ULTRAFAST PHOTOPHYSICS OF π – CONJUGATED POLYMERS FOR ORGANIC LIGHT EMITTING DIODE APPLICATIONS

by

Ella Olejnik

A dissertation submitted to the faculty of
The University of Utah
in partial fulfillment of the requirements for the degree of

Doctor of Philosophy

in

Physics

Department of Physics and Astronomy

The University of Utah

December 2013

The University of Utah Graduate School

STATEMENT OF DISSERTATION APPROVAL

The dissertation of **Ella Olejnik**

has been approved by the following supervisory committee members:

Zeev Valy Vardeny	, Chair	**08/23/2013**
Christoph Boehme	, Member	**08/23/2013**
Shanti Deemyad	, Member	**08/23/2013**
Ajay Nahata	, Member	**08/23/2013**
Pearl Sandick	, Member	**08/30/2013**

and by **Carleton Detar**, Chair/Dean of

the Department/College/School of **Physics and Astronomy**

and by **David B. Kieda**, Dean of The Graduate School.

ABSTRACT

In this work, we used the pump-probe photomodulation (PM) spectroscopy technique to measure the transient PM spectrum and decay kinetics in various π – conjugated polymers (PCPs) films and blends. Using two ultrafast laser systems, we covered a broad spectral range from 0.25 – 2.5 eV in the time domain from 200 fs to 1 ns with 120 fs time resolution. We also used continuous wave (CW) photomodulation spectroscopy, photoluminescence (PL), electro-absorption, and doping-induced absorption to study the photoexcitations and other optical properties of PCPs and guest/host blends.

In particular, we studied two different types of Poly(thienylenevinylene) polymer derivatives. One polymer type is the ordered region-regular (RR) and regio-random (RRa) – PTV in which the dark exciton, $2A_g$, is the lowest excited state. In these polymers, the photoexcited exciton shows very fast decay kinetics due to the internal conversion to the dark exciton, which results in weak PL emission; thus, these two polymers are nonluminescent. The other PTV derivative is the imide – PTV which is more luminescent due to the proximity of $1B_u$ and $2A_g$ states, that results in longer decay kinetics and a difference between the calculated value of the QEPL (9%) and the measured one (1%).

We also demonstrate transient strain spectroscopy in RR – PTV thin films, where the ultrafast energy release associated with the exciton decay gives rise to substantial

static and dynamic strains in the film that dramatically influences the film's transient PM response.

We also study the photophysics of poly(dioctyloxy) phenylenevinylene polymer with different isotopes, where we substituted hydrogen (H – polymer) by deuterium (D – polymer), and ^{12}C by ^{13}C isotopes. From the transient decay kinetics measurements, we found that the exciton recombination in DOO – PPV consists of two processes. These are: intrinsic monomolecular, and exciton-exciton annihilation (bimolecular). In the D – polymer, different probe frequencies of the main exciton photoinduced absorption band (PA_1) show a variety of decay kinetics that result from various photoexcitations that contribute to the spectrum. Comparing the transient PM spectrum at 1 ns time delay to the CW PM shows the formation of triplet excitons, which is possible due to singlet fission of mA_g (at 2.9 eV) into two triplets (2 X 1.4 eV).

In the last part of this thesis, we summarize our studies of organic light emitting diodes (OLED) devices based on a host/guest blend of polyfluorene polymer that is mixed with various percentages of $Ir(btp)_2acac$ molecules. In this mixture, the PFO (host) shows blue fluorescence, whereas the Ir-complex (guest) has red phosphorescence emission; thus, OLED based on this mixture can serve as a "white OLED." Since the PFO emission spectrum perfectly matches the absorption band of the Ir-complex, it induces an efficient energy transfer from the PFO host to the Ir-complex guest molecules, which we tried to time resolve by the transient PM method.

To my parents

TABLE OF CONTENTS

ACKNOWLEDGEMENTS

I would like to express my sincere gratitude and heartfelt thanks to my honorable advisor, Prof. Z. V. Vardeny, for his plentiful suggestions, constant guidance, support, and encouragement throughout all the years of my Ph.D. The research opportunity provided by Prof. Vardeny has been invaluable to me. I also express my sincere gratitude to my supervisory committee members, Prof. Christoph Boehme, Shanti Deemyad, Ajay Nahata, and Pearl Sandick, for their encouraging discussions and suggestions.

I would like to thank our collaborators, Prof. X. Jiang's group from the Department of Physics, University of South Florida, and Prof. C. Zhang's group from Department of Chemistry and Biochemistry, South Dakota State University for the PTV polymers and the related discussions.

A Ph.D. degree in experimental physics requires a lot of technical assistance, and this was available to me through the help of Drs. Randy Poslon and Mathew Delong. I am grateful for their help. I would also like to thank Mr. Leonard Wojcik for synthesizing the DOO-PPV polymer based on different isotopes, and his help with understanding the chemistry.

I would like to thank Dr. Josh Holt for introducing me to the ultrafast measurements and Dr. Sanjeev Singh for introducing me to the near-IR femtoseconds system at the Laser Institute.

I would like to thank my former group members, Drs. ChuanXiang Sheng, Golda Hukic, Tho Nguyen. Maria Navas, Bhoj Raj Gautam, and Bill Pandit, for their valuable suggestions, support, and collaboration.

My sincere thanks is extended to my current group members, Tek Prasad Basel, Uyen Huynh, Ryan McLaughlin, Yaxin Zhai, Peter Peroncik, and Dr. Dali Sun for their collaboration, support, and friendly suggestions.

Last but not least, I thank my family in Israel for their endless support, love, patience, care, and encouragement through all these years of my Ph.D.

Finally, I would like to thank the Department of Energy for their generous financial support, without which this work would not be possible.

CHAPTER 1

INTRODUCTION

1.1 π – conjugated polymers

Since the discovery of π – conjugated polymers (PCPs), they have been widely used for the fabrication of electronic and optoelectronic devices [1.1, 1.2] such as organic light emitting diodes (OLEDs) [1.3, 1.4], thin film transistors (TFTs) [1.5 – 1.7], photovoltaic cells [1.8, 1.9], optical switches, and modulators. In their neutral form, these polymers are semiconducting, with a typical optical gap of about 2 eV. However, upon doping, they behave as metals, with electrical conductivities approaching that of copper. The 2000 Nobel Prize in Chemistry was awarded to Heeger, McDiarmid, and Shirakawa for the first demonstration of conducting polymers (PCPs).

In addition to their unique properties among polymers to conduct electrical currents, they also have the advantage over the traditional inorganic semiconductors (such as silicon) because of their low manufacturing cost, environmentally friendly components, and completely flexible form factor.

From a fundamental point of view, the unique properties of conjugated polymers rely on the π-electrons delocalization along the backbone chains. They have intrinsic one-dimensional (1D) characteristics that are manifested by their optical and electronic

properties. The 1D ideal model, however, is flawed by interchain interactions with neighboring polymer chains or segments. In addition, polymers in general are very disordered systems compared to crystalline inorganics, on which solid-state physics has progressed. While much of the terminology was borrowed from inorganic solid-state physics, the physics is fundamentally quite different. Furthermore, experimental data from conjugated systems tend to be difficult to interpret and has led to discrepancies in the literature. The chemical structure of the most common π – conjugated polymers is shown in Figure 1.1.

1.2 Electronic and optical properties of π – conjugated polymers

In the ground state, the carbon atoms have 4 electrons with configuration $1s^2 2p^1_x 2p^1_y$. In bonding, these s and p atomic orbitals are hybridized to form sp^n orbitals. There are three types of sp^n hybridization: sp hybridization, found in linear molecules such as ethyne; sp^2 hybridization, typical planar molecules such as ethylene, benzene, and graphite; and sp^3 hybridization, characteristic of three-dimensional structures such as methane, ethane, or diamond [1.11]. Molecules with sp^3 orbitals are known as *saturated*, since every carbon is bonded to 4 neighboring atoms [Figure 1.2 (a)] and the energy gap is about 6 eV.

Conjugated polymers are typically sp^2 hybridized (unsaturated). The hybrid orbitals lie within the plane of the molecule, while the remaining $2p_z$ orbitals are oriented perpendicular to the plane [Figure 1.2 (b)] and overlap to form a delocalized π-molecular orbital [Figure 1.2 (c)]. The strong σ-bonds determine the shape of the backbone, whereas the π-electrons are more loosely bound and primarily responsible for the electronic and

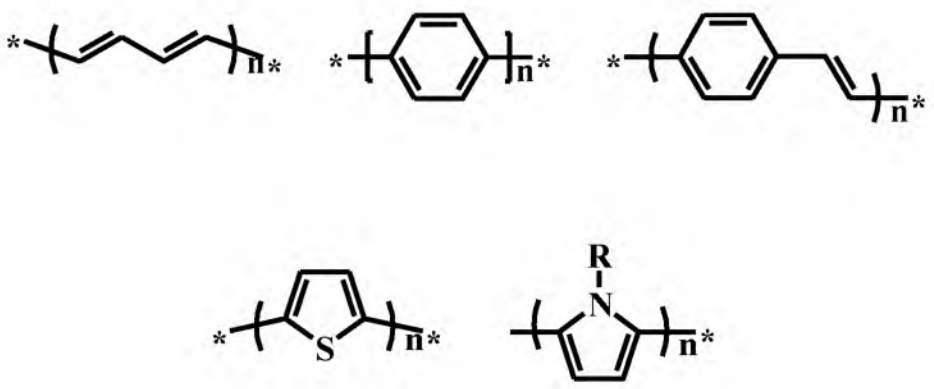

Figure 1.1: Example of a few common π – conjugated polymers.

optical properties of the polymer. These hybrid π-bonds form molecular orbitals, which are filled with electrons according to the Pauli exclusion principle up to the highest-occupied molecular orbital (HOMO), corresponding to the valance band in inorganic semiconductors. The next molecular orbital above that is called the lowest unoccupied molecular orbital (LUMO), analogous to the conduction band. Electrons in the ground-state π-orbital are delocalized across many monomers and are therefore considered in a "bonding" state. The π-electron can be excited to an "antibonding" π* configuration (e.g., the LUMO).

1.2.1 Symmetry groups

Polyenes ($C_{2n}H_{2n+2}$) are linear chains of CH units with sp^2 hybridization of p_z atomic orbitals. The symmetry of such a polymer is described by the point group C_{2h} [1.10] and the electronic wave functions are classified on the basis of their inversion and

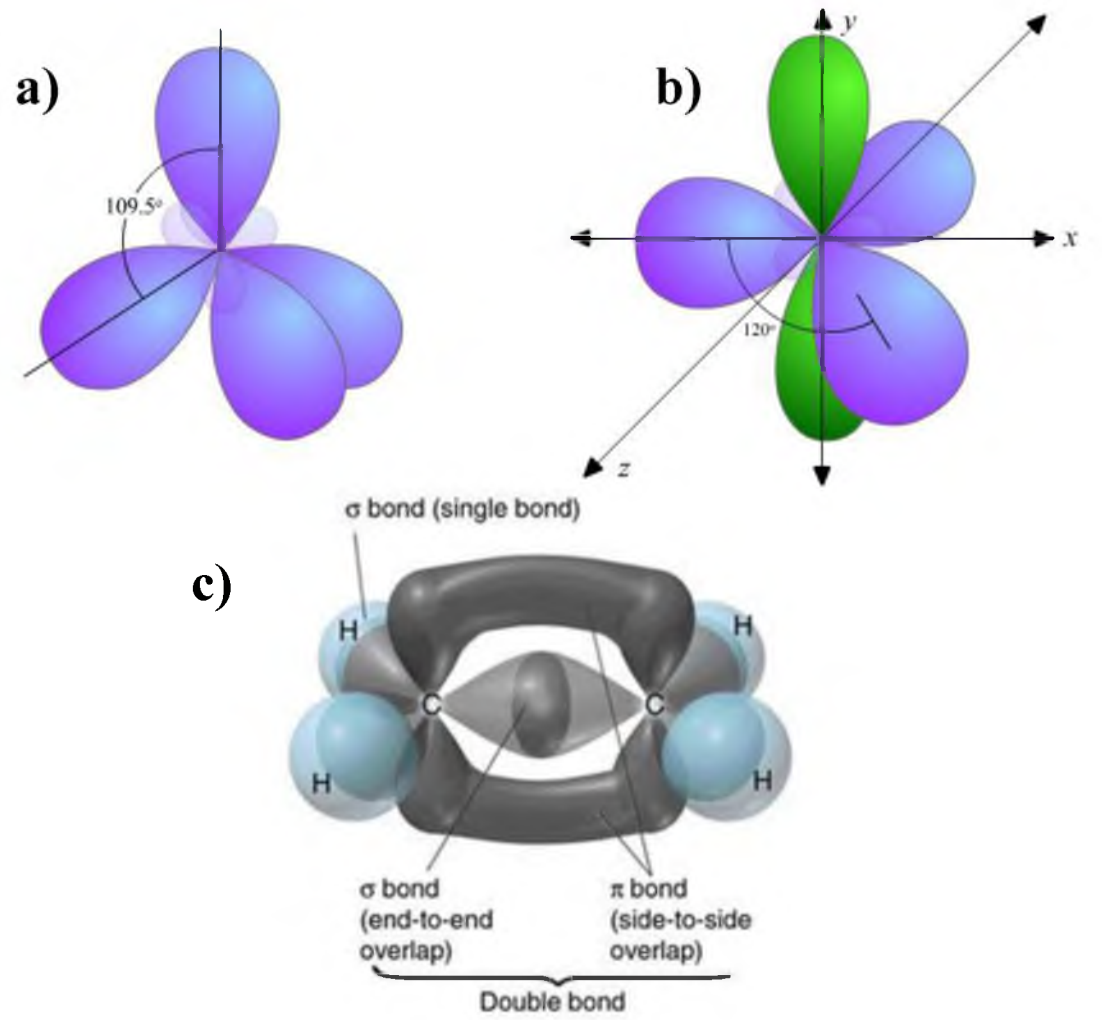

Figure 1.2: sp^n hybridization of the carbon atoms; (a) The sp^3 hybridization. (b) The sp^2p_z hybridization. (c) The formation of the π bonds.

rotation properties. We note that wave functions have to change within their degeneracy with respect to every symmetry operation belonging to the point group symmetry. If the orbital wave functions change (do not change) sign under inversion at the symmetry center, then they are dubbed as u (g), and denoted with b (a) if they change (do not change) sign under 180° rotation around the symmetry axis. The atomic 2p-orbitals change sign under reflection in the symmetry plane, so p-electron orbitals are only a_u or b_g.

The wave function describing the electronic states along a conjugated length is still distinguished by its g or u character, but now, in the molecular-orbital picture, the inversion properties are denoted with capital letters A or B. The π-electron states in polymers can then have either A_g or B_u symmetry according to:

$$a_u \otimes a_u = b_u \otimes b_u = A_g \tag{1.1}$$

$$a_u \otimes b_g = b_g \otimes a_u = B_u \tag{1.2}$$

Since all π-orbitals in the HOMO in PCPs are always doubly occupied, the ground state has A_g character. The next excited state (LUMO) has B_u character and the excited state above that (LUMO + 1) has Ag symmetry again, and so on. It is convenient to assign labels to excited states in PCPs according to these symmetry groups by the convention n^pX, where n is the overall quantum number (although a generic m or k may be used to describe the unknown, but high, quantum number of continuum states), p is the degeneracy of the quantum state: 1 for singlet and 3 for triplet, and X is its symmetry

character. Thus, the ground state exciton is often labeled as $1A_g$ where the p = 1 is understood.

Whenever electron-electron (el-el) and electron-phonon (el-ph) interactions can be neglected, the ordering of these excited states is:

$$1^1A_g < 1^1B_u < 2^1A_g \tag{1.3}$$

The energies of these configurations can be regarded as approximately equal to the sum of the orbital energies. However, as a consequence of both el-el and el-ph interactions, the energetic ordering of the first excited states may be reversed:

$$1^1A_g < 2^1A_g < 1^1B_u \tag{1.4}$$

The ordering of the first excited states affects the optical properties of the material. When the B_u excited stated has lower energy than the A_g excited state [Figure 1.3], the material is expected to show fluorescence, since the $B_u \rightarrow A_g$ transition is dipole allowed. This is the case of polythiophene and poly (p-phenylenevenylene)s. If, however, the B_u excited stated has higher energy than the A_g excited state, then the first excited state decays nonradiatively to the ground state, due to the dipole forbidden $A_g \rightarrow A_g$ transition, and no fluorescence occurs. This happens, for instance, in the case of trans-polyacetylene and PTV. A complete discussion about the interplay of electron-electron and electron-phonon coupling on state ordering is offered in Ref. [1.12].

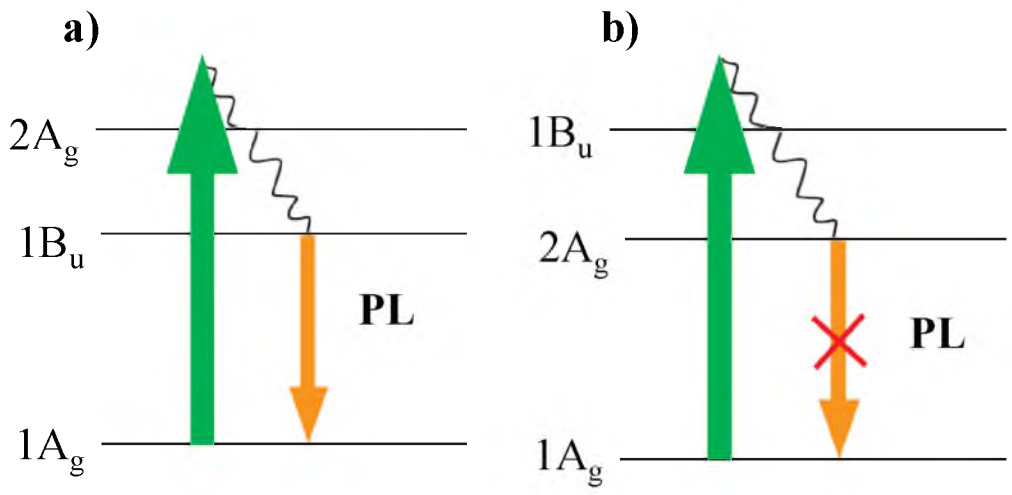

Figure 1.3: After excitation and relaxation, the polymer in (a) fluoresces due to the state ordering 1Ag < 1Bu < 2Ag, whereas in (b), the Ag → Ag transition is forbidden, so fluorescence does not occur.

1.2.2 The Franck-Condon principle

The calculation of transition dipole moments can be significantly simplified by the Franck-Condon principle. Basically, it assumes that electron transitions occur so quickly that the nuclei remain stationary. After an electronic transition has taken place, the nuclei respond by moving along the adiabatic potential energy surface of the excited state to a new equilibrium position, resulting in a change of the molecule to the excited state configuration. This configurationally change is known as "lattice relaxation" and the energy involved in it is the "relaxation-energy." Emission follows the same path in reverse. In the potential energy surface diagram, the transition is vertical, as represented in Figure 1.4.

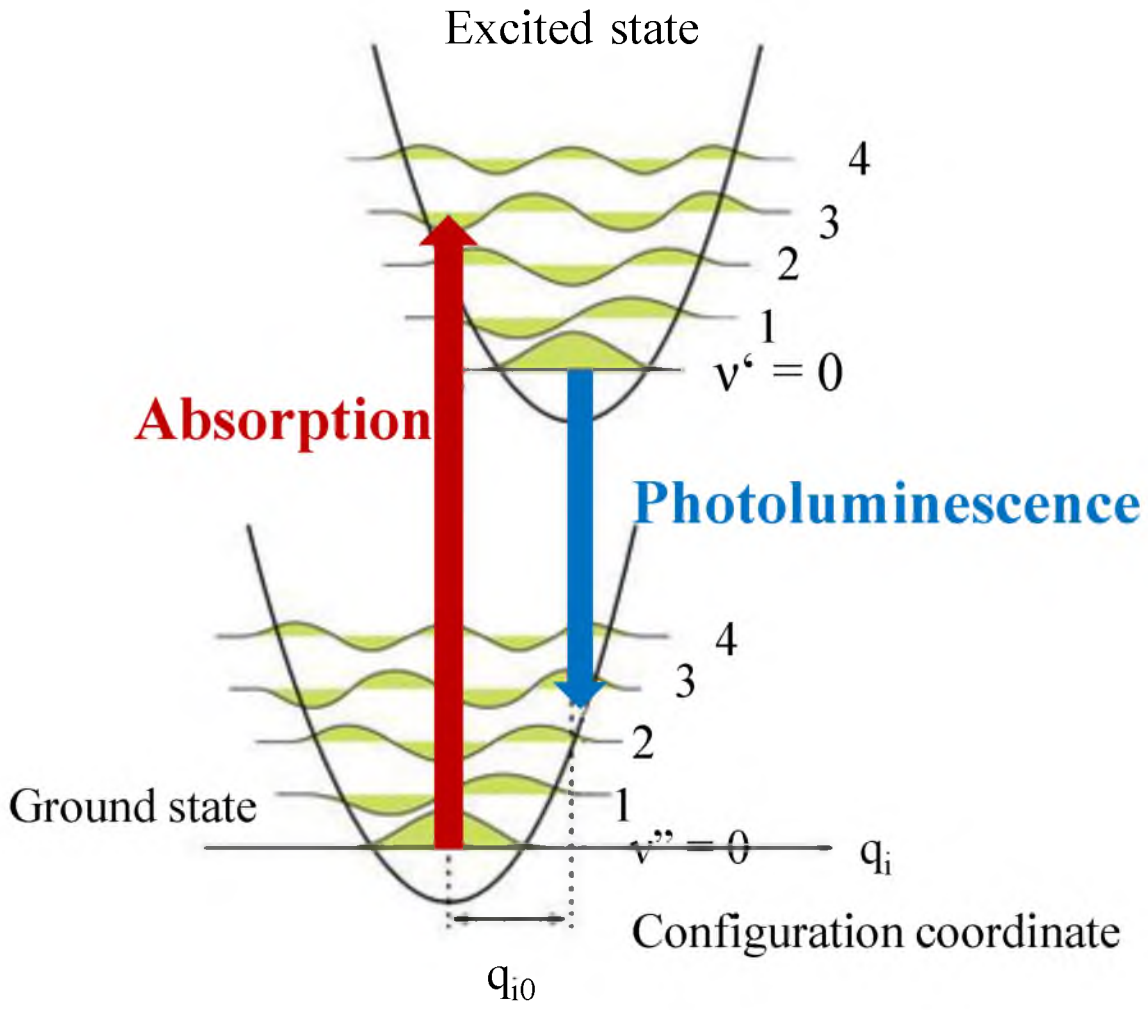

Figure 1.4: The potential energy surfaces of the ground and excited states with vibronic modes of the wavefunction plotted as a function of the conformational coordinates, Q. The Franck-Condon principle states that absorption and fluorescence electronic transitions are vertical.

Describing the nuclear motion in terms of the normal coordinates, or conformational coordinate, Q, for small displacements from the equilibrium position, each normal mode can be considered as a harmonic oscillator. The relaxation of the nuclear position to the bottom of the adiabatic energy curve leads to the so-called "Stokes-shift" between absorption and emission. In general, the emission spectrum is sharper than the absorption spectrum, since photogenerated excitons have time to migrate to the longer, lower energy chains.

The relative intensity of the transitions from the ground to the excited vibronic state [see Figure 1.4] is controlled by the overlap integral 0-vibronic ground state wavefunction and the 0/1/2/ .... -vibronic excited state wave functions. The overlap integral can be separated into an electronic and vibrational components. Within the Franck-Condon (FC) approximation, the exciton-phonon coupling strength is expressed by the Huang-Rhys (HS) parameter, S, and incorporated into the overlap integrals. The square of the vibronic integral is known as the Franck-Condon factor of the transition. If the equilibrium bond lengths in the ground- and first-excited states were equal, the 0 – 0 transition would have a FC factor of unity and all higher vibronic transitions would be zero (i.e., forbidden). In reality, bond lengths are longer in excited-states than in the ground state, and higher vibronic transitions become allowed, so-called "vibronic satellites" or "replicas." The distribution of emission intensities between the main peak and replicas depend strongly on the HR parameter S.

In the excited state, there is rapid ($\approx$ 200 fs), nonradiative relaxation of the photoexcitation into the lowest vibrational level, known as internal conversion. From there, the photon may be reemitted after typically 0.1 – 1 ns with via a transition to the

lowest vibronic level of the ground state (0 – 0 transition), the first vibronic level (0 – 1), etc. Vibronic spacing is rather similar in ground and excited states. Therefore, absorption and emission spectra often appear as mirror images [Figure 1.4].

1.2.3 Optical selection rules

Symmetry considerations play an important role in optical spectroscopy. A particle (quasi or otherwise) cannot change quantum states without conserving energy. A selection rule is a condition constraining the physical properties of the initial system and the final system that is necessary for a process to occur with a nonzero probability. Usually, in spectroscopy, a transition involves the emission or absorption of photon radiation.

Three quantum states must be considered in order to address the probability of a transition: the photon, the initial state, and the final state. The symmetry of a function with regard to a reflection of all coordinates through the origin is called its parity. Even though photons are bosons, photons have antisymmetric parity. This is also in agreement with the dipole interaction approximation where the dipole matrix element is odd under inversion or reflection. As a consequence of the odd photon parity, the initial and final wave functions of a transition must have opposite parity after absorbing/emitting a photon.

A photon also carries spin angular momentum $\pm \hbar$. The total (spin and orbital) angular momentum in the photon-dipole interaction must be conserved [1.29]; $\Delta\ell = \pm 1$, and, $\Delta m_\ell = 0, \pm 1$. ℓ is the angular momentum quantum number and m_ℓ is the magnetic quantum number (projection of angular momentum).

The oscillating electric field associated with a transition between an initial and final state can be seen as an electric dipole, and the transition probability is given by the matrix element between them. Decoupling the initial and final state by means of losing quantum mechanical phase coherence is required to absorb or emit a photon. Transition probability of a dipole is described by D^2, where the transition moment is given by $D = < i| \hat{\mu} |j >$ where $\hat{\mu} = \hat{e}r$ is the dipole operator. The equation above indicates that the transition probability is related to how well the dipole moment between two energy states can couple to the electric field of a photon, which is Fermi's Golden Rule [1.30].

From the nature of the electric dipole operator, we can conclude a few points; (i) The electric dipole operator conserves total spin, so transitions can only occur between states in the same spin manifold. Transitions between singlet and triplet states are forbidden in the dipole approximation (this rule may be overcome by spin-orbit coupling). (ii) The electric dipole operator is antisymmetric with respect to the inversion operator, which means that optical transitions are allowed only between gerade, g, and ungerade, u, states. (iii) The dipole operator is antisymmetric with respect to the particle-hole operator so that it connects only states of opposite e-h symmetry. It should be noted that selection rules do not absolutely prohibit transitions that violate them.

Even though the expression “forbidden transition” is often used, it does not mean that these transitions do not occur or cannot occur. These transitions are possible, they only occur at a lower rate. Also, extrinsic factors like disorder, applied electric fields, etc. may “break” the symmetry of the states and as a result, these transitions become allowed.

1.3 Excitation models for π – conjugated polymers

Su, Schriefer, and Heeger proposed a model (SSH) based on tight binding approximation calculations taking into account only the electron-phonon interaction, thus ignoring the electron-electron interaction [1.13]. They applied a semiclassical Huckel Hamiltonian that contains two components: the lattice kinetic energy, which is treated classically, and the electron-phonon interaction, which is treated quantum mechanically, as expressed in the following Hamiltonian:

$$H_{SSH} = \frac{K}{2}\sum_{n}(u_n - u_{n-1})^2 + \frac{M}{2}\sum_{n}\left(\frac{du_n}{dt}\right)^2 - \sum_{n,s}(t_0 + \alpha(u_{n+1} - u_n)(c^{+}_{n+1,s}c_n + c^{+}_{n,s}c_{n+1,s}) \quad (1.5)$$

where t_o is the hopping integral between the nearest neighbors for an undistorted chain, α is the electron lattice coupling constant, $c_{n,s}^{+}$ and $c_{n,s}$ are the creation and annihilation operators of an electron on site n with spin s, K is the spring constant due to the π-electrons, and u_n is the deviation of the n-th site from the equilibrium position in an undistorted chain with equal distance between sites.

The SSH model predicts that dimerization caused by strong electron-phonon interaction lowers the system energy, and opens an energy gap $\Delta = 4\alpha u$. Thus, the occupied electronic states in equilibrium are lowered, causing this configuration to be more stable [Figure 1.5 (b)]. In this way, the system no longer acts as a one-dimensional metal [Figure 1.5 (a)], but instead it has the properties of a semiconductor [1.14].

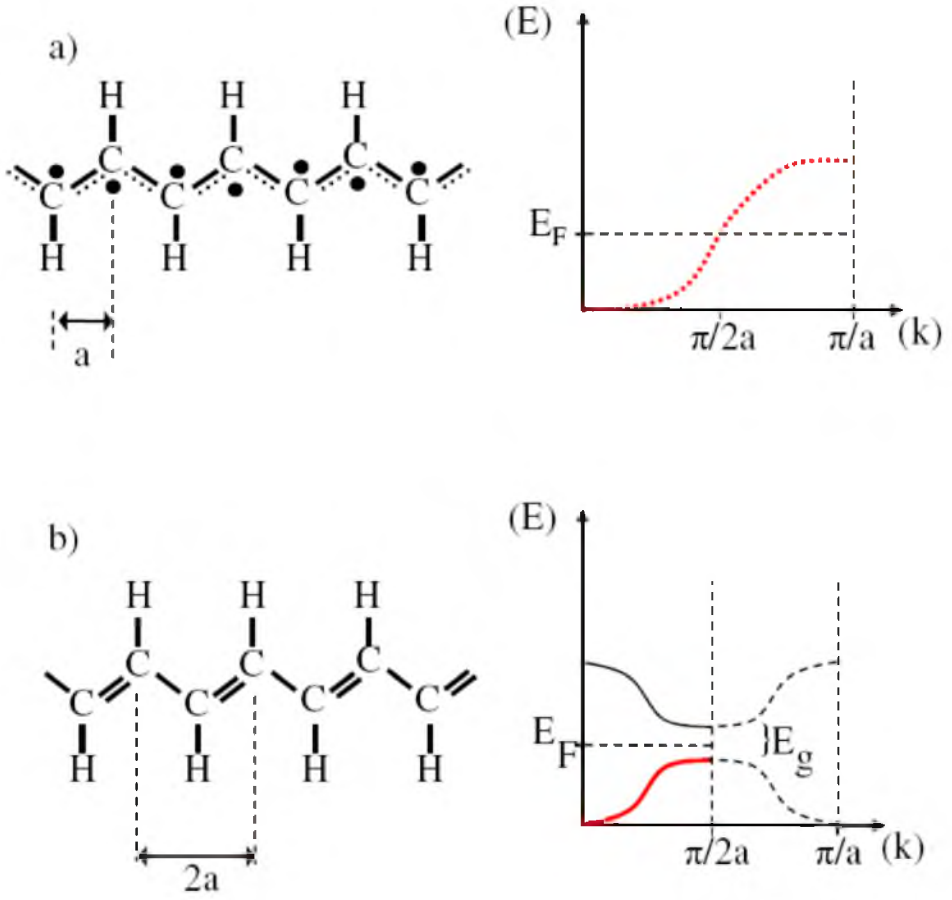

Figure 1.5: The nondimerized configuration which has a typical one-dimensional metallic behavior (a). The dimerized configuration which has the properties of a semiconductor (b).

Models including electron-electron interaction and 3D interchain coupling are based on Hubbard type Hamiltonians, where the Hubbard contribution to the Hamiltonian is:

$$H_{Hub} = U \sum_i n_{i,\uparrow} n_{i,\downarrow} \tag{1.6}$$

where U is the Coulomb repulsion between two electrons on the same site, $n_{i,\uparrow}$ and $n_{i,\downarrow}$ describe the density operators for electrons with spin up and spin down, respectively.

However, since the Hubbard model disregards electron-phonon interaction, which is quite strong in the polymer system, a combination of both SSH model and Hubbard model is more realistic, as has been used by Mazumdar and Dixit [1.15, 1.16] to explain the energy levels of excitations in the class of π – conjugated polymers. Since electron-electron interaction is so strong in one-dimensional polymers, the lowest optical transition is not a transition from the valence band into the conduction band, like in usual semiconductors, but instead an excitonic transition, where intrachain exciton binding energies as large as 0.4 to 0.8 eV have been inferred.

1.4 Photoexcitations in π – conjugated polymers

When the π – conjugated polymer is excited with above-gap photon energy, both short- and long-lived photoexcitations are created. These photoexcitations can be detected and characterized by transient and CW photomodulation (PM) techniques, where a pump beam generates the photoexcitations, and subsequently, the induced optical absorption spectrum due to the presence of photoexcited species is monitored with the probe beam in a broad spectral range from mid-IR to visible using different probe sources. The PM spectrum essentially measures difference spectra, i.e., the difference in the optical absorption ($\Delta\alpha$) of the polymer when it contains a nonequilibrium carrier concentration and that in the equilibrium ground state. Therefore, the optical transitions of the various photoexcitations are of fundamental importance.

1.4.1 Charged photoexcitations

1.4.1.1 Polaron and bipolarons excitations

In PCPs with nondegenerate ground state, or when a single charge is added to a trans – polyacetylene chain, then another charged excitation is possible. When an electron is taken away from the HOMO or added to the LUMO of a molecule, the molecular orbitals and the nuclei respond by relaxing to a new, localized position of minimum energy. Due to the strong coupling between the charge carrier and the local lattice deformation, removing an electron energetically costs less than the HOMO suggests, while an electron joining a molecule gains a bit more energy than the LUMO suggests. In other words, moving the HOMO and LUMO in a local neighborhood much closer in energy creates states within the energy gap which can be populated with charge carriers.

These midgap states are shown in Figure 1.6. They, usually, are dislocated symmetrically about the center of the energy gap and have alternate parity. The charge carrier that is coupled with the disturbed field produces a quasi-particle called a polaron. A polaron can be positively (P^+) or negatively (P^-) charged and carries a spin 1/2.

Polarons are typically detected optically by observing their associated absorption signature transitions, P_1 and P_2 [Figure 1.6]. The polaron excitations were first predicted by Su and Schrieffer [1.20]. The analytic solution for polaron was discussed Bishop and Campbell [1.19].

The bipolaron is a combination of two charge polarons [1.17]. As the polaron, here also there are two symmetrical states localized in the gap, but deeper in the gap compared with the polaron states. The bipolaron levels can be empty, which is a doubly

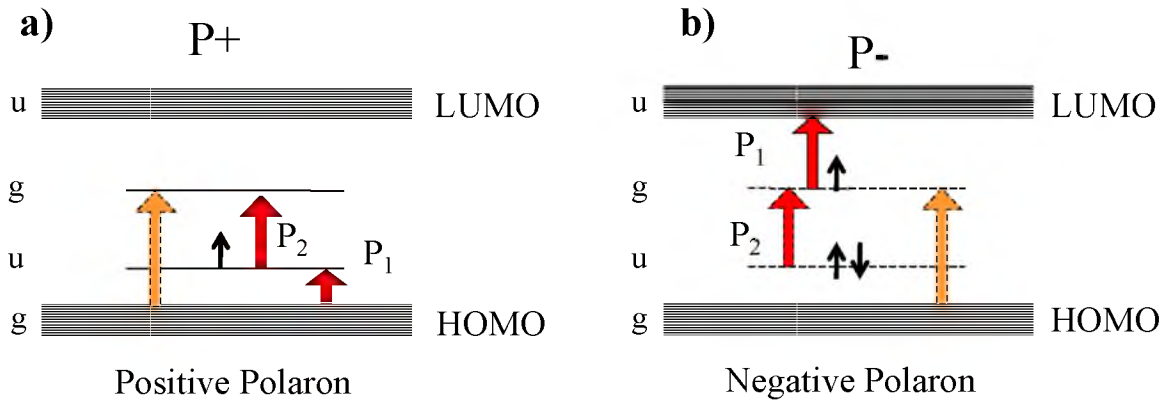

Figure 1.6: Optical transitions of the positive polaron (a) and negative polaron (b). The optically allowed transitions are shown with the red arrows and the forbidden optical transitions are shown with the dashed arrows.

charged positive bipolaron (BP++), Figure 1.7 (a), or fully occupied, which is a negative bipolaron (BP--), Figure 1.7 (b).

Therefore, the bipolaron is spinless. The bipolaron has one strong (allowed) and one weak (forbidden) optical transition.

1.4.1.2 Polaron pair excitations

The polaron pairs diagram is shown in Figure 1.8. A polaron pair (PP) is a bound pair of two oppositely charged polarons, P+ and P-, formed on two adjacent chains [1.18]. Thus, the polaron pair is neutral. The binding energy is mainly Coulombic in the case of polaron pairs.

The energy levels of a polaron pair are formed by the energy levels of the coupled P+ and P- , each polaron level is split into two due to the coupling, and as a result, there are four states in the gap. The Coulomb interaction between the oppositely charged polaron composing the pair causes the energy levels of the positive polaron to shift downward and those of the negative polaron to shift upward.

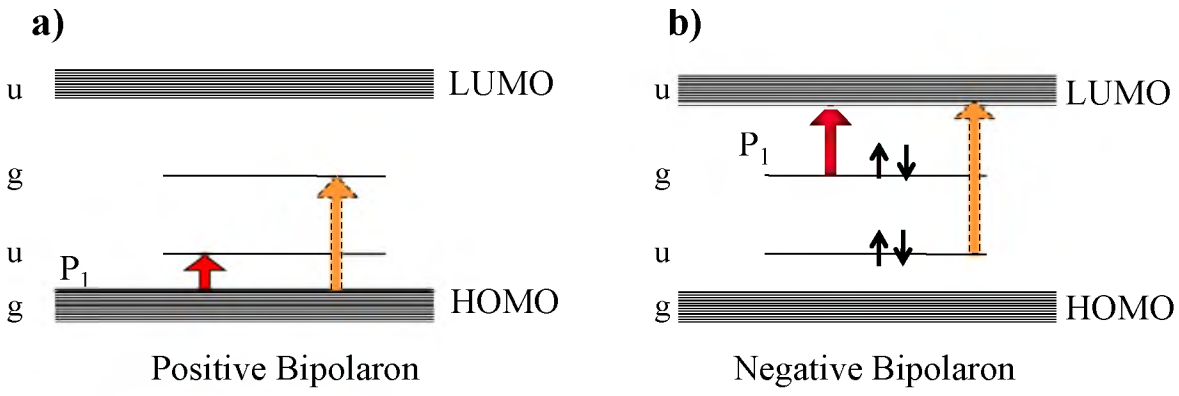

Figure 1.7: Optical transitions of the positive bipolaron (a) and negative bipolaron (b). The optically allowed transition is shown with the red arrow and the forbidden optical transition is shown with the dashed arrow.

As the polaron, the polaron pairs also have two strong transitions, PP_1 and PP_2, and a weak one, PP_3. For a loosely bound polaron pair, these transitions are not far from transitions P_1, P_2, and P_3 of the polaron. On the other hand, for a tightly bound polaron pair, a single transition, PP_2, is expected to dominate, since the energy of PP_1 is very low to be observed experimentally and PP_3 is close to the fundamental transition and thus difficult to separate. In this case, there are two states in the gap; the excitation is also known as a neutral interchain bipolaron or interchain polaron-exciton.

When the exchange interaction is small, the spin state of the PP is composed of four levels $|\pm 1/2, \pm 1/2>$. When the exchange interaction is large, the polaron pairs split into a singlet with spin 0 ("antiparallel spins") or a triplet with spin 1 ("parallel spins").

1.4.2 Neutral photoexcitations; excitons

Unlike polarons, excitons form when an electron is removed from the HOMO and placed in the LUMO, typically via the absorption of a photon. Excitons are bound states due to the Coulomb attraction between an electron excited in the conduction band and the

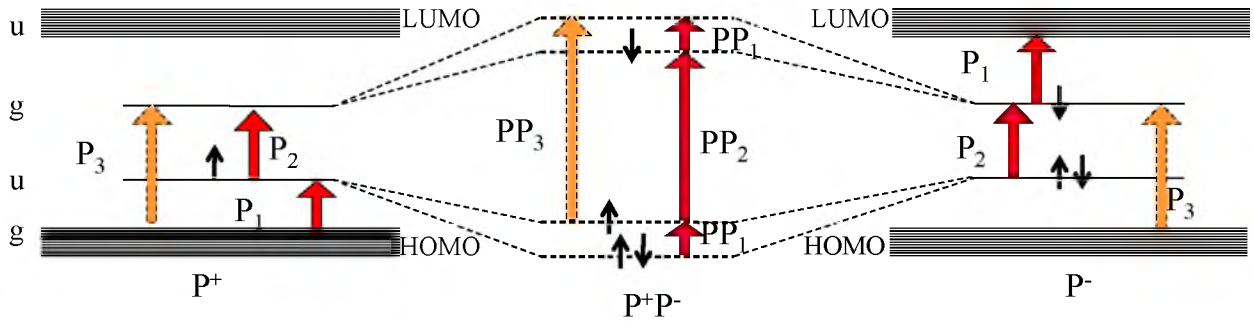

Figure 1.8: Optical transitions polaron pairs. The optically allowed transitions are shown with the red arrows and the forbidden optical transitions are shown with the dashed arrows.

hole left behind in the valence band (in the case of conjugated polymer, this corresponds to a $\pi - \pi^*$ excitation). Following the usual treatment of inorganic semiconductors, excitons in π – cojungated polymers can be classified as Frenkel or Wannier-Mott excitons [Figure 1.9].

When the electron and hole are tightly bound, the resulting exciton is strongly localized and is known as the Frenkel exciton [Figure 1.9 (a)]. The Frenkel exciton [1.22, 1.23] can be regarded as a correlated electron-hole pair that is located on the same molecular site and moves as a unit through the crystal lattice. Its radius, that is the average separation between the electron and the hole, is thus small ($<5^{o}A$) compared to the intermolecular spacing. The binding energy of such an exciton is of the order of 1 eV,

In the Wannier-Mott exciton [Figure 1.9 (c)], on the other hand, the exciton is delocalized over many atoms or molecules [1.24, 1.25], and often describes excitations in inorganic semiconductors where the dielectric constant, ε, is high by consequence of the electron-hole (e-h) Bloch functions and delocalized bands. The e-h Coulombic interaction is small compared to the bandgap of the material, with a binding energy of the order of

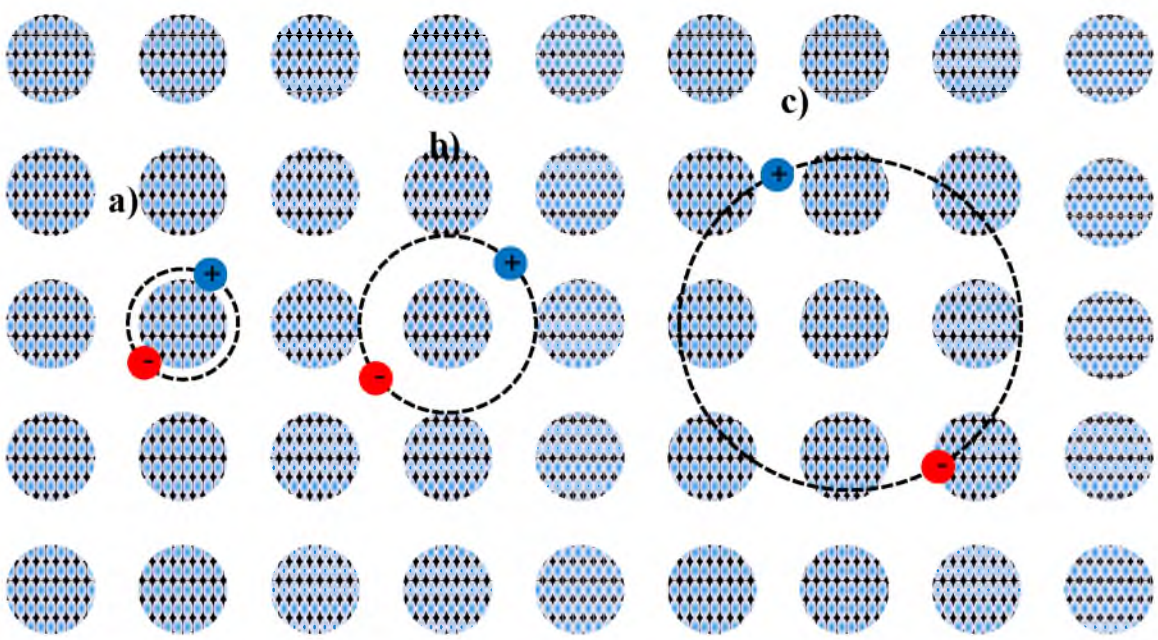

Figure 1.9: Schematic representation of (a) small-radius Frenkel exciton; (b) intermediate or charge-transfer exciton; and (c) large-radius Wannier-Mott exciton.

$E_b \approx 50$ meV and a radius of $r_{ex} \approx 40 - 100$ Å. Even though it is weakly bound and lives close to the conduction band, it carries no net charge, and resembles the Rydberg series of the hydrogen atom.

Excitons in conjugated polymers are usually considered to fall into an in-between regime of the Frenkel and Wannier-Mott extremes that are called charge transfer excitons [Figure 1.9 (b)].

However, there is still debate in the field about the magnitude of the exciton binding energy in organic systems. Experimental values currently report the binding energy of the lowest energy transition of PPV to range from 0.1 eV [1.26], to 0.2 – 0.5 eV [1.27], to around 1 eV [1.28].

1.4.2.1 Singlet and triplet excitons

The electron and hole in an exciton can be associated in a singlet or triplet state with spin 0 or 1, respectively, but both maintain a neutral charge. The wave function describing a two-particle system must be antisymmetric in spin and electron coordinates. It is obtained from the Slater determinant:

$$= \frac{1}{\sqrt{2}} \begin{vmatrix} \psi_i(r)\chi_i(\sigma) & \psi_i(r')\chi_i(\sigma') \\ \psi_j(r)\chi_j(\sigma) & \psi_j(r')\chi_j(\sigma') \end{vmatrix} \tag{1.7}$$

where $\psi_i(r)$ and $\chi_i(\sigma)$ are the electronic and spin part of the wave function, respectively. When taking into account the different total spin quantum number S:

$$^{S=0} = \frac{1}{2}\,[\psi_1(1)\psi_2(2) + \psi_2(1)\psi_1(2)][\uparrow(1)\downarrow(2) - \uparrow(2)\downarrow(1)] \tag{1.8}$$

$$^{S=1} = \frac{1}{2}\,[\psi_1(1)\psi_2(2) - \psi_2(1)\psi_1(2)][\uparrow(1)\downarrow(2) + \uparrow(2)\downarrow(1)] \tag{1.9}$$

$$^{S=1} = \frac{1}{2}\,[\psi_1(1)\psi_2(2) + \psi_2(1)\psi_1(2)][\uparrow(1)\uparrow(2)] \tag{1.10}$$

$$^{S=1} = \frac{1}{2}\,[\psi_1(1)\psi_2(2) + \psi_2(1)\psi_1(2)][\downarrow(1)\downarrow(2)] \tag{1.11}$$

where ↑ and ↓ represent the spin up and spin down projection of χ. In the noninteracting limit, singlet (S = 0) and triplet (T = 0) are degenerate, but electron-electron correlation

splits the energy level with triplet taking the lower energy. The transitions between singlet and triplet states are not allowed unless spin-orbit coupling becomes significant.

Figure 1.10 shows a picture of exciton bands. The lowest exciton is B_u with singlet and triplet antisymmetric with respect to inversion about the bond center. The next excited state is A_g with smaller binding energy E_b than the Bu state. Excitons can form in the continuum band. States above the continuum band onset are usually labeled mA_g and kA_g; the coefficients m and k represent high states which are in the continuum where the exact index is unknown.

Upon light absorption, a singlet exciton in the ground state, S^0 ($\ell = 0$), is excited to the first excited state, S^1 ($\ell = 1$). The inverse transition $S^0 \leftarrow S^1$ provides the required angular momentum to emit photon. The triplet to singlet transition, $S^0 \leftarrow T^0$, is forbidden since here $\Delta\ell = 0$. Because of the forbidden character of the dipole transition, an exciton in the triplet configuration has a relatively long lifetime compared to that of singlet excitons, from the order of a few microseconds up to seconds.

The emission of light from the lowest-lying triplet state is called phosphorescence. In order to see triplets in the picosecond time-domain, high intersystem crossing (ISC) rate (which may be provided by oxygen or other magnetic center), or high incident intensity to split a singlet into two triplets, a process called singlet fission [1.21], is required.

The triplet is lower in energy, as explained by Hund's Multiplicity Rule: for the same configuration, the lower energy state is the one which has the higher total spin. The common explanation for Hund's rule is that states with parallel spins are more spatially separated and thus the electron-electron repulsion is less, and the energy is thus lower.

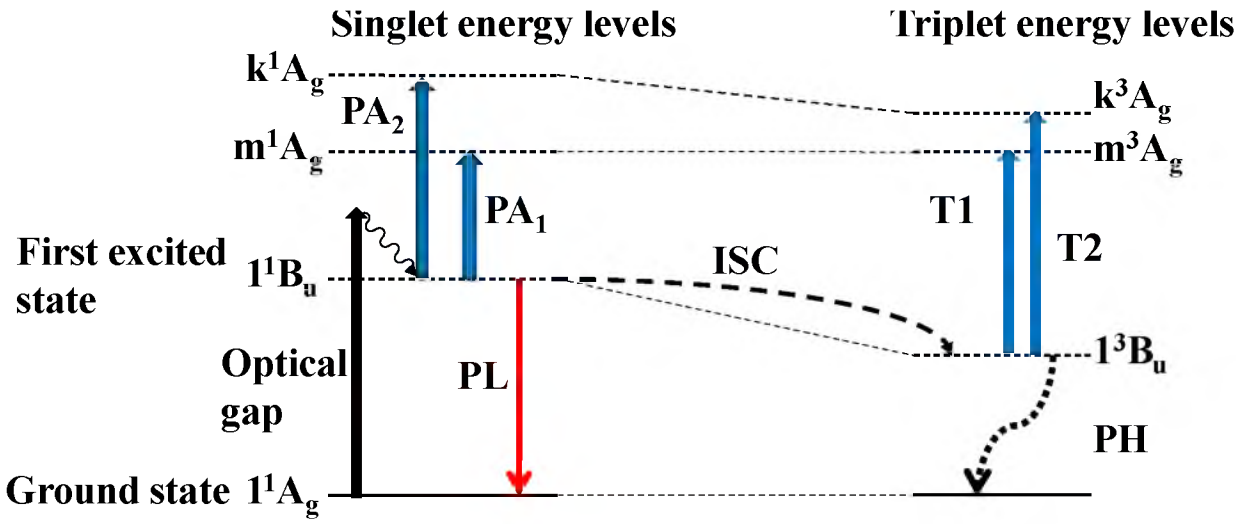

Figure 1.10: Photoexcitation model in conjugated polymers with nondegenerate ground states.

In summary, several decay process can take place for singlet excitons [1.31]; 1) they can recombine radiatively (PL in ≈ 100 ps, PH in ≈ 10 μs); 2) they can recombine nonradiatively (at recombination centers by emitting phonons); 3) become trapped (by self-trapping or at defect centers); 4) convert to the triplets (through intersystem crossing via extrinsic spin exchange centers, ≈ 10 ns), or 5) dissociate into polaron pairs.

1.5 Excimer, pi-dimer, and exciplex species

A variety of interchain species may be introduced when two adjacent chains interact with each other. Excimers and pi-dimers only exist in the excited state. They are formed when two neighboring polymers share their π-electrons in the excited state but not in the ground state [1.32 – 1.34]. These emissive excited state complexes have a dissociative ground state, that is, the ground state of the dimer spontaneously dissociates

into two ground-state molecules. Furthermore, the excimer cannot be directly excited optically. Instead, an intramolecular singlet exciton is photoexcited that at a later time delocalizes over two molecules, forming the excimer. Excimer formation is accompanied by a strong geometric distortion along the intermolecular axis that, when combined with the dissociative nature of the ground state, leads to featureless, strongly Stokes-shifted emission of films in comparison to dilute solution. Excimer formation was observed in PPV-based films [1.35], leading to quenching of luminescence due to their large nonradiative decay in this polymer.

An interchain excited state, called an exciplex, can also be formed when an *unequal* sharing of π-electron density between chains or a partial degree of charge transfer occur [1.34].

While excimers exist only in the excited state, interchain interaction may also lead to ground-state interactions, with formation of aggregate states [1.33]. Upon aggregation, both the ground- and excited-state wave functions are delocalized over several polymer chains. The aggregate is therefore directly accessible by spectroscopic means.

1.6 Reference

[1.1] T. A. Skotheim, R. L. Elsenbaumer, and J. R. Reynolds, Handbook of Conducting Polymers, 2nd ed., New York: M. Dekker, 1998.

[1.2] G. Malliaras and R. Friend, Physics Today, 58, 53, (2005).

[1.3] J. H. Burroughes, D. D. C. Bradley, A. R. Brown, R. N. Marks, K. Mackay, R. H. Friend, P. L. Burns, and A. B. Holmes, Nature, 347,539, (1990).

[1.4] D. Braun and A. J. Heeger, Applied Physics Letters, 58, 1982 (1991).

[1.5] J. H. Burroughes, C. A. Jones, and R. H. Friend, Nature, 335, 137, (1988).

[1.6] B. Crone, A. Dodabalapur, Y. Y. Lin, R. W. Filas, Z. Bao, A. LaDuca, R. Sarpeshkar, H. E. Katz, and W. Li, Nature, 403, 521, (2000).

[1.7] F. Garnier, R. Hajlaoui, A. Yassar, and P. Srivastava, Science, 265, 1684 (1994).

[1.8] N. S. Sariciftci, L. Smilowitz, A. J. Heeger, and F. Wudl, Science, 258, 1474 (1992).

[1.9] G. Yu, J. Gao, J. C. Hummelen, F. Wudl, and A. J. Heeger, Science, 270, 1789 (1995).

[1.10] Ashcroft, N. and Mermin, N. Solid State Physics. Holt, Rinehart and Winston, New York, (1976).

[1.11] Pauling, L. J. Am. Chem. Soc. 53, 1367, (1931).

[1.12] Barford, W. Electronic and Optical Properties of Conjugated Polymers. Oxford University Press, (2005).

[1.13] W. P. Su, J. R. Schrieffer, and A. J. Heeger, PRB, 22, 2099, (1980).

[1.14] Peierls, R. E. Quantum Theory of Solids. Oxford: At the Clarendon Press, (1955).

[1.15] S. Mazumdar and S. N. Dixit, PRL, 51,292, (1983).

[1.16] S. Mazumdar and S. N. Dixit, Synthetic Metals, 28, 463, (1989).

[1.17] A.J. Heeger, S. Kivelson,.R. Schrieffer, W.P. Su, Rev. Mod. Phys. 60, 781 (1988).

[1.18] P.A. Lane, X. Wei, Z.V Vardeny, PRB, 56, 4626, (1997).

[1.19] D.K. Campbell, A.R. Bishop, Nucl. Phys B 200, 297 (1982).

[1.20] W.P. Su, J.R. Schrieffer, Proc. Nat. Acad. Sci. USA 77, 5626 (1989).

[1.21] Sheng, C.-X. Photophysics of Quasi-one-dimensional Excitons in π-conjugated Polymers and Semiconducting Single-walled Nanotubes. PhD thesis, University of Utah, (2005).

[1.22] Scholes, G. D. and Rumbles, G. Nat. Mater. 5, 683 (2006).,

[1.23] Davydov, A. S. Theory of Molecular Excitons. Plenum Press, New York, (1971).

[1.24] Cojan, C., Agrawal, G. P., and Flytzanis, C. PRB 15, 909, (1977).

[1.25] Wannier, G. H. Phys. Rev. 52, 191 (1937).

[1.26] Hide, F., Garcia, M. D., Schwartz, B., and Heeger, A. Acc. Chem. Res. 30, 430, (1997).

[1.27] Schwartz, B. Ann. Rev. Phys. Chem. 54, 141, (2003).

[1.28] Chandross, M., Mazumdar, S., Liess, M., Lane, P. A., Vardeny, Z. V., Hamaguchi, M., and Yoshino, K. PRB 55, 1486, (1997).

[1.29] Ellis, A. M. J. Chem. Ed. 76, 1291, (1999).

[1.30] Pope, M. and Swenberg, C. Electronic processes in organic crystals. Clarendon Press Oxford University Press, Oxford, New York, (1982).

[1.31] Skotheim, T. A. and Reynolds, J. R. Conjugated polymers: theory, synthesis, properties, and characterization. CRC Press, (1998).

[1.32] S. A. Jenekhe and J. A. Osaheni, 265, 765, (1994).

[1.33] R. Farchioni and G. Grosso, Organic Electronic Materials : Conjugated Polymers and Low Molecular Weight Organic Solids, Berlin ; New York: Springer,(2001).

[1.34] D. D. Gebler, Y. Z. Wang, D. K. Fu, T. M. Swager, and A. J. Epstein, The Journal of Chemical Physics, 108, 7842, (1998).

[1.35] I. D. W. Samuel, G. Rumbles, and C. J. Collison, PRB, 52, 11573, (1995)

CHAPTER 2

EXPERIMENTAL SETUP

Probably the best way to identify and characterize photoexcitations in π – conjugated polymers (PCPs) is to study the change in their optical absorption. When PCPs absorb a photon, states are created within the optical gap of the polymer, which change the optical absorption spectrum. The best way to study the change in the optical absorption is to use the technique of photomodulation (PM). By introducing modulation into the optical system, small changes in optical properties can be detected.

2.1 Ultrafast excitation source

2.1.1 Femtosecond Ti:sapphire setup

The femtosecond laser source that has been used in this study is a Ti:Sapphire laser system that consists of a home-made Ti:Sapphire oscillator and Ti:Sapphire regenerative amplifier [Figure 2.1]. The oscillator is passively mode-locked, and was assembled at the University of Utah Laser Institute based on the "Kapteyn-Murnane 11 fs scheme" [2.1]. It yields a pulse laser output of ~ 400 mW at 800 nm, with pulse duration of ~ 30 fs with repetition rate of 76 MHz. The oscillator is pumped by a cw 5W diode laser (532 nm) Millenia Pro (Spectra Physics), and its cavity contains two fused silica prisms to compensate the dispersion caused by the 4.75 mm long Ti:sapphire crystal.

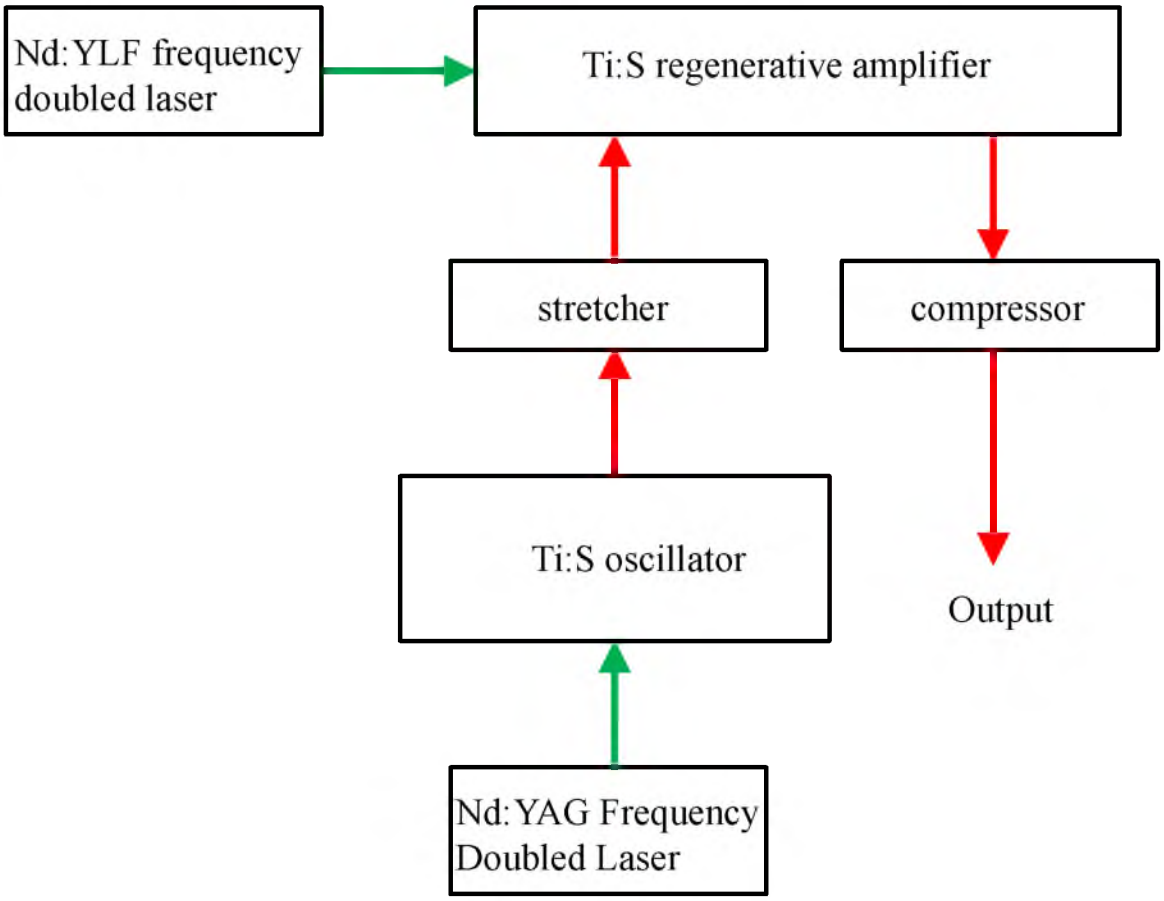

Figure 2.1: Schematic diagram of Ti:Sapphire regenerative amplifier laser system.

The oscillator can run either in cw mode or in passive mode-locked pulse mode. The mode locking is achieved by fine adjustment of one of the prisms in the cavity. The output stability of this oscillator is crucial to the stable performance of the amplifier. Usually, the fluctuations in the output power of the oscillator are < 1%. The output power of the oscillator is monitored by a fast-scan auto-correlator that measures the pulse duration of the pulse train. The output beam of the oscillator is fed into the regenerative amplifier cavity. The Ti:sapphire regenerative amplifier provides high-power pulses with ultrashort pulse duration.

The Ti:sapphire regenerative amplifier, which is home-made, was built based on the configuration provided by Positive Light Inc. [2.2]. It is pumped by a Coherent Evolution15 with ~ 200 ns Q-switched Nd:YLF laser at 527 nm at a repetition rate of 1 kHz. The Ti:sapphire regenerative amplifier is used to amplify single pulses from the Ti:sapphire. The output pulse energy can be five orders of magnitude higher compared to that of the oscillator, due to the lower repetition rate and amplification that happens in the system. The output pulse power of the amplifier is about 300 mW or 0.3 mJ/pulse with 1 kHz repetition rate at 800 nm wavelength and pulse duration of ~ 120 fs. There are three major parts of the Ti:Sapphire regenerative amplifier setup, which are: "stretcher," "amplifier," and "compressor." The "stretcher" role is to stretch the ultrashort pulses into long pulses by delaying different frequency components of the pulse with respect to each other using group velocity dispersion. This is done in order to avoid damaging the optical components inside the cavity due to the high peak power. The stretched pulses enter the "amplifier" cavity, where they are amplified by 5 – 6 orders of magnitude. The pulses are finally recompressed by the "compressor," which works in a way just the opposite to that of the "stretcher" part.

2.1.1.1 Characterization of the output signal

In order to have good ultrafast transient spectra measurements, the ultrashort pulses have to be monitored and optimized to have good quality. Since the pulse duration in the femtosecond time scale is beyond the time domain measured by standard electronic equipment, therefore, the output pulses from the amplifier are characterized by the autocorrelation technique [2.3, 2.4]. In this technique, the beam is split (50/50) into two

"arms" having almost equally optical paths that go through different delay stages, and subsequently, they meet again at the surface of a nonlinear BBO crystal. The second harmonic generation (SHG) signal is produced where the pulses overlap both spatially and temporally. Because the beam waist at the overlap area is much larger than the pulse width, then the intensity distribution of the second harmonic beam corresponds to the intensity of the autocorrelation function which is given by:

$$G(t) = \int I(t')I(t'-t)dt' \tag{2.1}$$

The signal from the crystal can be monitored by a UV detector. The pulses spectra from the amplifier are shown in Figure 2.2; the temporal domain is shown in Figure 2.2 (a), whereas spatial domain of the pulse is shown in Figure 2.2 (b).

2.1.2 White light supercontinuum generation

White light supercontinuum is an important femtosecond light source. It is used as a probe beam in the time-resolved pump-probe spectroscopy. Focusing the high-power pulses from the amplifier onto a transparent substance generates white light supercontinuum. The output pulses show substantial spectral broadening. White light supercontinuum generation has been observed in many different materials, including solids, liquids, and gases. There are several optical nonlinear processes responsible for white light supercontinuum generation such as self-phase-modulation, four-wave-mixing, Raman scattering, self-focusing, etc. However, in case of femtosecond pulses, self-phase

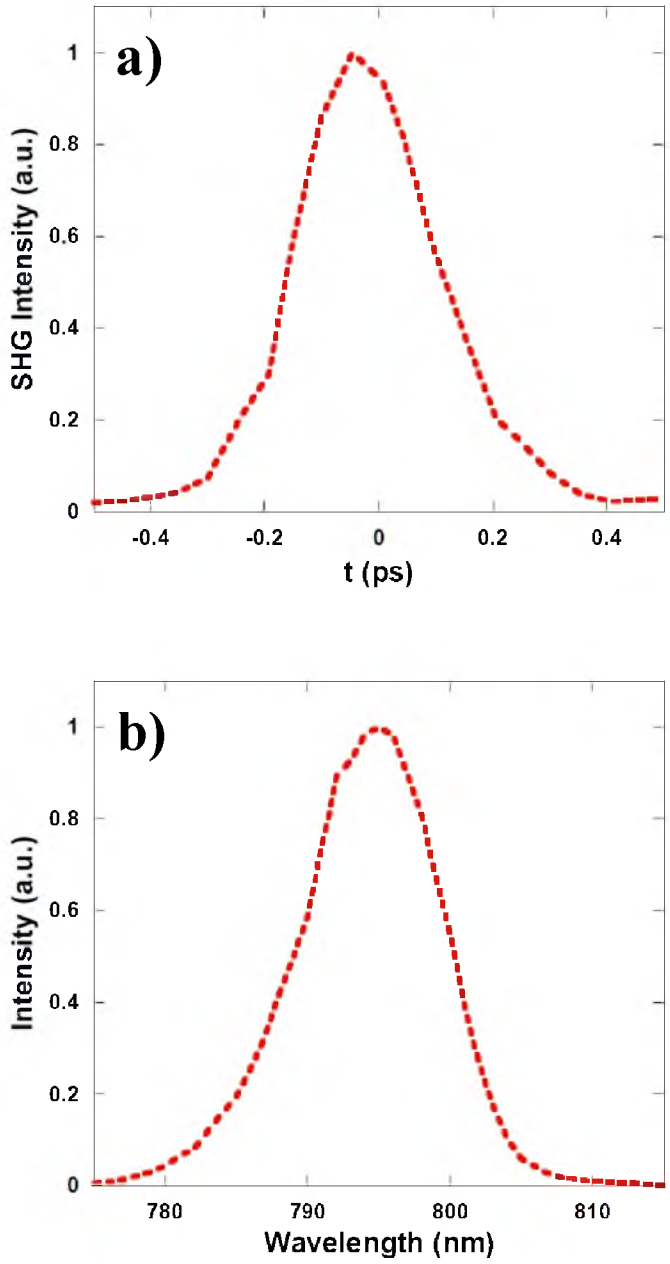

Figure 2.2: Characterization of fundamental pulses at 800nm; (a) temporal profile measured by autocorrelation, and (b) spectral profile.

modulation due to the nonlinear refractive index of the transparent medium is the dominant mechanism [2.5].

In our laboratory, white light supercontinuum is created by focusing a small portion of the pulsed light beam (< 10 mW) of the fundamental 800 nm light beam from the amplifier onto a 1 mm thick sapphire plate. This yields an output pulse train of a broad spectrum from 450 nm to 1000 nm, but the spectrum is not uniform, as shown in Figure 2.3. A notch filter was used after the sapphire plate to remove the residual 800 nm fundamental laser from the white light supercontinuum probe pulses. If we do not do that, then the high intensity of the fundamental beam would saturate the monitoring photodiode, and in addition, it can also damage the polymer film sample. Generating a stable white light supercontinuum out of the 800 nm amplified laser pulses train is very important; it depends on many factors such as the stability of the incident pulse, the intensity of the pulse, the pulse width, the bulk material, etc. In order to achieve a good stable white light supercontinuum, the following conditions have to be met: minimum intensity fluctuations, maximum compression (this leads to the shortest possible pulses within the given system), and minimum intensity of the fundamental 800 nm beam. This intensity can be controlled by neutral density filters and/or aperture (or pinhole), which makes the fundamental beam circular by blocking the unwanted peripheral beam. After the aperture, the light beam is focused onto the transparent sapphire plate using an appropriate lens, and the generated white light supercontinuum is collimated by another lens.

The white light supercontinuum contains chirp pulses due to group velocity dispersion present at different frequency parts of their spectrum. Because of this chirp,

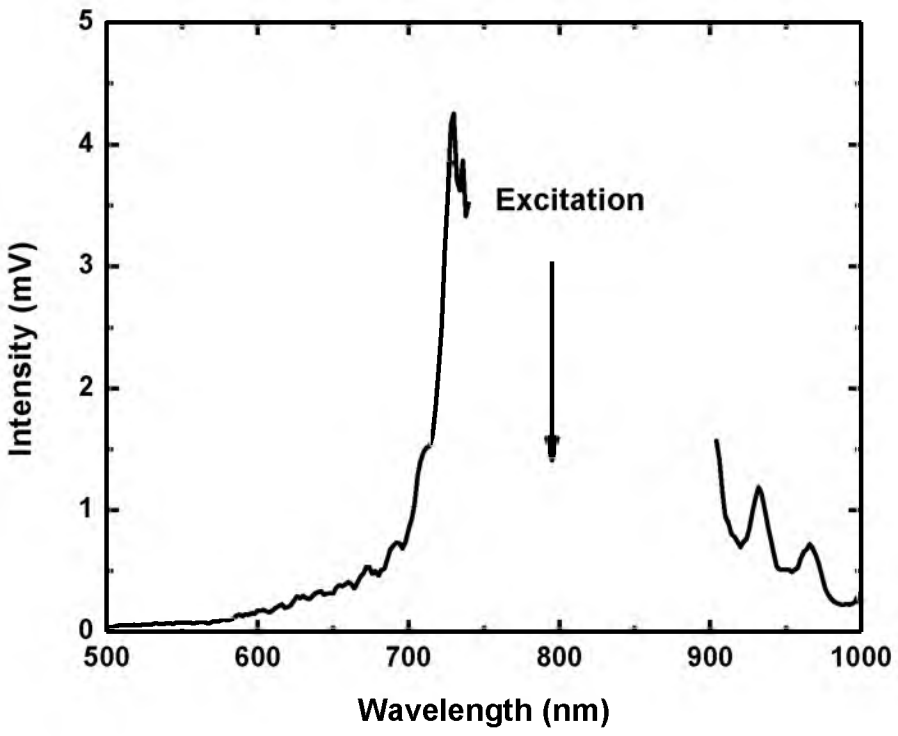

Figure 2.3: Characterization of white light continuum (WLC) source; Spectrum of WLC generated by 800 nm fundamental laser.

the redder part of the supercontinuum spectrum is delayed compared to the bluer part. This has to be taken into account when measuring the transmission spectrum at a fixed time delay in the pump-probe transient PM experiments. The way to correct for the chirp is by two-photon-absorption (TPA) measurements which give the "zero-time" position at each wavelength of the pulse spectrum. The "zero-time" positions are plotted as a function of the wavelengths in Figure 2.4. There is a time difference of about 2 ps between the blue (450 nm) and the near IR (780 nm) that is very large compared to the pulse duration of ~ 120 fs. The "zero-time" positions were fitted with a second-order

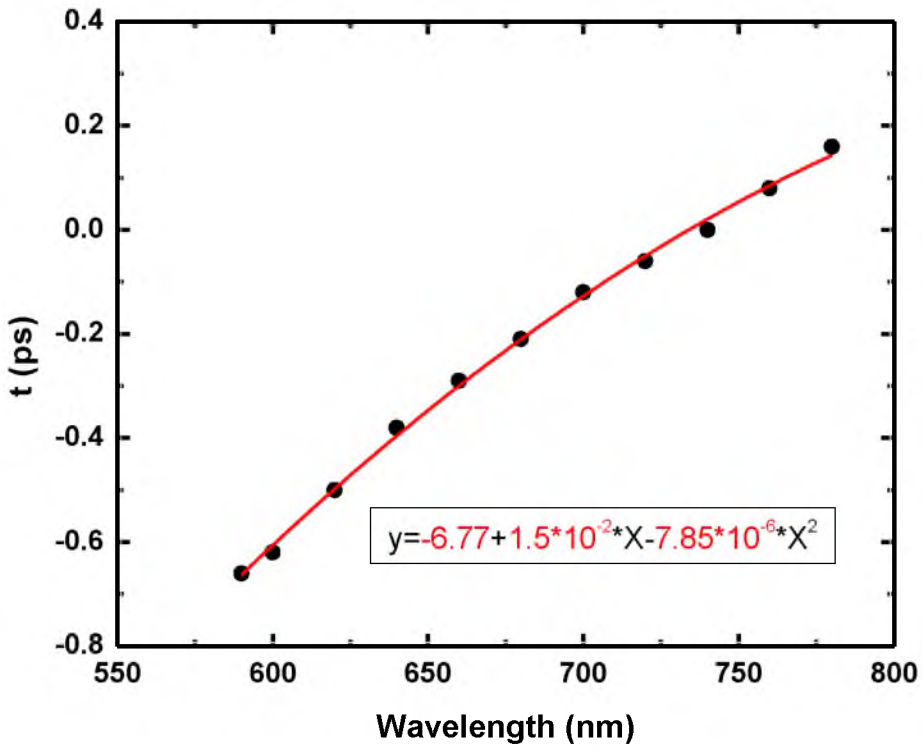

Figure 2.4: The "zero-time" positions (black dots) are plotted as a function of the wavelengths with a fitting of a second-order polynomial function (red curve). The insert shows the fitted function.

polynomial function [Figure 2.4, insert]. This calibration was used while performing the pump-probe measurements.

2.1.3 Low-energy high repetition-rate system

In addition to the high-energy low repetition-rate ultrafast laser system, a low-energy high repetition-rate ultrafast system is used. This system is based on an optical parametric oscillator (OPO) (OPAL, Spectra-Physics), which covers the midinfrared range, 0.1 – 1.1 eV. A 10 Watt, 532 nm CW solid-state laser (Millennia Xs, Spectra-

Physics) pumps a 100 fs Ti:Sapphire pulsed laser with a repetition rate of 80 MHz (Tsunami, Spectra-Physics), which in turn pumps the OPO system.

2.2 Ultrafast transient spectroscopy

Transient photoinduced absorption (PA(t)) is the time-dependent change in the material absorption when it is illuminated (or subjected to the pump pulses). An absorbed optical pump pulse with high intensity populates the excited states with neutral and charged excitations.

When a material is illuminated, the light can be reflected, absorbed, or transmitted. The relation between the intensities of the incident (I_0), transmitted (It), reflected (I_r), and absorbed (I_a) lights is given by:

$$I_o = I_r + I_t + I_a \tag{2.2}$$

where $I_r = RI_0$ and $I_t = TI_0$

Absorbance (A) is the loss of the transmitted light intensity (T) in the material and is given by:

$$A = -\ln T = -\ln \frac{I_t}{I_0} \tag{2.3}$$

The optical absorption coefficient, α is defined by the density of optical absorbers N, times the optical cross-section, σ of those absorbers that depends on the wavelength:

$$\alpha(\lambda) = N(\lambda)\sigma(\lambda) \tag{2.4}$$

The Lambert-Beer law: $$I_t = I_0(1-R)e^{-\alpha d} \tag{2.5}$$

where d is the optical thickness of the sample.

From Equations 2.2 to 2.5, the absorbance can be derived:

$$A = \alpha d - \ln(1-R) \tag{2.6}$$

and

$$\begin{aligned} I_a &= I_0 - I_r - I_t \\ &= I_0(1-R)(1-e^{-\alpha d}) \\ &= \begin{cases} 0 & \alpha d \approx 0 \\ I_0(1-R)\alpha d & \alpha d \ll 1 \end{cases} \end{aligned} \tag{2.7}$$

If the reflection is neglectible, then:

$$A = \alpha d \tag{2.8}$$

$$I = e^{-\alpha d} \tag{2.9}$$

The energy per pulse is given by:

$$\varepsilon_{pulse} = \int_0^{\tau} P(t)dt = N\hbar\omega \tag{2.10}$$

τ is the pulse duration, P(t) is the instantaneous power, and N is the number of photons per pulse.

The average power (which can be measured directly with a power meter) is:

$$\bar{P} = \frac{1}{\tau}\int_0^{\tau} P(0)\,dt = \varepsilon_{pulse} = r\varepsilon_{pulse} \tag{2.11}$$

where r is the repetition rate and equal to $1/\tau$.

From Equations 2.10 and 2.11, we can get the number of photons per pulse; N.

$$N = \frac{\bar{P}}{r\hbar\omega} \tag{2.12}$$

The difference in the transmission is ΔT; the transmission with light and without light is:

$$\Delta T = T_L - T_D \tag{2.13}$$

The relation between transmission in the dark and the transmission in the light is given by:

$$T_L = T_D e^{-\Delta\alpha d} \tag{2.14}$$

$$\frac{T_D + \Delta T}{T_D} = 1 + \frac{\Delta T}{T_D} \tag{2.15}$$

$$\Delta\alpha = -\ln\left(1 + \frac{\Delta T}{T_D}\right) \tag{2.16}$$

For $\Delta T << T_D$ where the difference in the transmission is much smaller than the transmission, we can get that:

$$\Delta\alpha d \approx - \Delta T/T_D \tag{2.17}$$

2.2.1 Kinetic analysis

According to Equation 2.17, the measured transient photomodulation (PM) signal, which is the fractional change in transmission T, is proportional to the change in the absorption, which can be written from Equation 2.4 assuming that the cross-section σ does not change with time, then

$$\Delta\alpha = \Delta N(t)\sigma \tag{2.18}$$

From (2.17) and (2.18), we can get:

$$-\frac{\Delta T}{T}(t) = N(t)\sigma d = \Delta\alpha(t) d \tag{2.19}$$

Here, σ is the optical cross-section of the material, and d is the optical depth. In other words, the measured PA signal is proportional to the photoexcitation density N(t). To understand the mechanism of the photoexcitation dynamics in the time – domain, we use a simple model that distinguishes between the generation and recombination processes. These processes are described by a single rate equation for the photoexcitation density:

$$\frac{dN(t)}{dt} = G(t) - R(N), \tag{2.20}$$

where N is the photoexcitation density at a given time, G is the photoexcitation generation rate, and R is the recombination rate. Under steady state (SS) conditions (e.g., in CW measurements), Equation 2.20 becomes

$$\frac{dN}{dt} = G - R = 0 \tag{2.21}$$

meaning G = R. The generation rate is

$$G = \frac{\alpha\eta}{\hbar\omega V} I_L = aI_L \tag{2.22}$$

where I_L is the intensity of the excitation laser that is absorbed by the material, α is the absorption coefficient at the pump photon energy, η is the quantum efficiency, $\hbar\omega$ is the

excitation photon energy, V is the volume of excitation, and a is a coefficient. G(t) is proportional to g, the generation rate, that is proportional to the pump intensity I_L.

2.2.1.1 Monomolecular recombination kinetics

Transient PA dynamics depend on various generation and recombination conditions. The simplest recombination is the monomolecular recombination (MR) where only a single excited species is involved in the process. Subsequently the recombination rate depends directly on the excited state population, N, and $R = N/\tau$. The generation rate, G is assumed to be zero in transient spectroscopy after the excitation pulse ends. In this case, Equation 2.20 becomes

$$\frac{dN(t)}{dt} = -\frac{N}{\tau} \tag{2.23}$$

And the solution for this equation is

$$N(t) = N(0)e^{-t/\tau} \tag{2.24}$$

In steady state, Equation 2.20 becomes

$$\frac{dN}{dt}\Big|_{SS} = G - \frac{N_{SS}}{\tau} = 0 \tag{2.25}$$

And the solution

$$N_{SS} = G\tau = aI_L\tau \tag{2.26}$$

This means that the photoinduced absorption signal, ΔT/T, depends linearly on the excitation laser intensity, if MR occurs in CW spectroscopy.

2.2.1.2 Bimolecular recombination kinetics

Bimolecular recombination (BR) kinetics takes place when two excited-state quasi-particles are involved in the recombination process. In this case, R is proportional to the population squared, or $R = bN^2$, where b is the proportionality coefficient and Equation 2.20 becomes

$$\frac{dN}{dt} = -bN^2 \tag{2.27}$$

And the solution to this equation is:

$$N(t) = \frac{N(0)}{1 + tbN(0)} \tag{2.28}$$

In the steady state, Equation 2.20 becomes

$$\frac{dN}{dt}\Big|_{SS} = G - bN_{SS}^2 \tag{2.29}$$

So $N_{SS} = (G/b)^{1/2} = (aI_L/b)^{1/2}$. BR kinetics in CW spectroscopy shows PA sublinear power law dependence with excitation laser intensity, having an exponent of 0.5.

2.2.2 Transient pump-probe photomodulation

The transient pump-probe PM or transmission experiments give information about the spectral evolution of the photoexcitations in the ps time interval. In the time - resolved pump-probe measurements, two laser beams are used. One is a high-intensity pulsed beam, the pump, which generates the photoexcitations in the sample. The other pulsed beam is a time-delayed beam, the probe, which measures the resulting change in the transmission as a function of the pump-probe delay time.

The experimental setup for the pump-probe PM transient measurement is shown in Figure 2.5. The output from the Ti:Sapphire amplifier is a pulse train at 1 kHz repetition rate with pulse duration of ~ 120 fs at 800 nm. The beam is divided by a 90/10 beam splitter into two beams, pump and probe. The delayed pump beam (90% of the power) is frequency doubled to 400 nm (~ 3.1 eV) using a nonlinear BBO crystal. The probe beam (10% remaining power) is used to create broadband 1.24 – 2.76 eV white light supercontinuum in a 1 mm thick sapphire plate. The broad probe spectral range 0.12 – 2.76 eV used in our measurement is obtained by combining the low-intensity and high-intensity laser systems, as shown in Figure 2.6.

The time resolution in our pump-probe setup over the entire spectral probe range is ~ 120 fs, as confirmed by autocorrelation. The delay of the pump beam with respect to the probe beam is determined by a computer controlled translation stage with an accuracy of 0.1 μm (or 0.03 fs). Spectral resolution of about 4 nm is achieved by a CM110

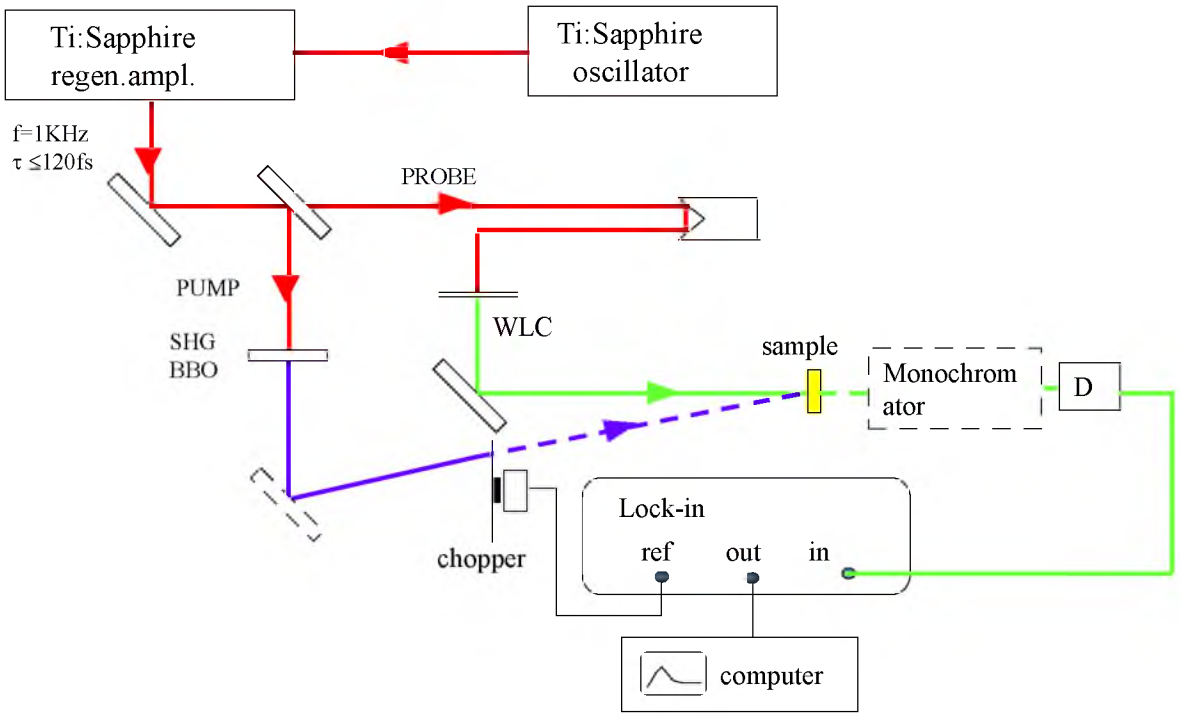

Figure 2.5: The experimental setup for the pump-probe measurement.

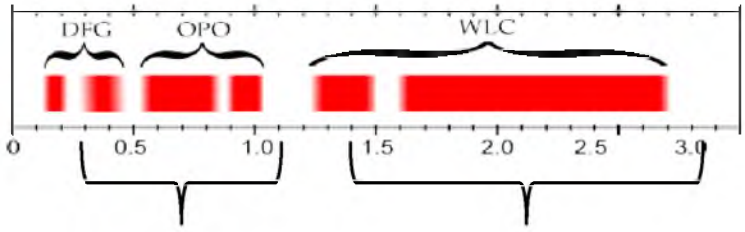

DFG : Difference Frequency Generation; OPO : Optical Parametric Oscillator;
WLC: White Light Continuum

Figure 2.6: The broad probe spectral range which is obtained by combining the low-intensity and high-intensity laser systems.

Digikröm monochromator with 0.6 mm entrance and exit slits. The pump beam is modulated by a mechanical chopper at exactly half the frequency of a Ti:Sapphire laser system, and the change in transmission of probe, ΔT, is monitored by Si photodiode with a phase-sensitive technique provided by a lock-in amplifier.

Using the transient PM technique, a sensitivity of $\Delta T/T \approx 10^{-5}$ is easily achieved across all the probe range. Transient pump-probe PM measurements are done in two modes: (i) as a function of time at a fixed wavelength; and (ii) as a function of wavelength at a fixed time delay. In the latter measurement scheme, the chirp of white light supercontinuum has to be taken into account, as explained above. While measuring the transient PM spectrum, a chirp-free program is used that moves the translation stage according to the calibration of the white light supercontinuum at different wavelengths.

All measurements were done using thin films of pi-conjugated polymers in a dynamic vacuum of ~ 150 μtorr to prevent degradation and oxidation in the presence of intense laser light. The pump intensity in the pump-probe measurement was usually kept lower than 0.3 mJ/cm^2, which ensures linearity of the response. The probe intensity should be much lower than the pump intensity to avoid any excitation of the sample (like TPA). The pump and probe beams were focused onto the sample film in order to overlap with each other concentrically, with the diameter of 500 μm for the pump and 100 μm for the probe. The alignment was done by a dedicated telescopic microscope.

Two types of signals can be distinguished according to their increase or decrease in intensity; i) $\Delta\alpha < 0$, which is dubbed photoinduced absorption (PA) due to creation of new states, ii) $\Delta\alpha > 0$, could be either photoinduced bleaching (PB) when an optical transition (from the ground state) is depleted by another process, or, alternatively

stimulated emission (SE) due to the stimulated radiation of the material by the presence of a photon from the probe beam. The SE spectrum can be easily separated from the PB spectrum because it resembles the PL spectrum of the sample.

Figure 2.7 shows a typical pump-probe PM measurement in a MEHPPV film and auto-correlation of the system setup that determines the "zero-time" position and the temporal response of the measurement system. The pump excitation energy is 3.1 eV and the probe is set at 1.34 eV.

2.3 Two-photon absorption

Most of the π – conjugated polymers belong to the C_{2h} symmetry group, which has four irreducible representations, namely A and B with even (g) and odd (u) parity; these are: A_g, B_u, B_g, and A_u. The ground state is an Ag character (^1A_g). One-photon absorption can occur only between states of opposite parity: A_g and B_u states. On the other hand, two-photon absorption (TPA) occurs between the same parity states: the ground state (^1A_g) and higher A_g states.

The two-photon absorption coefficient is proportional to the imaginary part of the third-order nonlinear susceptibility $\chi^{(3)}$ [2.6, 2.7]. It is a very weak transition compared with the linear absorption. In order to measure TPA, a very high peak power of ultrashort pulses is required. There are several methods to measure TPA such as Z-scan [2.8], two-photon luminescence, etc. Here we have used another method that is based on ultrafast nondegenerate pump-probe spectroscopy.

The two-photon absorption spectrum is measured with the help of pump-probe correlation technique at time delay t = 0. In the TPA experiment, the pump beam is set at

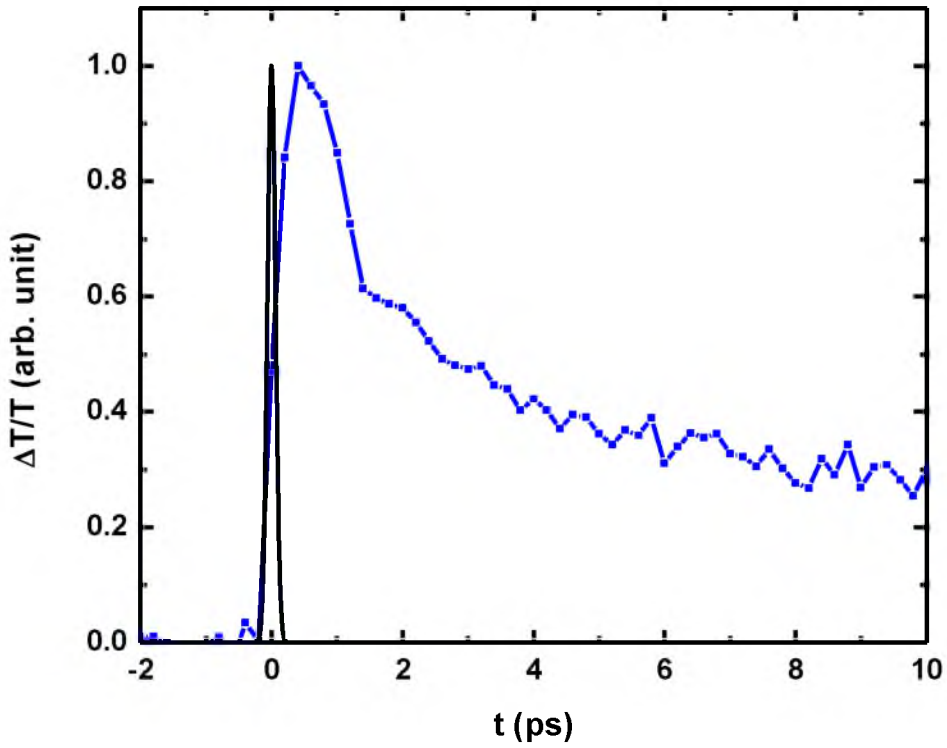

Figure 2.7: A typical pump-probe measurement of the excited state in MEHPPV film and auto-correlation of the system setup that determines the zero position and the temporal response of the measurement.

1.55 eV, which is below the polymer optical gap. Basically, this is the main difference between the TPA measurement and normal pump-probe measurement in which the pump is set at 3.1 eV, namely above the optical gap.

Since the excitation photon energy is below the optical gap, there is no real intermediate electronic level involved in the TPA, and thus the transition is instantaneous. The probe is the WLC beam having a spectral range from 1.2 – 2.9 eV. The temporal and special overlap between the pump and the probe beams leads to a photoinduced absorption (PA) signal at t = 0. This PA signal has a temporal profile similar to the pump-

probe cross-correlation function, which is interpreted here as two-photon absorption, namely one photon from the pump beam and the other photon from the probe beam.

Figure 2.8 shows TPA time-resolved response at 3.45 eV in D – DOO-PPV thick film using a 1.55 eV pump and 1.9 eV probe beams, together with the cross-correlation function of the system. The PA signal reaches maximum at t = 0 when the pump and probe pulses overlap in space and time, and follows the cross-correlation response of the pump and probe pulses.

2.4 Other optical measurement systems and techniques

2.4.1 Absorption and emission

As discussed earlier, the first excited singlet state is $1B_u$. Because of the differences in the configuration coordinate between the electronic ground state and the electronic excited state, phonons can be excited together with the electronic excitation. Therefore, the probability for transition depends on the overlap of the phonon ground state wave function and the final electronic excited state wave function. As a result, the absorption of the optical gap has a broad spectrum line, as can be seen from Figure 1.5.

The experimental measured quantity is the optical density (OD), which is defined as, $OD = -\log_{10}\frac{T}{T_0}$ where T is the transmission of the sample and T_0 is the transmission of the optical system without the sample. The absorption coefficient α is defined by the expression $T = T_0 e^{-\propto d}$, where d is the sample thickness.

Photoluminescence (PL) spectroscopy is an important tool for studying the optical and electronic properties of solid state material. PL in conjugated polymers is associated with the transition from $1B_u$ to the ground state $1A_g$.

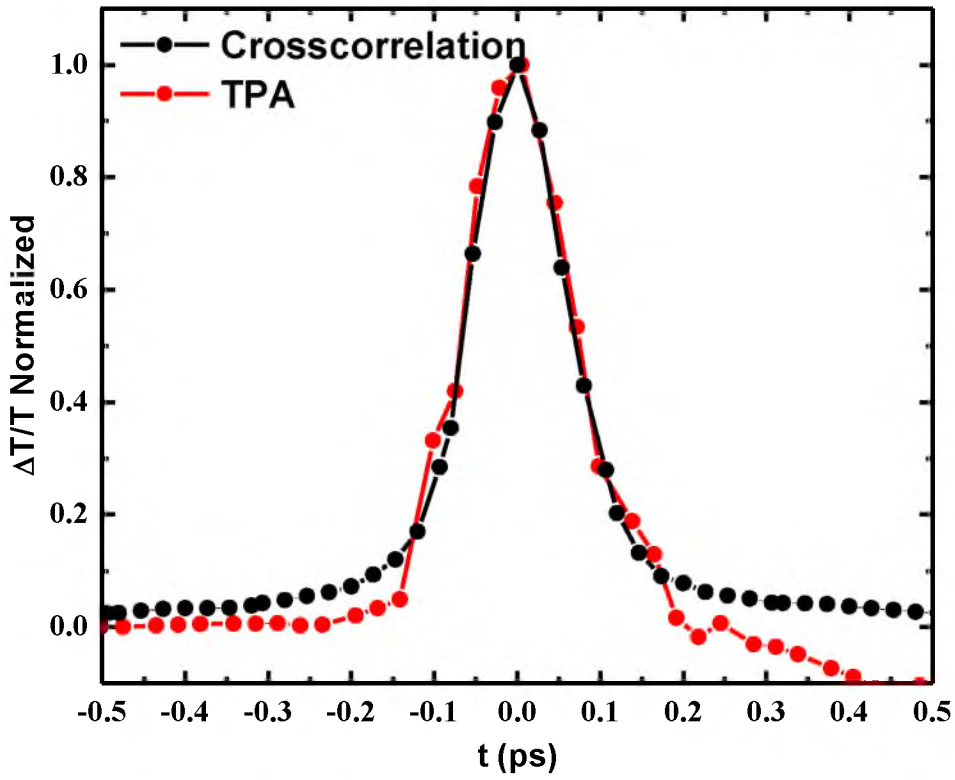

Figure 2.8: TPA time-resolved response at 3.45 eV in D – DOO-PPV thick film (red) using 1.55 eV pump and 1.9 eV probe beams; the cross-correlation function of the system shows in black.

PL in conjugated polymers gives important information about the nature of the excited states. The PL spectrum of conjugated polymers usually shows an emission peak, which is red shifted relative to the absorption threshold ("stokes shift") and vibronic structure due to simultaneous phonon emission. The PL line is in general narrower than the absorption spectrum, since the PL occurs due to transitions from the lowest excited state while the absorption scans all available states, which broaden the spectrum due to inhomogeneity.

Optical absorption spectra in the ultraviolet, visible, or near-infrared was measured with a CARY17 spectrophotometer. The system which we used to measure PL is shown in Figure 2.9.

2.4.2 Photoinduced absorption

Photoinduced absorption (PA) spectroscopy is a useful tool for investigating the nature of the photoexcited species in π-conjugated polymers [2.9 – 2.11]. The photoinduced absorption technique is used to study the new optical transitions due to the new energy levels that formed in the excited state.

In the PA experiments, the change in the transmission of the sample, ΔT, is measured. By photoexciting the sample with a modulated laser beam (pump beam), the excited states are populated with neutral and charged excitations. The result is additional absorption bands in the band gap. The detecting "probe beam" from an incandescent light source creates the new optical transitions.

The PA method is detecting the sample absorption difference between the excited state and the ground state. This is done by measuring the transmission of the sample with (T_L) and without (T_D) the "probe beam."

The relation between the induced absorption coefficient α and the difference in transmission ΔT is given by:

$$\Delta T = T_L - T_D \tag{2.30}$$

$$T_L = T_D e^{-\alpha_L} \tag{2.31}$$

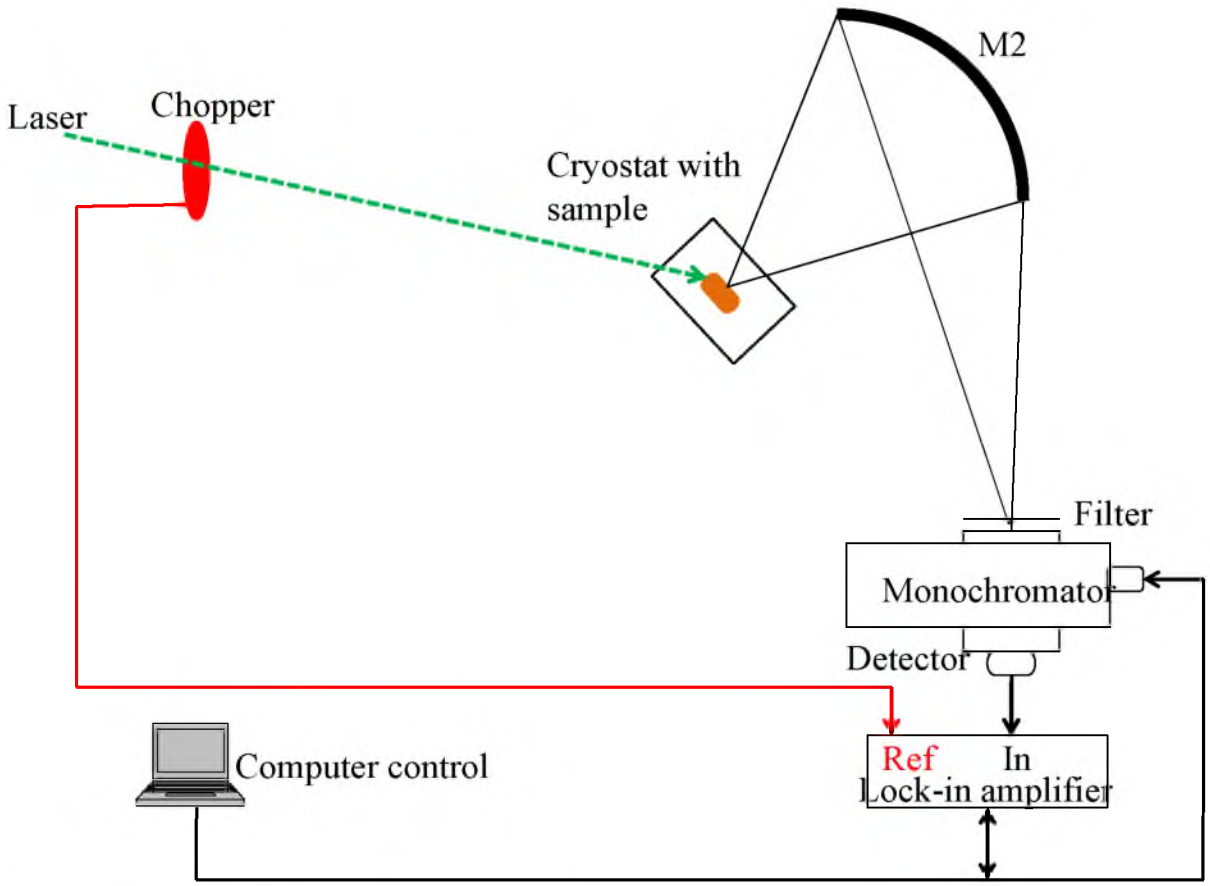

Figure 2.9: Experimental setup for the PL measurement.

From Equations 2.30 and 2.31 we get:

$$e^{-\alpha_L} = 1 + \frac{\Delta T}{T_D} \Rightarrow -\ln\left(1 + \frac{\Delta T}{T_D}\right) = \alpha_L \qquad (2.32)$$

If $\Delta T_D << T_D$, then:

$$\alpha_L \approx -\frac{\Delta T}{T_D} \tag{2.33}$$

Two types of signals can be detected: the photoinduced absorption ($+\alpha_L$), which is associated with the absorption due to creation of new states, and the photoinduced bleaching ($-\alpha_L$), caused by, e.g., interband transition.

2.4.2.1 Modulation spectroscopy

PA dependencies on the modulation frequency, ω, and excitation intensity, I_L, have been used to determine the photoexcitations lifetime, τ , and the recombination mechanism. Modulation spectroscopy is a useful tool for measuring and understanding the kinetics of the photoexcitations [2.12].

In the PA experiment, the modulated signal follows the density of the excited states N(t).

The pump beam is being modulated by a chopper at frequency ω and the PA is being measured by using a Lock-in amplifier [Figure 2.10]. The Lock-in amplifier analyzes the first harmonics of the photoinduced signal, which is defined as:

$G(t) = g(1 + \cos(\omega t))$, where g denotes the generation rate and is proportional to the pump intensity, I_L. Two signals are detected by the lock-in;

The in-phase signal: $$N(t)_Q = \int_{period} N(t)\sin(\omega t)dt \tag{3.34}$$

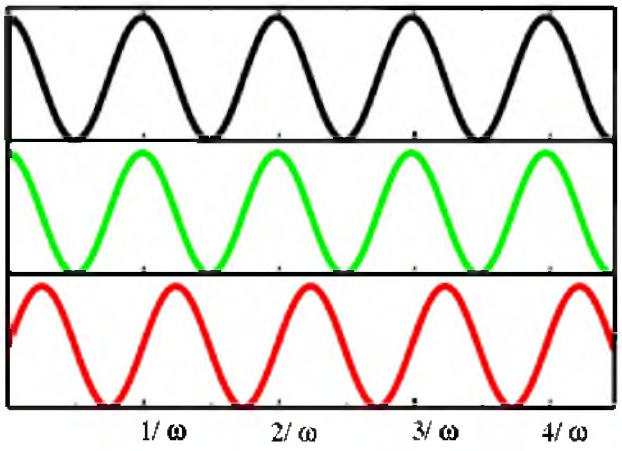

Figure 2.10: The illustration of the model laser intensity (the top panel), in-phase (center panel) and Quadrature (bottom panel) lock-in amplifier response as a function of time.

And the out-of-phase (Quadrature):

$$N(t)_Q = \int_{period} N(t)\sin(\omega t)dt \tag{3.35}$$

The setup for PA measurements is shown in Figure 2.11 for the pump beam; we used the Ar^+ laser at 488 nm (2.41 eV). The pump was chopped by either a mechanical chopped or acousto-optical modulator. For the probe beam, we used a Tungsten lamp or glowbar lamp. The light transmitted by the sample was filtered and dispersed by an Acton monochromator and detected by a series of semiconductors detectors: Si, InSb, and MCT, using the phase-sensitive Lock-in detection technique. The sample was placed on a cold finger in a cryostat with a temperature controller and kept in vacuum using a rotation pump.

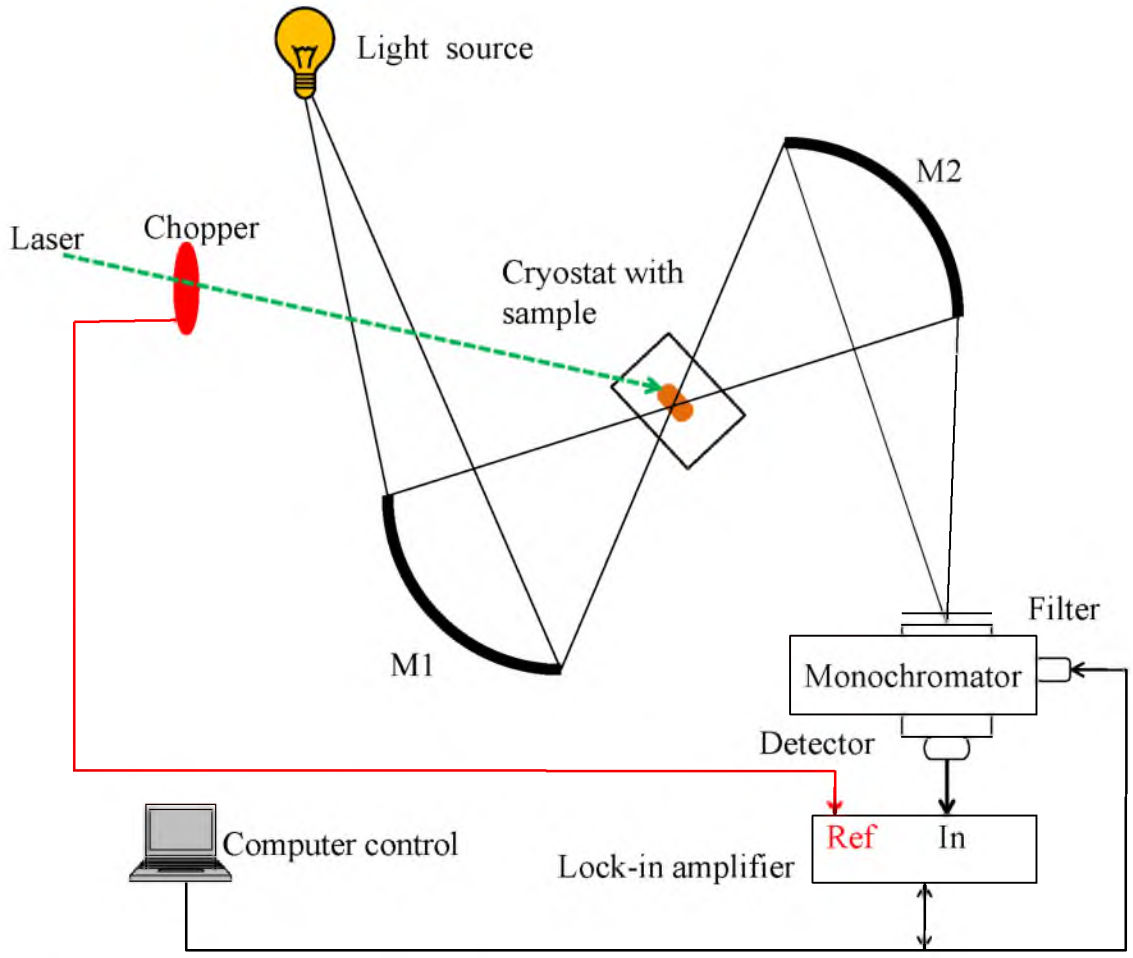

Figure 2.11: Experimental setup for the PIA measurement.

2.4.3 Electroabsorption

In electroabsorption (EA) technique, we measure changes in the absorption spectrum of the sample with the application of an electric field. Electroabsorption has been a very important method to characterize the optical properties of π-conjugated polymers. It can give information for both even and odd parity of states. The signal is proportional to the imaginary part of the third-order nonlinear susceptibility; $\chi^{(3)}$;

$$\frac{\Delta T}{T} \cong -\Delta\alpha d = \frac{4\pi\omega}{nc} Im[\chi^3(-\omega;\omega,0,0)F^2 d] \tag{3.36}$$

In the above relation, F is the applied electric field, and, d and n are film thickness and refractive index, respectively [2.13]. The modulation frequency of the electric field, f ~ 300 Hz, so that f << ω, and thus can be considered zero with respect to the optical frequency of electromagnetic wave used in the measurement.

The EA measurement needs a special device structure that is in the form of an interdigitated electrode array, as shown in Figure 2.12 (a). The substrate is a 1 inch diameter, 2 mm thick sapphire plate. A 50 nm titanium film is sputtered on the substrate, which is followed by 150 nm of gold deposition. Finally, the interdigitated electrodes are patterned using photolithography with a 40 micron gap between the adjacent electrodes. Our sample is deposited on such a substrate with optical density of 0.2 – 0.4 to allow substantial EA signal even for photon energy above the polymer optical gap. The experimental setup for the EA measurement is shown in Figure 2.12 (b). A xenon or tungsten light source is used as a probe. The probe light is dispersed via the grating monochromator, guided through the sample and focused onto a UV enhanced Si detector by a couple of curved mirrors. The sample is kept in a cold finger cryostat under dynamic vacuum of 150 torr. A high AC voltage of 200 – 300V is applied to the electrodes using a function generator and step-up transformer. A very high electric field of ~ 105 V/cm may easily be achieved between the electrodes, because of their small spacing of ~ 40 μm gap. The electric field is modulated at 520 Hz, and the EA signal (namely changes in the probe transmission) is detected at 2f, using a phase-sensitive Lock-in amplifier technique.

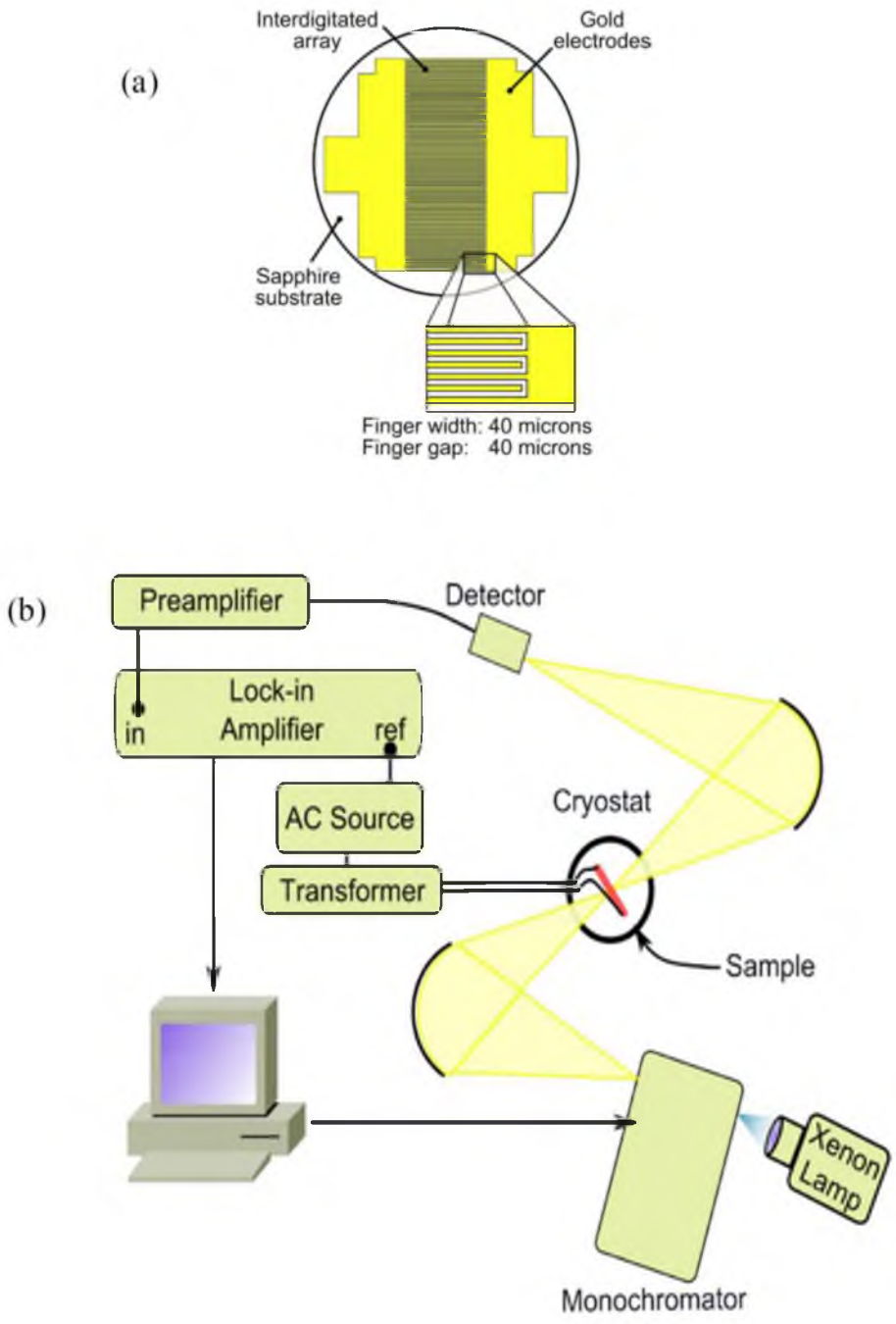

Figure 2.12: Experimental setup for electroabsorption (EA) spectroscopy (a) sapphire substrate with interpenetrating finger electrodes used in EA measurement (b) experimental arrangements.

2.5 Reference

[2.1] M. Asaki, Optics letters, 18, 977, (1993).

[2.2] Positive light incorporation, Los Gatos, California.

[2.3] AC-1 Interferometric Autocorrelator Kit, Clark Instrumentation.

[2.4] J.-C. Diels, and W. Rudolph, Ultrashort Laser Pulse Phenomena: Fundamentals, Techniques and Applications on a Femtosecond Time Scale, 2nd ed., San Diego: Academic Press, (2006).

[2.5] The Supercontinuum Laser Source, New-York: Springer-Verlag, (1989).

[2.6] R. W. Boyd, Nonlinear Optics, San Diego: Academic Press, (1992).

[2.7] Y. R. Shen, The Principles of Nonlinear Optics, New York: J. Wiley, (1984).

[2.8] S. V. Frolov, Z. Bao, M. Wohlgenannt, and Z. V. Vardeny, PRB 65, 205209 (2001).

[2.9] J. Orenstein, Z. Vardeny, G.L. Baker, G. Eagle, S. Etemad, PRB 30, 786 (1984).

[2.10] Z. Vardeny, E. Ehrenfreund, O.Brafman, M. Nowak, H. Schaffer, A.J. Heeger, F. Wudl, PRL. 56, 671 (1986).

[2.11] O. Epshtein, G. Nakhmanovich, Y. Eichen, E. Ehrenfreund, Synth. Metals, 119, 585 (2001).

[2.12] Y. Eichen, G. Nakhmanovich, V. Gorelik, O. Epshtein, J.M. Poplawski, E. Ehrenfreund, J. Am. Chem. Soc. 120, 10463 (1998).

[2.13] S. A. Jeglinski, "Electroabsorption spectroscopy of conjugated polymers and carbon fullerenes and conjugated-polymer light-emitting-devices," Thesis (Ph D), Department of Physics, University of Utah, Salt Lake City, 1996.

CHAPTER 3

PHOTOEXCITATIONS OF NONLUMINESCENT CONJUGATED POLYMERS

3.1 Introduction

The π-conjugated polymers may be divided into two principal classes: namely, polymers with degenerate ground states, and polymers with nondegenerate ground states (NDGS) [3.1]. Usually, NDGS polymers have high photoluminescence (PL) quantum efficiency (PLQE), and therefore may be attractive for organic light-emitting diodes [3.2]. The ultrafast photoexcitation dynamics of luminescent NDGS polymers are well understood. Upon photon absorption into a high-energy singlet exciton, there is an ultrafast thermalization to the lowest exciton, namely, the 1^1B_u exciton, followed by PL or recombination via nonradiative channels [3.3].

In rare occasions, NDGS polymers have weak PL emission; poly(thienylene-vinylene) (PTV) is such a polymer [3.4]. It has a lower optical gap (1.7 – 1.8 eV) compared to other NDGS polymers and thus could, in principle, provide a better match with the solar spectrum for organic solar cell applications [3.5, 3.6]. However, so far PTV-based solar cells have shown low power-conversion efficiency, indicating poor charge photogeneration [3.7].

It has been proposed that low intrinsic PLQE in π – conjugated polymers results from the order of the electronic excited states [3.1, 3.8]. In this model, if the lowest even-parity (dark) exciton, or 2^1A_g, lies below the 1^1B_u exciton, (i.e., $E[2^1A_g] < E[1^1B_u]$), it may circumvent the PL emission. In this case, according to Kasha's rule, the photogenerated $1B_u$ exciton undergoes ultrafast internal conversion to the dark 2^1A_g exciton, therefore eliminating further PL emission. This process, however, has not been yet identified in PTV, and thus, the origin of its weak PL emission is still unclear; it might be extrinsic or intrinsic in origin.

Moreover, in NDGS polymers with weak intrinsic PL, there is a substantial amount of energy that is released very fast via the $1^1B_u \rightarrow 2^1A_g$ internal conversion process and subsequent 2^1A_g decay to the ground state; this leads to thermal stress that is accompanied by transient strain [3.9, 3.10]. Thus, the fascinating phenomena that nonluminescent NDGS polymers may undergo upon photon absorption make them unique materials for ultrafast and nonlinear optical investigations. However, the photophysics of only a few NDGS polymers have been studied in detail, where cis-(CH)x [3.11] and polydiacetylene [3.12] are the exceptions.

In this chapter, we studied the ultrafast photophysics of derivatives of the π – conjugated polymer Poly(thienylenevinylene) (PTV). One is ordered PTV polymer with controlled 100% region-regularity (RR –), which is a nonluminescent polymer. Another one is regiorandom PTV (RRa – PTV), where the polymer side groups are randomly oriented. The last one is imide – PTV, which, by changing the side groups, becomes a luminescent material. The last part of this chapter presents transient strain spectroscopy

(TSS), which is caused by thermal stress. This phenomena occurs in nonluminescent NDGS polymers.

The work was done in collaboration with Prof. X. Jiang's group from the Department of Physics, University of South Florida and the materials were synthesized by Prof. C. Zhang's group from the Department of Chemistry and Biochemistry, South Dakota State University.

3.2 Materials

Figure 3.1 shows the chemical structures of the RR – PTV, RRa – PTV (a), and the imide – PTV (b). All materials were synthesized by Prof. C. Zhang's group from the Department of Chemistry and Biochemistry, South Dakota State University. The detailed synthesis process of the ordered PTV polymer with 100% region-regularity (RR –) and region-random PTV (RRa – PTV), can be found in the paper published by Prof. C. Zhang [3.13]. The imide – PTV contains two subunits. In one, the imide group is attached to a thiophene ring, which is neighbored by two thiophene rings. In addition, the nitrogen atom of the imide group is attached to two 2-methylundecane ($C_{12}H_{25}$). Basically, this subunit has a three thiophene ring complex with imide and alkyl group extensions. This subunit is bounded by another subunit that contains a vinylene group. All materials were originally dissolved in dichlorobenzene (~ 10 mg/ml) and the solutions were drop cast into films on sapphire and CaF2 substrates to allow broadband optical spectroscopies.

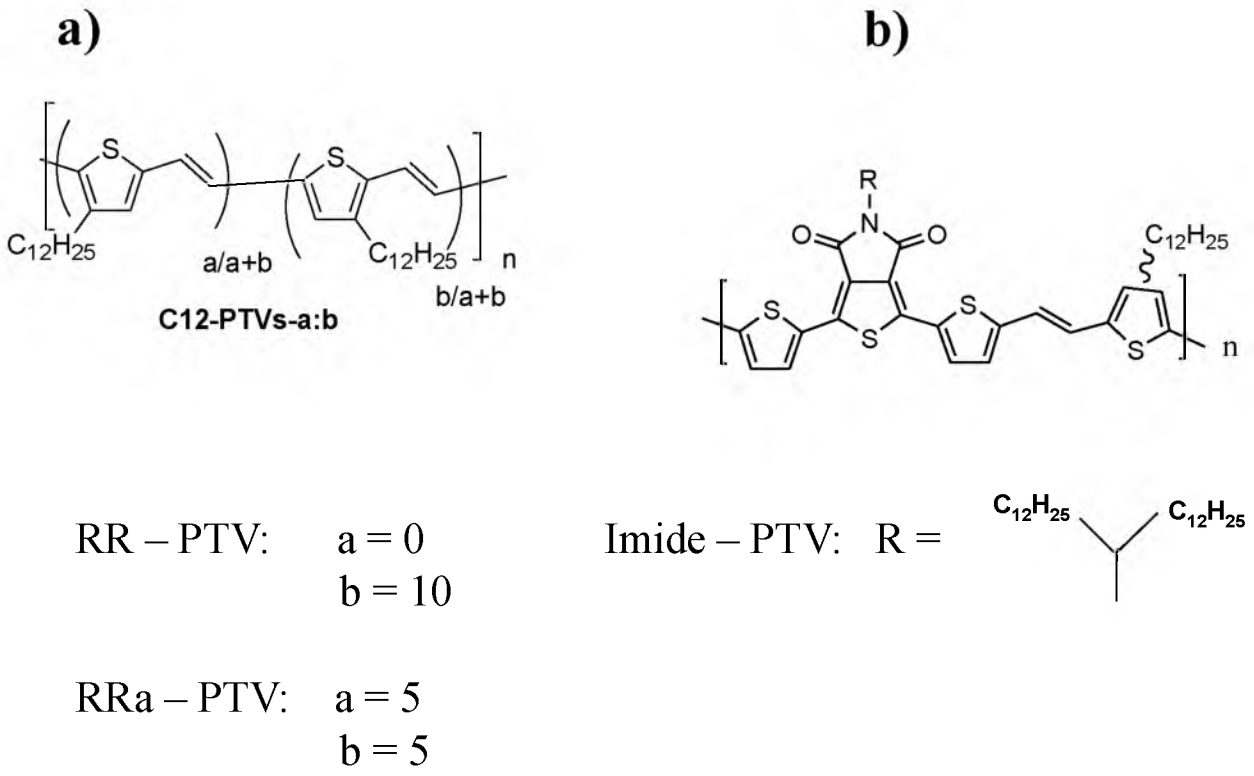

Figure 3.1: The chemical structures of (a) RR – PTV with 100% region-regularity (with a = 0 and b = 10) and regiorandom PTV (with a = 5 and b = 5) where the polymer side groups are randomly oriented. (b) imide – PTV.

3.3 Linear absorption and photoluminescence spectra

Figure 3.2 shows a normalized O.D. and PL spectra of the RR – PTV and imide – PTV. The linear absorption, in terms of optical density (O.D.), was measured using a Cary17 spectrometer. The photoluminescence (PL) was measured using the PL setup [Chapter 2]. For the absorption spectrum, a broad featureless band is observed at ≈ 2 eV for the RR – PTV and 2.23 eV for the imide – PTV. Vibronic levels are apparent in the spectra of both polymers, but they are less pronounced in the RR – PTV polymer. This is

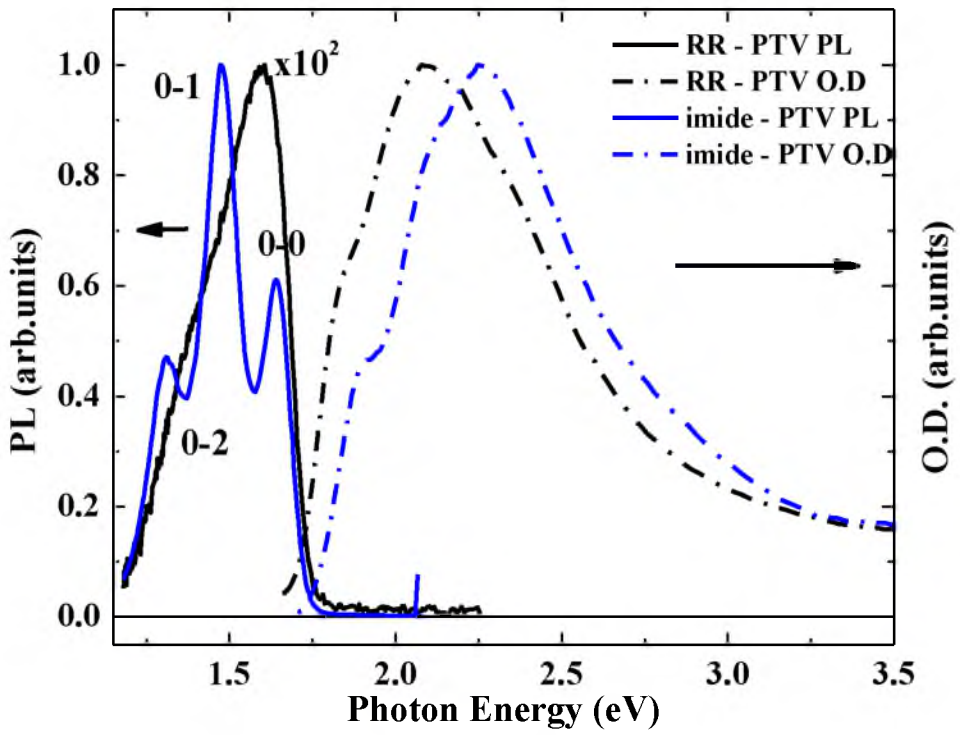

Figure 3.2: The normalized absorption and PL spectra of RR – PTV and imide – PTV.

due to the inhomogeneous broadening as a result of the distribution of conjugated lengths within the sample [3.14].

The emission spectra of both polymers are quite different. The imide PTV shows a nice PL band with two clear phonon sideband replicas while the RR – PTV has a broad PL band without obvious phonon sidebands. The broad PL band of the RR – PTV can be from inhomogeneity in the film morphology since the solubility of this polymer is not good [3.13, 3.15]. The relative strength of the PL intensity of the imide – PTV is two orders of magnitude stronger than the RR – PTV. This is correlated with the PLQE measurements: 10^{-4} for the RR – PTV and 10^{-2} (1%) for the imide – PTV.

The PL spectra are Stokes-shifted from the absorption edges. This observation has been explained by relocation of the photogenerated excitons to the lower energy (longer conjugation length) chain segments before radiative decay has time to occur [3.14]. Therefore, the observed PL emission mainly originates from the lowest energy segments leading to the observed Stokes shift and reduced inhomogeneous broadening when compared to the absorption spectra.

3.4 Photoexictations of RR – PTV film

Figure 3.3 shows the transient PM spectra in RR-PTV film at various times *t* following pulse excitation. Figure 3.3 (a) shows the transient PM spectra of the visible and NIR range. Figure 3.3 (b) shows the transient PM spectra of the MIR range. The PM spectrum is dominated by two PA bands, namely, PA_1 at ≈ 0.95 eV and PA_2 at ≈ 1.6 eV (both bands with broad tails toward lower energies) and PB above 1.81 eV. In addition, the transient PM spectra present a derivative-like feature having zero crossing (isosbestic point) at ≈ 1.81 eV (further details on the PB signal in section 3.3.2).

The transient PM spectra below 1 eV, i.e., PA_1 decays very fast and almost disappears at 2 ps. On the other end, PA_2 decays longer and the transient PM spectrum still exists at 50 ps. The PB decay is longer and still presents a transient PM spectra at 1 ns.

Figure 3.4 shows the decay dynamic of the transient PM spectra at different probe frequencies. The decay at probe frequencies 1 and 1.34 eV have the same dynamics and it is faster than the decay at probe frequencies 1.61 and 1.72 eV. It is clear that the two PA bands do not share the same dynamics. Whereas PA_1 decays almost completely within ≈

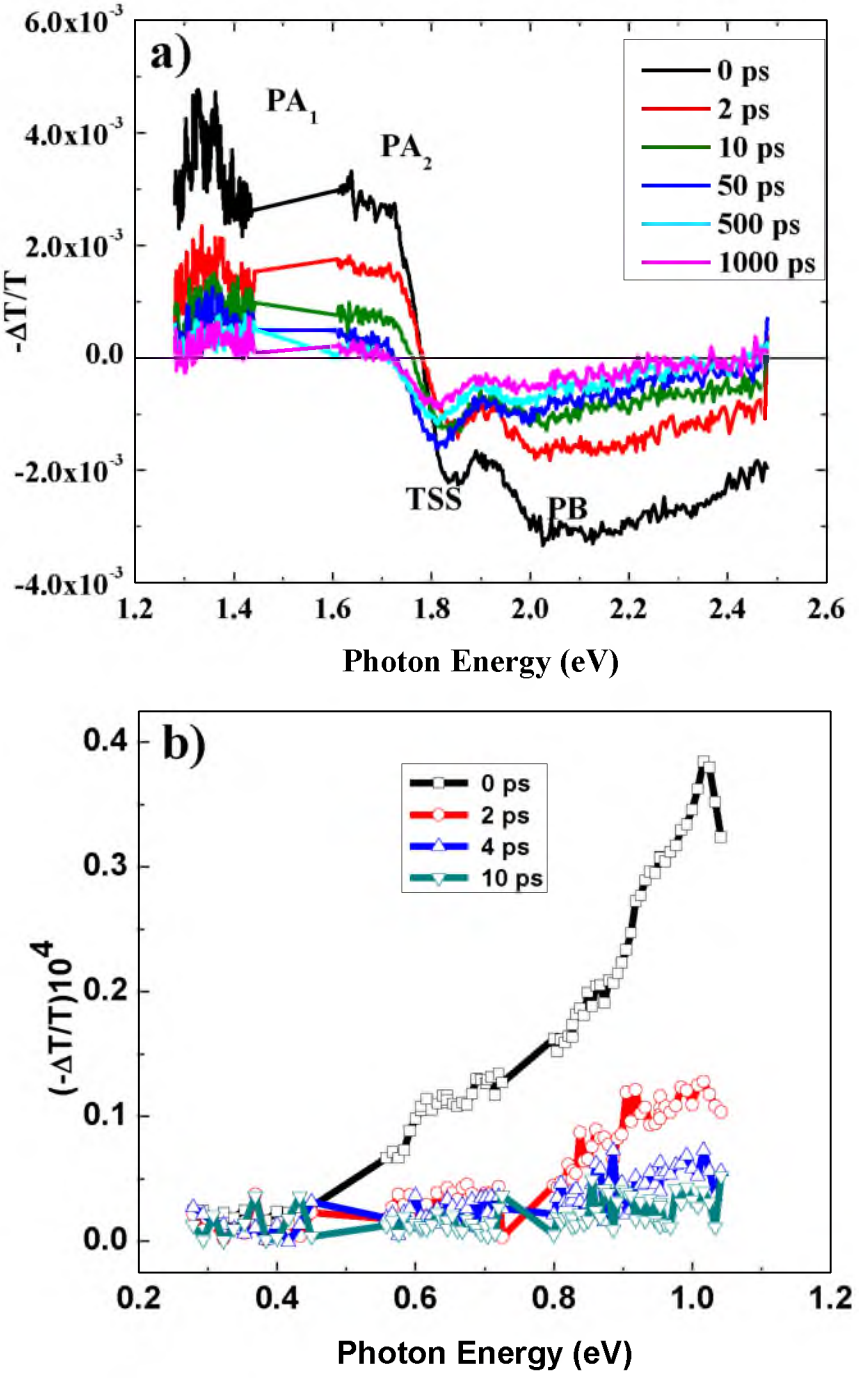

Figure 3.3: The transient PM spectrum of RR – PTV at different probe delay; (a) The range 2.6 to 1.2 eV at high pump intensity. (b) The range 1 to 0.3 eV at low pump intensity.

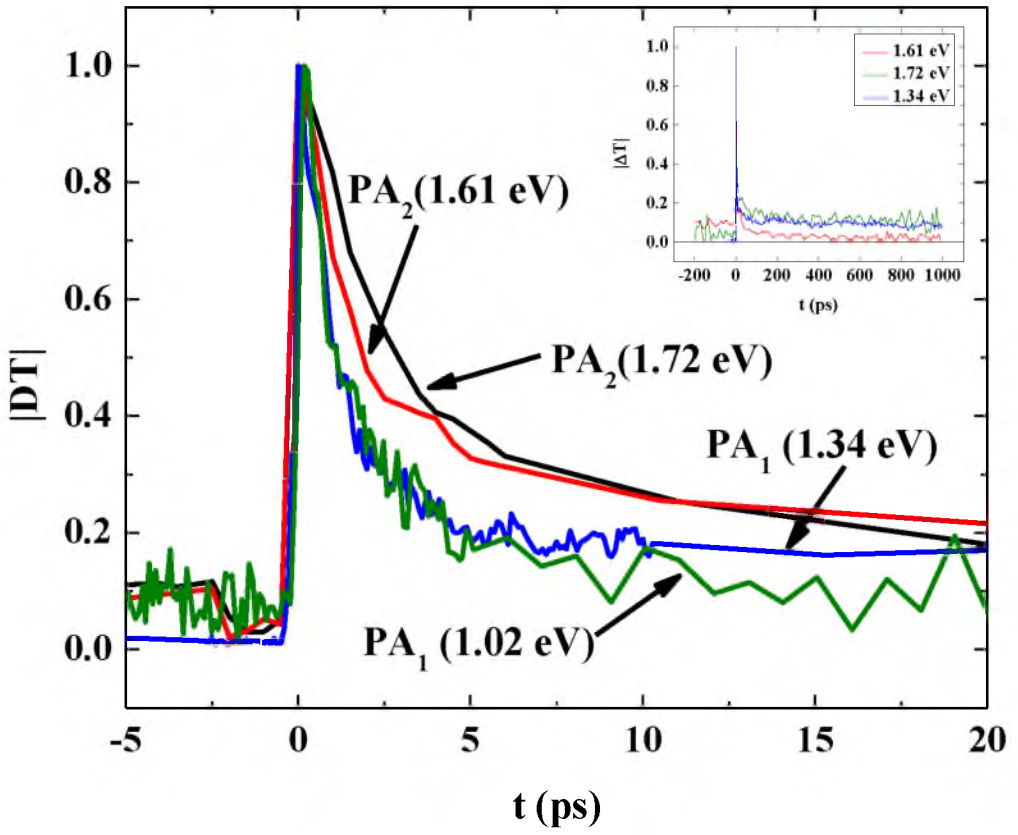

Figure 3.4: The decay dynamic of the transient PM spectra at different probe frequencies.

0.5 ps, the decay of PA_2 is longer (≈ 2.3 ps) into a plateau that indicates the formation of a relatively stable photoexcitation. We therefore conclude that the two PA bands do not belong to the same photoexcitation.

When using the transient PM spectroscopy, the pump-probe cross-correlation function is necessary to extract information on the sample response function for times, *t*, below or with the same time resolution of the experimental apparatus. This is needed in PTV to determine whether or not the photoexcitation is instantaneously generated.

This is done using deconvolution, in order to find the output signal;

If the $$Output\ signal(t) = \int f(t)g(t-\tau)d\tau \quad (3.1)$$

Or $$Output\ (\omega) = F\omega)G(\omega) \quad (3.2)$$

Then $$F(\omega) = Output\ signal(\omega)/G(\omega) \quad (3.3)$$

where the output signal (t) is the convolution between the decay kinetic, f(t), and the system response (which is the cross-correlation between the pump and the probe), g(t). Output signal (ω), F(ω), G(ω) are the fourier transform functions of the output signal (t), f(t), g(t), respectively.

Figure 3.5 shows the PA formation and decay evolution near t = 0 of PA_2 (a) and PA_1 (b), where the data (black solid circles) are fitted with an exponential formation and decay processes (blue line), taking into account the pump-probe cross-correlation function (red line) [3.16]. The insert of Figure 3.5 (a) shows the system cross-correlation and the fitted Gaussian function, which was measured with the low rep. rate laser system using up-conversion of the pump and probe photons in a the BBO crystal [more on cross-correlation in Chapter 2]. PA_2 was fitted with the equation:

$$f(t) = A(1 - e^{-t/\tau_{rise}})e^{-t/\tau_{decay}} \quad (3.4)$$

where A is a constant, τ_{rise} is the time of the formation of PA_2; τ_{decay} is the time that takes PA_2 to decay. From the fitting, we find: τ_{rise} = 0.24 ps and τ_{decay} = 1.1 ps. PA_1 was fitted with the equation:

$$f(t) = Ae^{-t/\tau_{decay}} \quad (3.5)$$

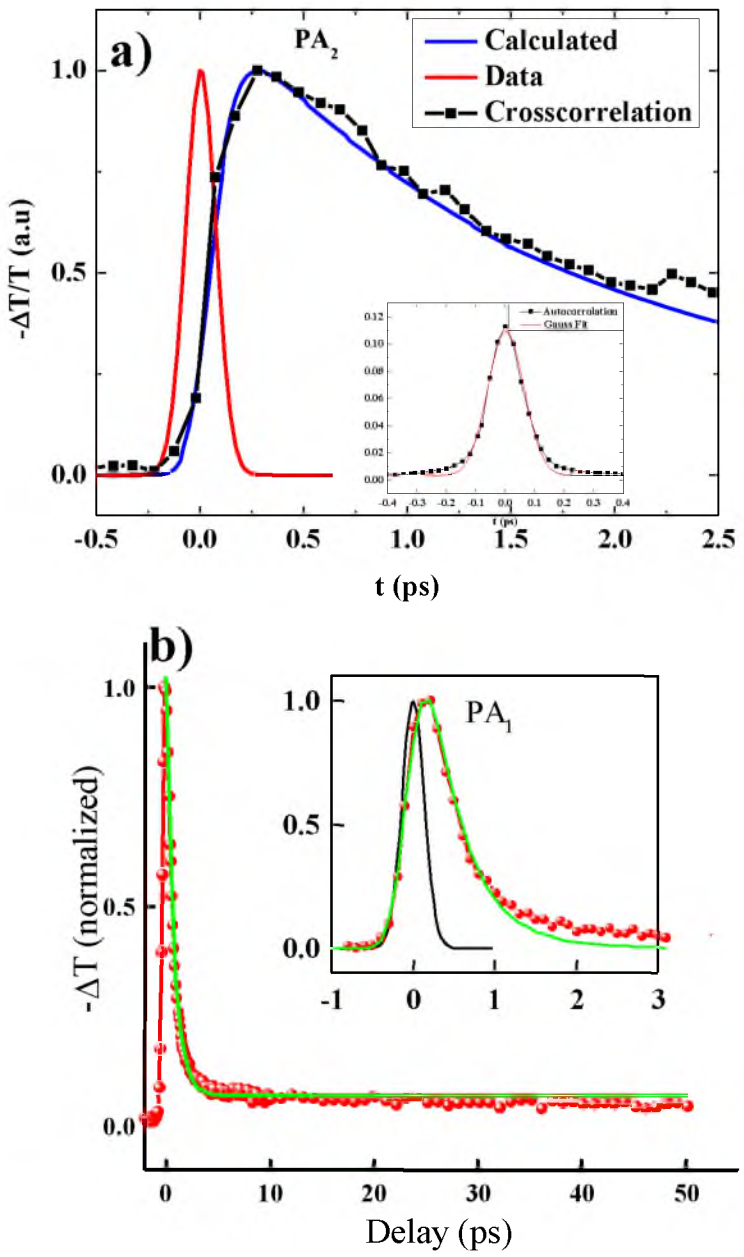

Figure 3.5: The PA formation and decay evolution near t = 0 of PA_2 (a) and PA_1 (b). The data (black solid circles) are fitted with an exponential formation and decay processes (blue line), taking into account the pump-probe cross-correlation function (red line). The insert shows the system cross-correlation and the fitted Gaussian function.

where A is a constant, τ is the time that takes PA_1 to decay. From the fitting we find τ = 0.7 ps.

When looking at the PA responses near t = 0, it is clear that PA_1 is instantaneously generated, whereas PA_2 is formed at a delay of ≈ 200 fs. We therefore conclude that PA_2 does not originate from the primary photoexcitation in RR – PTV but rather is formed at the expense of PA_1, and during its decay process.

Figure 3.6 shows the transient PM spectra in RRa – PTV film at various times t following pulse excitation at the range 1.8 to 1.2 eV. The PM spectrum is dominated by two PA bands, at ≈ 1.7 (PA_2) and 1.3 eV (PA_1) and PB above 1.75 eV. In addition, the PB and PA_2 bands spectrally overlap since, at longer time delay (≈ 50 ps), the PA band at 1.7 eV become PB.

Both PA_1 and PA_2 decay very fast. It is clear that the two PA bands do not share the same dynamics. Whereas PA_1 disappeared almost completely within ~ 2 ps, the decay of PA_2 is longer (~ 10 ps) into a plateau that indicates the formation of a relatively stable photoexcitation. The RRa – PTV PA spectrum behaves similar to the RR – PTV PA.

Figure 3.7 shows the EA [Figure 3.7 (a)] and TPA [Figure 3.7 (b)] spectra of RR – PTV. Similar to EA spectra in many other polymers, the EA spectra show a derivative – like band around E(1^1B_u) that is due to the Stark shift of the 1^1B_u exciton, followed by several vibration replicas and an absorption band at m^1A_g due to electric field d-induced symmetry breaking [3.17].

However, the m^1A_g band in RR – PTV is very small, indicating that the aggregates in the film also affect the EA spectrum [3.13]. We assume that the 0 – 0

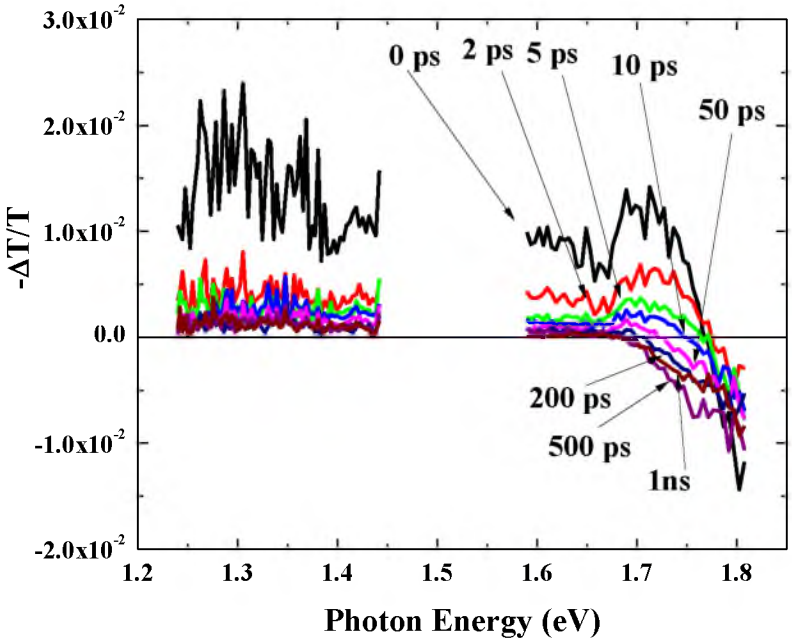

Figure 3.6: The transient PM spectrum of RRa – PTV at different probe delay at the range 2.6 to 1.2 eV at high pump intensity.

transition in the $1^1Bu \rightarrow m^1Ag$ band, which determines the EA band at m^1A_g, [3.8, and 3.17], is partially suppressed in aggregates, so that the vibronic replicas in the m^1A_g EA band are relatively more apparent. In any case, from the dominant features in the EA spectrum, we obtain the energy levels of two important essential states, [3.8] namely, $E(1^1B_u) \approx 1.75$ eV and $E(m^1A_g) \approx 2.35$ eV [at the onset of the EA m^1A_g band as seen at the inset of Figure 3.7 (a)].

The TPA illustrates the optical transitions between the ground state $1A_g$ and other states with A_g symmetry. These transitions become allowed when measuring two-photon absorption (TPA). From Figure 3.7 (b), we can obtain the energy level of k^1A_g, which is $E(k^1A_g) \approx 3.1$ eV.

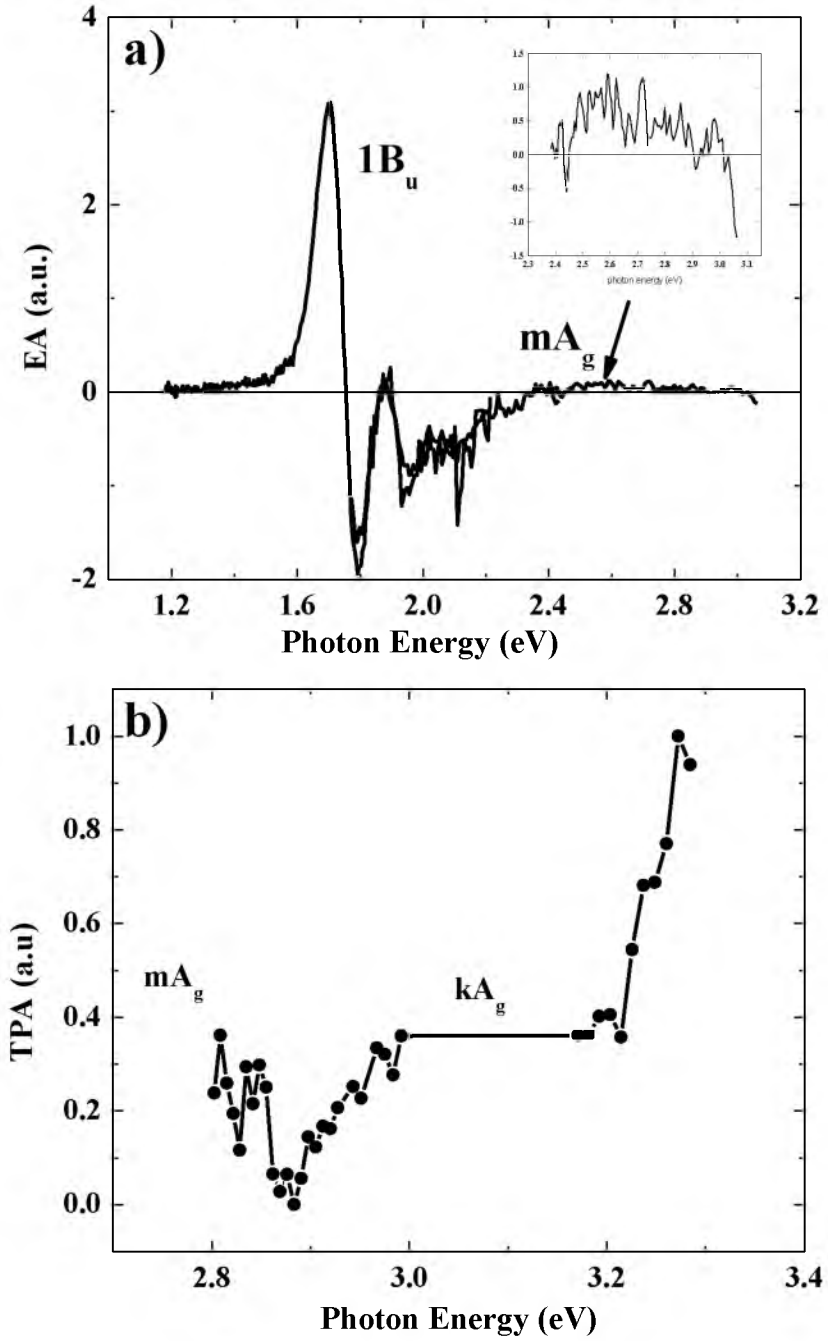

Figure 3.7: The RR – PTV states from; (a) The EA spectrum of RR-PTV. The spectral EA features related to 1^1B_u and m^1A_g are assigned. The inset is a blow-up of the EA spectrum from 2.4 to 3.0 eV that includes the m^1A_g state. (b) The TPA spectrum of RR – PTV. The k^1A_g and m^1A_g states are assigned.

This gives the energy difference between the states $\Delta E \approx 0.8$ eV between 1^1B_u and m^1A_g, and $\Delta E \approx 1.33$ eV between 1^1B_u and k^1A_g. These values are essential for understanding the PA band that originates from the photogenerated 1^1B_u excitons in the film [3.3].

3.4.1 Discussion

The band PA_1 is generic to many π-conjugated polymers, and it has been previously identified [3.3] as being due to optical transitions from the photogenerated 1^1B_u exciton into the m^1A_g exciton [3.8]. Therefore, we infer that PA_1 in RR – PTV is also due to the photogenerated 1^1B_u exciton. Its ultrafast decay kinetics, however, indicate that there is another state at lower energy ($<E[1^1B_u]$), into which the photogenerated 1^1B_u exciton decays; this should be the elusive dark exciton, 2^1A_g. As a check of this proposed scenario, we estimate the PLQE from the fast 1^1B_u decay and compare it to the PLQE η-value measured by an integrated sphere. For this estimate, we used the relation: $\eta = \tau / \tau_{rad}$, where τ is the exciton lifetime and τ_{rad} ($\approx$1 ns) [3.18] is the 1^1B_u radiative lifetime. Using a PA_1 lifetime of $\approx$ 0.5 ps, we thus estimate $\eta(PTV) \approx 3 \times 10^{-4}$, which is in good agreement with the measured η-value of $\approx 2 \times 10^{-4}$. Within this decay scenario, PA_2 is a transition from the 2^1A_g state. This optical transition, however, should be into an odd-parity exciton, namely, the n^1Bu exciton, which is also part of the polymer essential states [3.8]. The stabilization of PA_2 at later time ($t > 5$ ps) into a plateau indicates that some of the 2^1A_g excitons become trapped, similar to the classic polymer t-(CH)x [3.19]. As the consequence of the two transient PA bands, and the cw PL and the EA spectrum, we construct the essential-states structure and related optical

transitions in Figure 3.8. The RRa – PTV polymer shows a similar behavior to the RR – PTV. Therefore, we conclude that the lowest excited state is also 2^1A_g.

3.5 Photophysics studies of imide – PTV

3.5.1 CW photoinduced absorption (PA) and doping photoinduced absorption (DIA)

The CW photoinduced absorption (PA) measurement of the PTV derivatives films were performed using a pump-probe experiment at 80 K. The sample was photoexcited at 2.34 eV using an Argon laser beam as a pump, and photoinduced absorption was monitored by a tungsten probe beam in the spectral range from 0.3 to 1.8 eV. Figure 3.9 (a) shows the PA spectra of the RR – PTV and imide – PTV films.

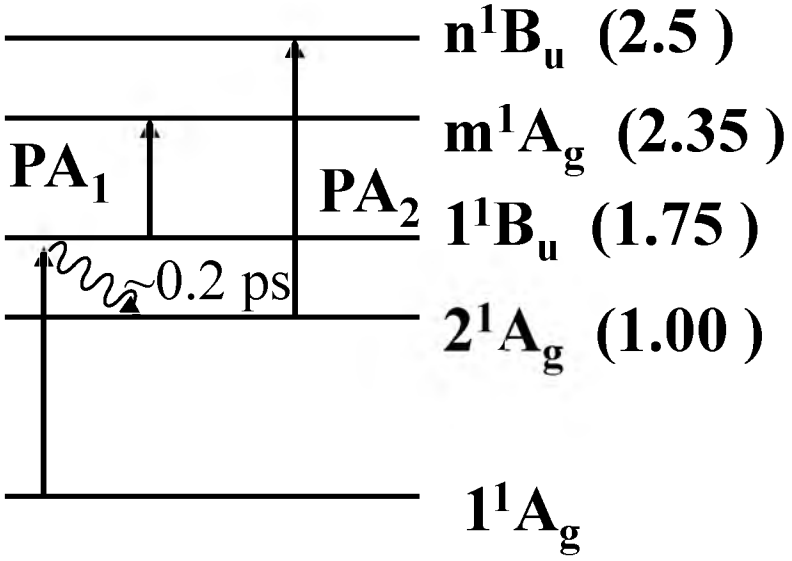

Figure 3.8: A diagram of the RR - PTV essential states and associated optical transitions.

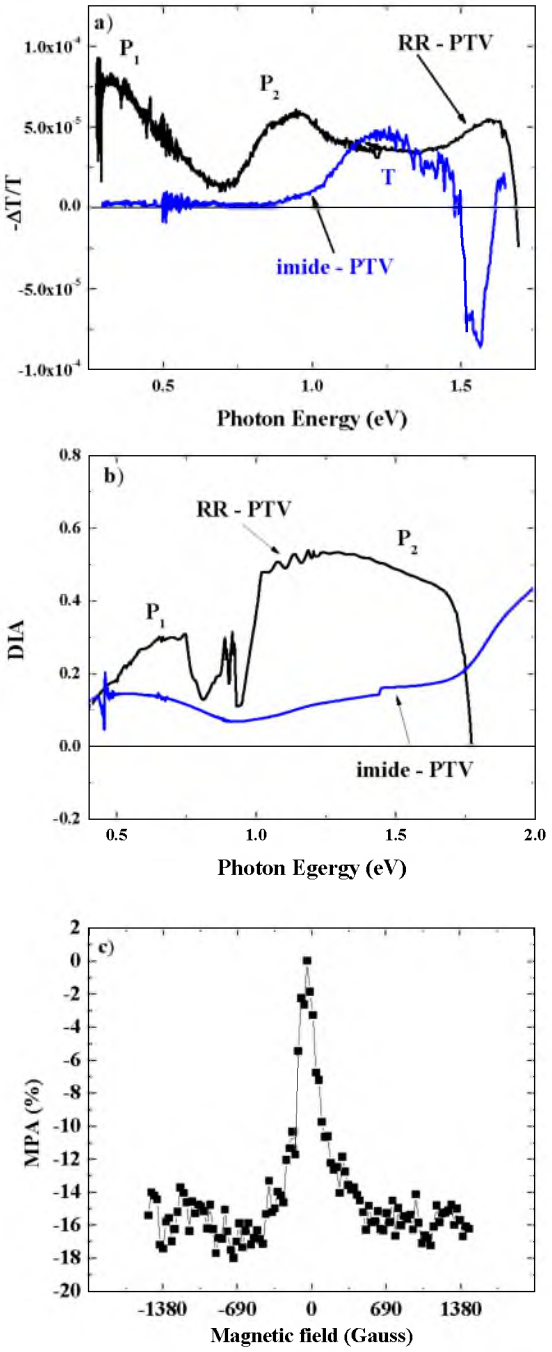

Figure 3.9: CW studies of imide – PTV polymer; (a) The PA spectra of the RR – PTV imide – PTV after exposure to Iodine. (b) The DIA spectra of the RR – PTV and imide – PTV after exposure to Iodine. (c) MPA (B) response of imide – PTV measured at 1.2 eV, showing a FWHM associated with zero-field splitting parameter $D/g\mu_B \approx$ 30 mT.

The PA spectrum of the RR – PTV shows a broad band with peaks at ≈ 1 and 0.4 eV. Compare to the PA spectrum of the imide – PTV, which shows a broad band with a peak at ≈ 1.2 eV. In order to identify the nature of these PA bands, doping-induced absorption was performed [Figure 3.9 (b)].

DIA is one of the most reliable techniques to identify the presence of long-lived photoexcitations in conjugated polymer films. By doping the film and measuring DIA, we can discover the charged photoexcitations in the conjugated polymer. Subsequently, by comparing the PA spectrum with the DIA spectrum, we can distinguish between the charge and neutral long-lived photoexcitations. In the DIA measurement, first, the transmission of the undoped sample, T_u, is measured. Next, the film is doped by exposure to a dopant vapor for 1 to 2 minutes. Subsequently, the transmission of the doped sample T_D is measured. In the end, the DIA spectrum, $\Delta T/T$, is obtained by taking the difference of transmission before and after doping, and then normalizing by transmission before doping the sample. For our measurements, we used Iodine, I_2, vapor as a dopant.

Polymers are one-dimensional chains, and in this model, the added charge carrier (from the dopant) to the polymer chain forms a spin ½ polaron with two localized states in the energy gap. Out of three possible transitions, only two of them are allowed and therefore, polarons have two optical transitions, namely P_1 and P_2.

In the DIA measurement of the RR – PTV, the DIA spectrum clearly shows two PA bands. Thus, we can conclude that charge long-lived photoexcitations are generated in the RR – PTV polymer, since the two PA bands that were discovered in the CW PA are P_1 and P_2.

On the other hand, the PA spectrum of the imide – PTV (were measured by Tek Basel and Evan Lafalce) does not show two clear PA bands. This led us to the conclusion that long-lived charge photoexcitations are not generated in the imide – PTV polymer, and the only long-live photoexcitations that are produced are triplet excitons.

Figure 3.9 (c) shows the magneto-photoinduced absorption (MPA) response [3.25] of imide – PTV film measured by Tek Basel at 1.2 eV. The principal TE zero-field splitting (ZFS) parameter, D, is $D/g\mu_B \approx 30$ mT. Even though it is smaller compared with other polymers (for example MEH – PPV with $D/g\mu_B \approx 63$ mT [3.25]), nevertheless it proves that the CW PA signal is due to triplet excitons.

Therefore, we conclude that the CW PA band is dominated by triplet excitons. The weak PA bands that we see in the CW DIA can be due to disorder and impurities in the film. We conclude that although the imide – PTV and RR – PTV are both derivatives of PTV; nevertheless, they show completely different behavior, which is clearly noted in their CW PA spectrum.

3.5.2 Transient photoinduced absorption of imide – PTV

Figure 3.10 (a) shows the transient PM spectra in imide-PTV film at various times *t* following pulse excitation at the range 2.6 to 1.2 eV at high pump intensity. The PM spectrum is dominated by two PA bands, namely, PA_2 at $\approx$ 1.7 eV and PA_2* at $\approx$ 1.3 eV (both bands with broad tails toward lower energies). The PB band was not observed.

Figure 3.10 (b) shows the transient PM spectra in imide – PTV film at various times *t* following pulse excitation at the range 1 to 0.3 eV at low pump intensity (which was measured by Uyen Huynh). The PM spectrum is dominated by one PA band,

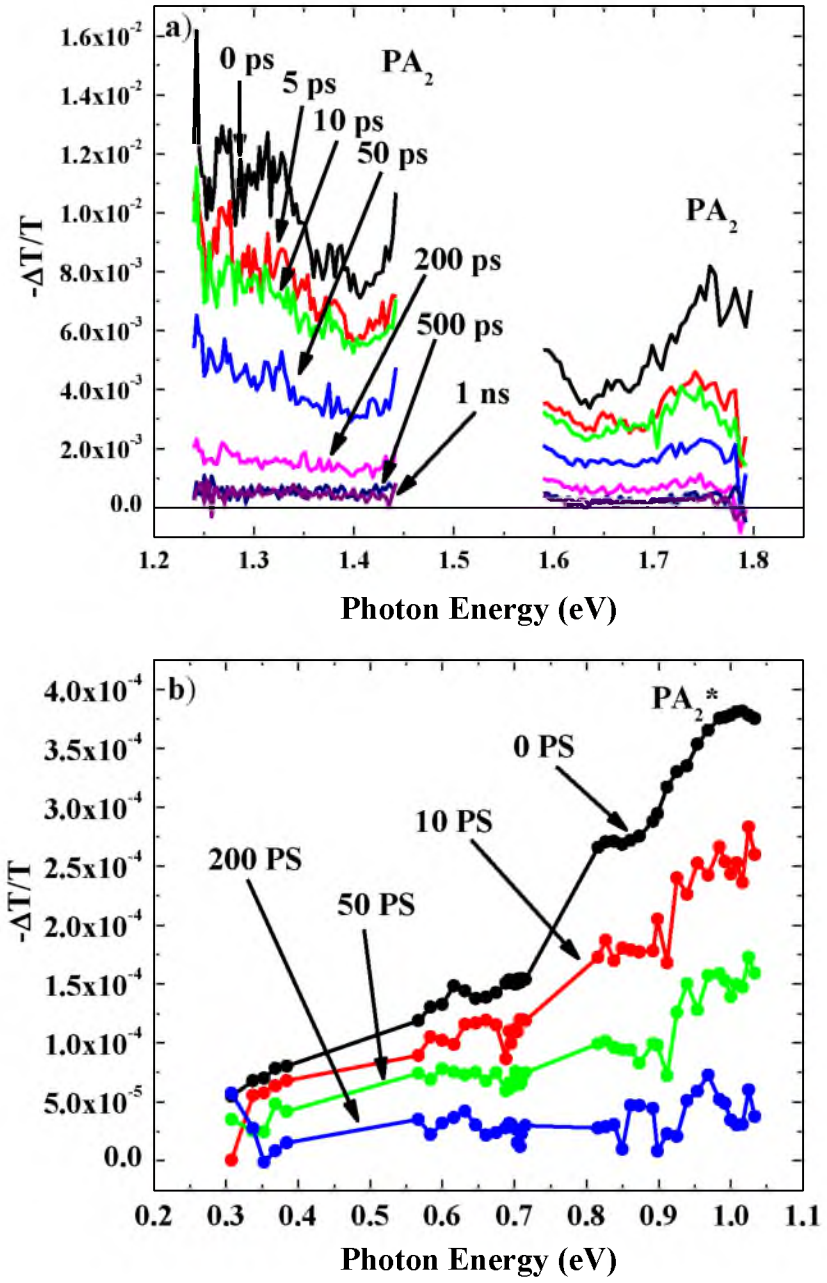

Figure 3.10: The transient PM spectrum of imide – PTV at different probe delay; (a) The range 2.6 to 1.2 eV at high pump intensity. (b) The range 0.3 to 1 eV at low pump intensity.

namely, PA_2* at ≈1 eV with a broad tail toward lower energies. The PA band, PA_1, was not observed below 0.5 eV.

Figure 3.11 (a) shows the decay kinetics at different probe frequencies. Both PA_2 and PA_2* decay with a similar time constant, τ. PA_2 decays with time constant of τ = 60 ps and PA_2* decays with time constant of about τ = 95 ps. The similarity of the time constants indicates that the two PA bands belong to the same photoexcitation, PA_2. By comparing the decay kinetics of the imide PTV and RR – PTV, it is obvious that the PA_2 band of the RR – PTV decays a lot faster than the PA_2 band of the imide – PTV.

Figure 3.11 (b) shows the PA formation and decay evolution near t = 0 of PA_2 (1.63 eV) of the imide – PTV and RR – PTV. The PA_2 of the imide – PTV is formed immediately compared to the PA_2 formation of the RR – PTV, which suggests that 1^1Bu undergoes a very fast internal conversion to a lower energy level as the RR – PTV but is not detected in our time resolution.

Figure 3.12 shows the EA spectra of imide – PTV and RR – PTV (which were measured by Tek Basel and Evan Lafalce). The EA spectra show a derivative-like band around $E(1^1B_u)$ that is due to the Stark shift of the 1^1B_u exciton, followed by several vibration replicas, and an absorption band at m^1A_g due to electric field-induced symmetry breaking. From the dominant features in the EA spectrum, we obtain the energy levels of two states: $E(1^1B_u) \approx 1.85$ eV (compare with 1.75 eV for RR – PTV) and $E(m^1A_g) \approx 2.5$ eV (compare with 2.55 eV for RR – PTV).

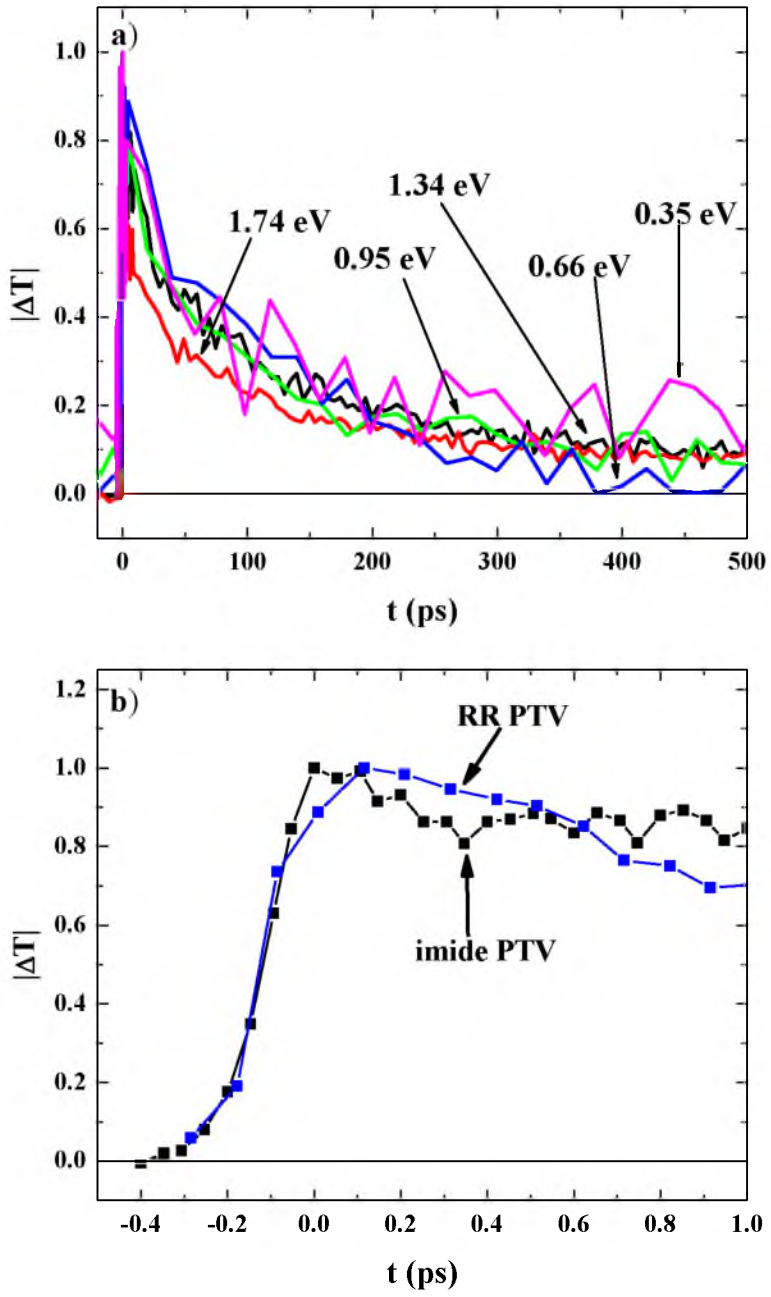

Figure 3.11: The decay dynamic of (a) the transient PM spectra at different probe frequencies. (b) PA_2 formation and decay evolution near t = 0 of PA_2 (1.63 eV) of the imide – PTV and RR – PTV.

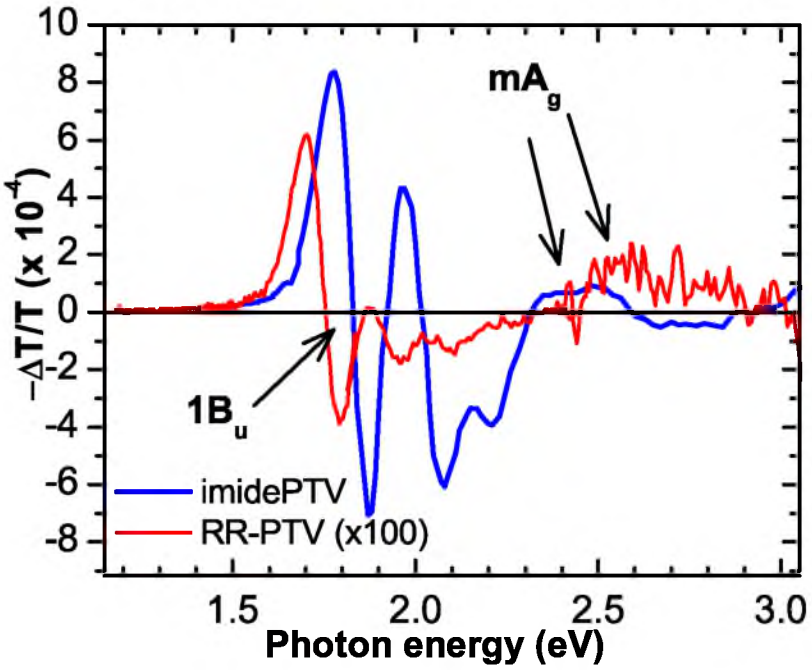

Figure 3.12: The EA spectrum of imide – PTV and RR – PTV. The spectral EA features related to 1^1B_u and m^1A_g are assigned.

3.5.3 Discussion

The band PA_2 is generic to many π – conjugated polymers. It is usually interpreted as the transition of 1^1B_u to k^1A_g [3.3]. In RR – PTV polymer, the band PA_2 is due to the transition $2^1A_g \rightarrow n^1B_u$ since 2^1A_g is the lowest excited state. This is in agreement with the weak PLQE (both measured and calculated), η, which is low since the transition from the lowest excited state (namely the $2A_g$) to the ground state is forbidden.

In the imide – PTV polymer, we found from the CW measurements (PA, DIA, MPA) that charged excitons (polarons) are not photogenerated in the film. Only triplets excitons dominate the cw spectrum. By comparing the spectra of the CW PA (or the background of the mid-IR measurement) and transient PM of the imide – PTV [Figure

3.13], we see that both of them do not show the same spectrum. This indicates that the PA band in the ps time domain is not due to triplet excitons.

The PA transient spectrum does not show a PA band in the 0.5 – 0.7 photon energy range, which is $1B_u \rightarrow mA_g$ energy range. Additionally, this transfer belongs to a single species, since the decay does not depend on the probe photon energy and we sign this transition to be $2A_g \rightarrow nB_u$.

In addition, in the imide – PTV polymer, the calculated PLQE from the 1^1B_u decay is $\eta = \tau / \tau_{rad} \approx 9\%$, which is quite different from the measured η-value of ≈ 1%. If the 1^1B_u is the lowest excited state, then we expect the value of the measured (1%) and calculated (9%) of the PLQE to agree with each other.

This means that this PA is due to some mixed state of $1B_u$ and $2A_g$ as the polymer has emission but does not have 1 ns radiative lifetime. This can explain the difference between the calculated value of the QEPL (9%) and the measured one (1%).

The difference between the time constant, τ, of the imide – PTV and the RR – PTV can be explained with thermal activation [3.21, 3.22] where because of the overlap in the energy parabolas of $2A_g$ and $1A_g$, the RR – PTV decays faster than the imide – PTV [Figure 3.14 (a, b)].

Several groups have studied PTV recently [3.23] and concluded that the PA transient band is due to triplets from singlet fission, where the exciton $1B_u$ decays into two triplets [3.23, 3.24, Figure 3.14 (c)]. On the other hand, our results support the claim that $2A_g$ is the lowest excited state.

Figure 3.14 (a) and (b) shows the difference between the polymers RR, imide – PTV. Figure 3.14 (c) shows the different points of view.

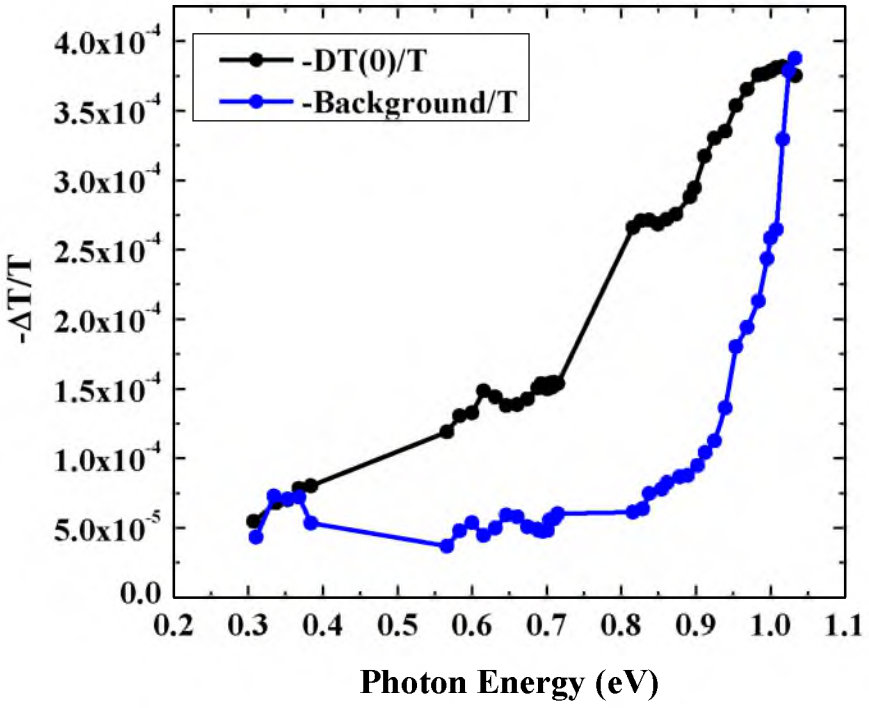

Figure 3.13: Comparison of the background and transient PM of the imide – PTV in the mid-IR range.

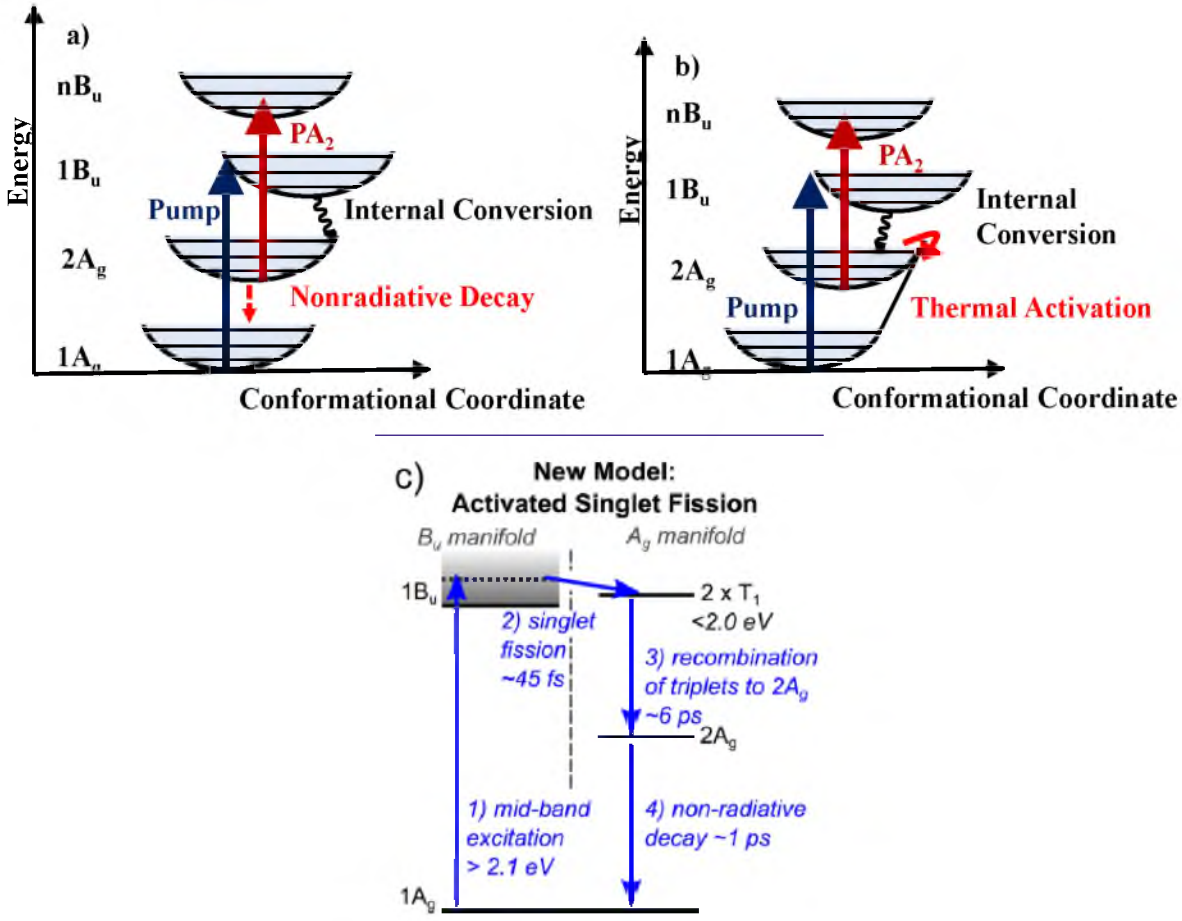

Figure 3.14: The states levels of the PTV polymer. (a) The states levels of the RR – PTV polymer. (b) The states levels of the imide – PTV. (c) Another model from [3.23]

3.6 Thermo-optical strain waves

3.6.1 Thermo-optically generated acoustic waves

Figure 3.15 shows two examples of transient photomodulation in RR – PTV. The decay kinetic of both examples has two components; one is the initial ultrafast component of transient PM response, which is followed by a much slower component. The slower component is overlaid with an oscillatory component, as shown in Figure 3.15. The slower component is the subject of this discussion. We will show that the ΔT/T oscillation vs. the probe time delay is produced by transient strain due to acoustic waves induced by the pump pulse, which is absorbed in the polymer film and has a dependence on the film thickness. The thinner film with d ≈ 60 nm has a shorter period compared with the thicker film with d ≈ 300 nm and a longer period. The ΔT/T oscillations were measured at probe energy of 1.81 eV. We measured $\tau_T \approx 120$ ps for a film thickness d ≈ 60 nm [Figure 3.15 (a)], and $\tau_T \approx 630$ ps for a thicker film of d ≈ 330 nm [Figure 3.15 (b)]. We can conclude that the second ΔT(t) component contains a propagating wave response that bounces back and forth in the film, due to successive reflection at the two film boundaries with τ_T determined by the "round-trip" time. The oscillation period, τ_T, is different in (a) and (b). The inset to (a) and (b) shows in more detail the PB decay and TS onset response.

It is possible to obtain the sound velocity, v, from the round-trip time given by the oscillation period, where

$$v = 2nd/\tau_T \tag{3.6}$$

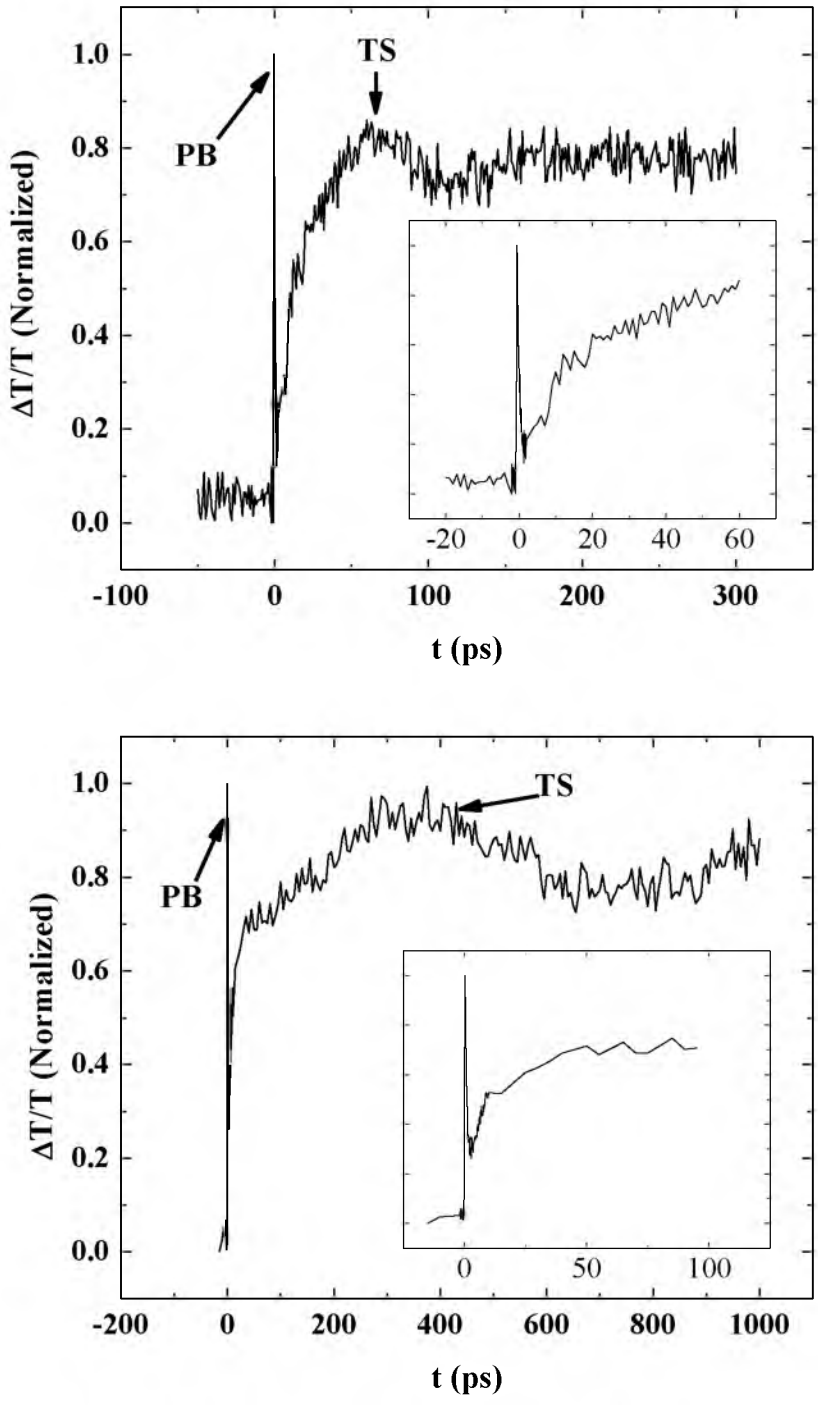

Figure 3.15: The transient PM response at $\hbar\omega$(probe) = 1.80 eV of two RR – PTV films with different thicknesses: (a) d ≈ 60 nm, and (b) d ≈ 330 nm. The ultrafast electronic response (PB) and the transient strain (TS) response that show an oscillatory component are assigned.

n = 1 if the film has two free surfaces or n = 2 if the film has one free surface. If we assume poor bonding of the polymer film to the substrate, then $\eta_{ds}(x,t)$ changes its sign at each film interface, thus forming an oscillatory $\Delta T(t)$ response component. From our data, we obtain for RR – PTV film, $v \approx 1$ nm/ps, which is in good agreement with sound velocities in other polymer films [3.10].

In nonluminescent conducting polymers, the pump pulse is absorbed in a thin layer ξ of about 300 Å, and within less than 10 ps, much of the energy is released to phonons due to thermalization and nonradiative recombination of the hot photogenerated carriers. The subsequent nonquilibruim phonon distribution can be roughly characterized by an increase $\Delta\Theta(x)$ in the effective temperature. As a result, the temperature of the layer ξ increases, and its thermal expansion creates a stress, which then causes a strain pulse to propagate into the film. The strain pulse bounces back and forth in the film upon reflection off the interfaces [3.9 – 3.11]. This process is illustrated in Figure 3.16.

The temperature increase, Θ_T, is proportional to the absorbed pump light intensity. Therefore, $\Theta(x)$ is given by:

$$\Theta(x) = \Theta_o + \Theta_T e^{-\alpha x} \tag{3.7}$$

This process can be described with the following wave equation [3.9]:

$$\rho \frac{\partial^2 u}{\partial t^2} = 3B \frac{1-\vartheta}{1+\vartheta} \frac{\partial^2 u}{\partial x^2} - 3B\beta \frac{\partial \Delta\Theta(x)}{\partial x} \tag{3.8}$$

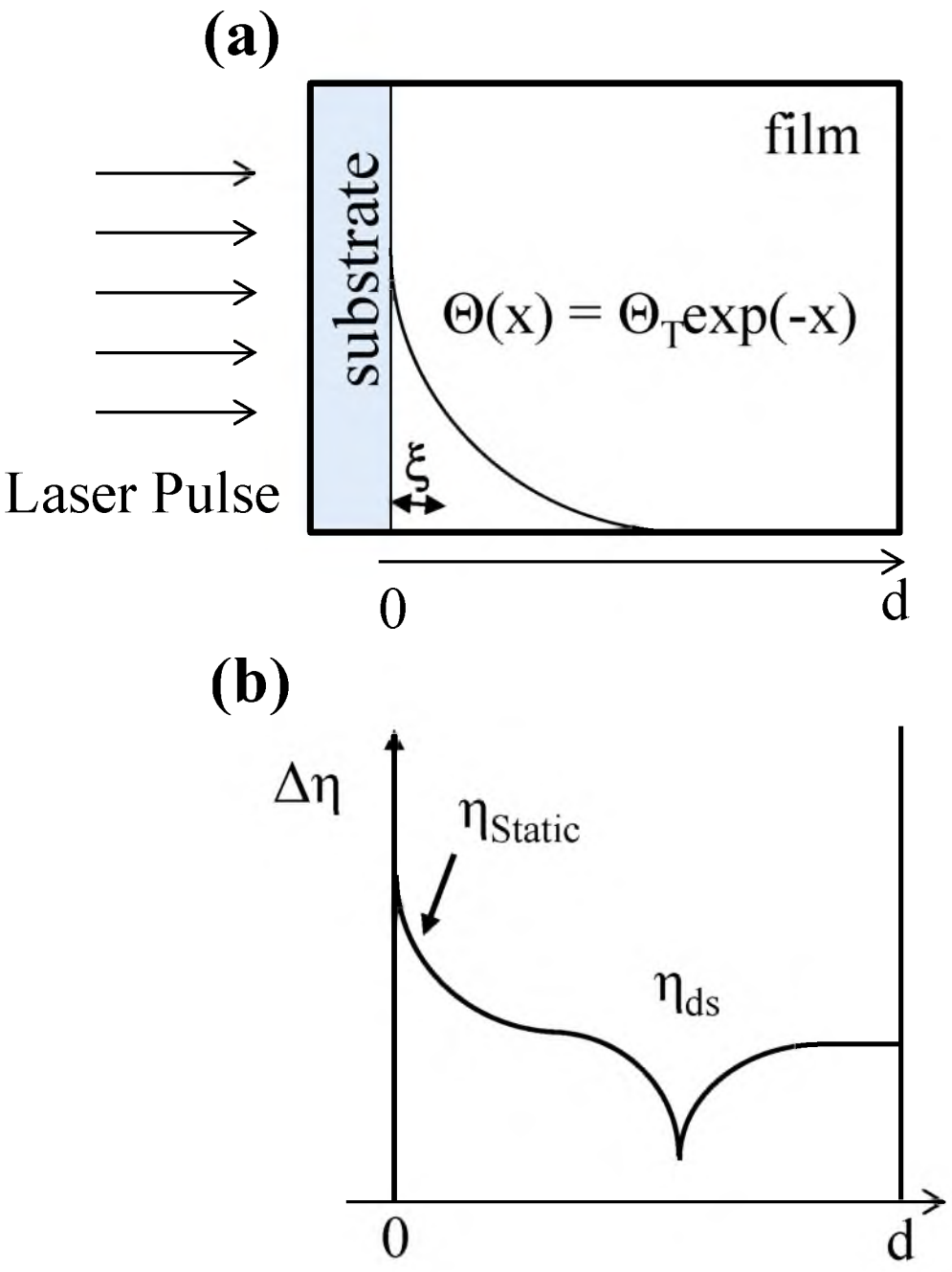

Figure 3.16: Strain generation in nonluminescent conducting polymer film. (a) Thermo-optical excitation of a strain wave. (b) An illustration of the propagate strain wave in the film.

where ρ is the film density, B is the bulk modulus, υ is the Poisson's ratio (which is 0.33 for many polymers), β is the linear expansion coefficient (~ 10^{-4} K^{-1}), and u(x) is the displacement.

The strain, η(t), is given by

$$\eta = \partial u/\partial x \tag{3.9}$$

Equation 3.8 can be written as:

$$u_{xx} = v^2 u_{xx} = f(x) \tag{3.10}$$

where *v* is the longitudinal sound velocity given by:

$$v^2 = \frac{v-1}{v+1}\frac{B}{\rho} \tag{3.11}$$

and

$$f(x) = \frac{-3B\beta}{\rho}\frac{\partial\Theta(x)}{\partial x} \tag{3.12}$$

assuming zero displacement at the interface between the substrate and the film at z = 0. Then the solution for Equation 3.10 is given by [3.9, 3.11]:

$$\eta(x,t) = K[e^{-\frac{x}{\xi}}\left(2 - e^{-\frac{vt}{\zeta}}\right) - e^{-\frac{|x-vt|}{\zeta}}] \quad (3.13)$$

where x is the distance into the film from the photoexcited film surface, K is a constant proportional to the heat transferred to the film from the pump pulse. Equation 3.13 can be described with static strain and dynamic strain. $\eta_{ss}(x)$ is the static strain, which takes the profile of the pump absorbed energy in the film ($e^{-x/\xi}$), whereas $\eta_{ds}(x, t)$, is the dynamic strain wave that bounces from the film interfaces. The first term, $\eta_{ss}(x)$, in Equation 3.13 is time-independent for $t \gg \xi/v$, while the second one, $\eta_{ds}(x, t)$, corresponds to a portion of the strain that propagates back and forth inside the film. Equation 3.13 describes the strain for times before the propagating strain pulse first reaches the free surface (z = d); upon arrival at this surface, $\eta_{ds}(x, t)$, the dynamic strain, is reflected with a change in sign, but $\eta_{ss}(x)$, the static strain, remains intact near the substrate-film interface. Figure 3.17 shows a simulation of the pulse propagation in the film vs. the displacement, *x* (a) and vs. time, t (b).

3.6.2 Transient strain spectroscopy

Transient strain spectroscopy (TSS) is defined as the method of detecting electronic states by measuring transient strain-modulated absorption [3.10, 3.11].

The physics behind TSS is simple: the propagated strain wave causes $\alpha(\omega)$ to shift, as a result, changing the transmission at a given probe frequency (ω). The resulting strain-induced $(\Delta T/T)_{TSS}$ is

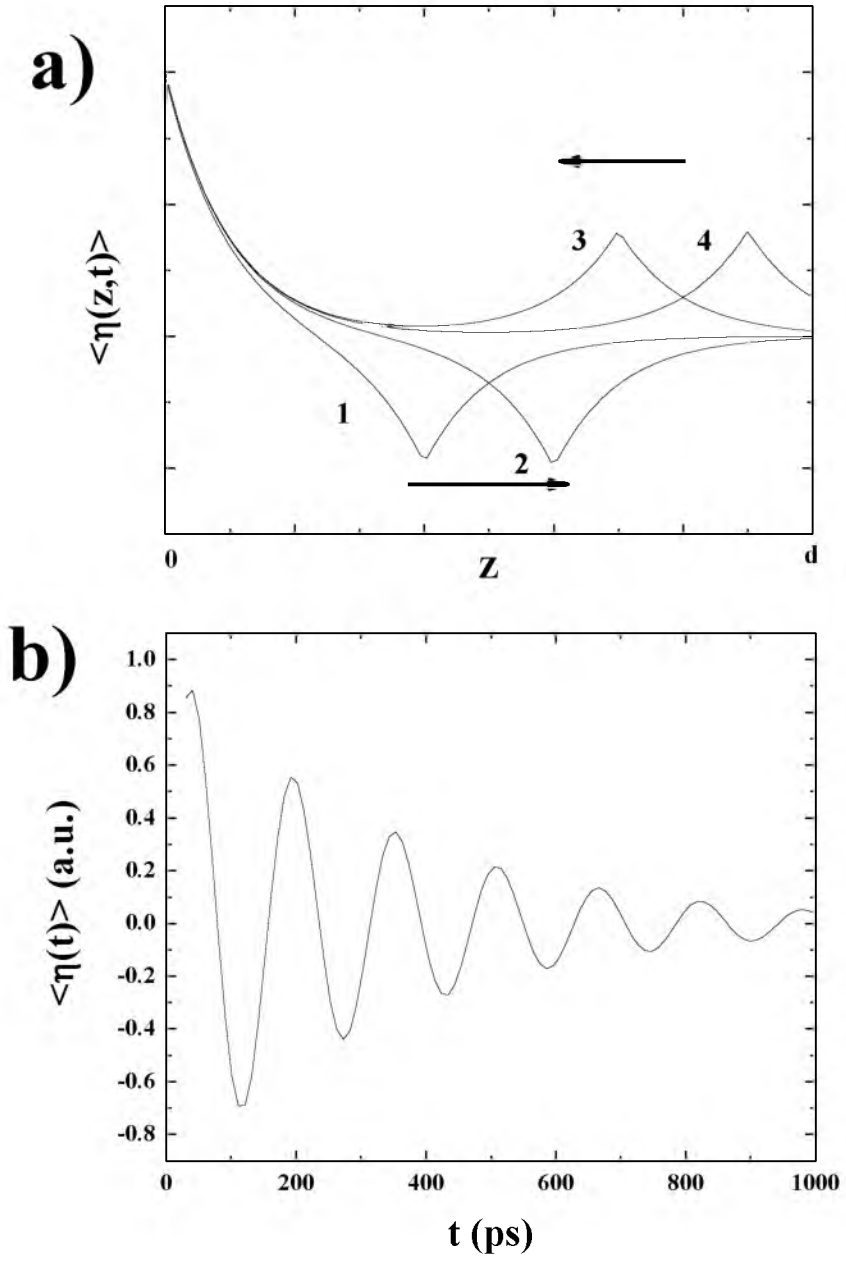

Figure 3.17: Simulation of the strain oscillations. (a) η(x). (b) η(t).

$$-\frac{\Delta T}{T} = \Delta\alpha d = \frac{\partial\alpha}{\partial(\hbar\omega)}\frac{\partial E_g}{\partial\eta} < \Delta\eta > d \tag{3.14}$$

α and Δα are the absorption and the photoinduced change at the probe frequency ω, Eg is the band gap, $\partial Eg/\partial\omega$ = A is the deformation potential. From Equation 3.14, we can say that the resulting strain photoinduced modulation signal is following the first derivative of the absorption.

$$\left(\frac{-\Delta T}{T}\right)_{TSS} \propto \frac{\partial\alpha}{\partial\omega} \tag{3.15}$$

Figure 3.18 (a) shows the initial PB spectrum and its time evolution of the thin film (d ≈ 60 nm). The PB spectrum at t = 0 has similar features as in the absorption spectrum of the film [Figure 3.2]; there is a prominent PB band at 1.83 eV (1^1B_u), followed by a phonon side band at ≈ 2.03 eV. However, at t > 10 ps, the PB spectrum dramatically changes; it does not resemble the absorption spectrum any longer, but rather follows the absorption derivative spectrum, $\partial\alpha(\omega)/\partial\omega$ [Figure 3.18 (b)]. At the same time, ΔT(t) near the isosbestic point at $\hbar\omega$ = 1.80 eV starts increasing [Figure 3.15 (a)], showing the onset of a second ΔT component. The fit between the spectra of $(\Delta T/T)_{TSS}$ and $\partial\alpha(\omega)/\partial\omega$ is quite good. The difference between them can be due to the inhomogeneity in the film.

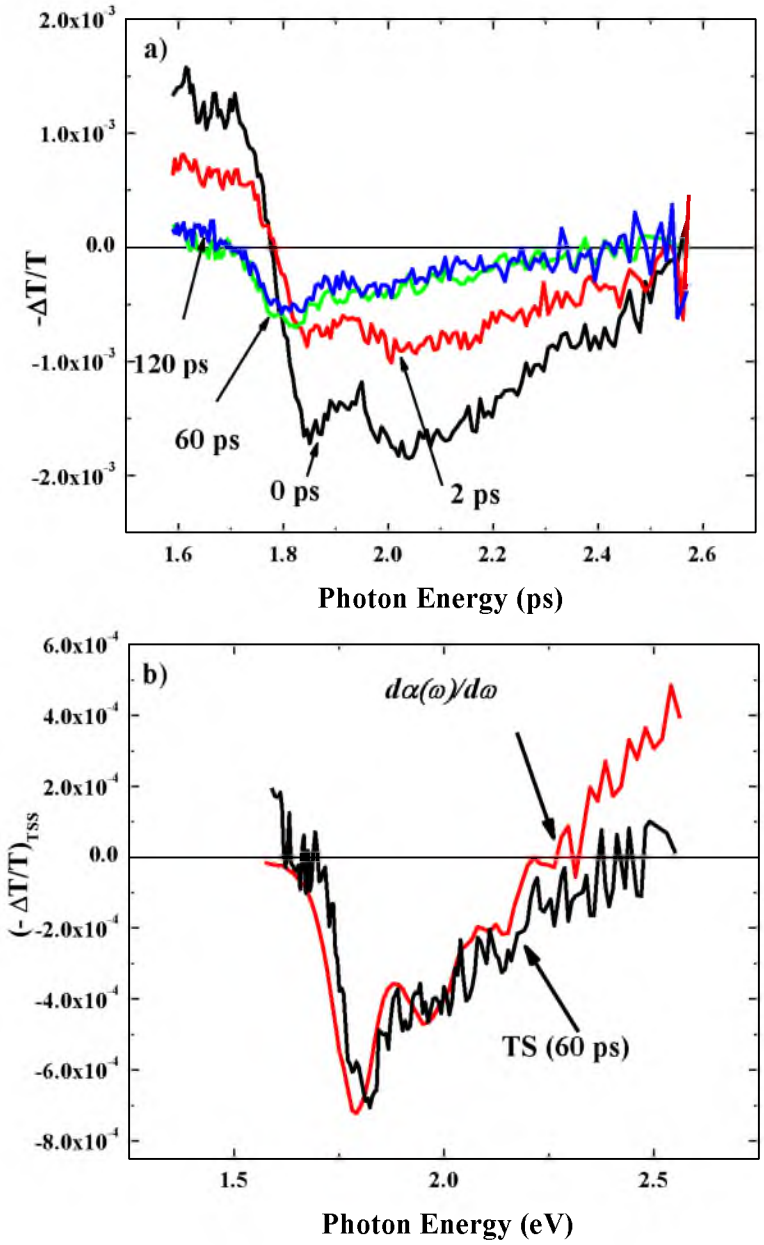

Figure 3.18: The PM spectra of RR – PTV film of d ≈ 60 nm in the $\hbar\omega$(probe) interval 1.6 – 2.6 eV; (a) which shows the evolution of the PB response. (b) Comparison of the PB spectrum at 60 ps (dominated by the TS response) with the spectrum of the absorption derivative, $\partial\alpha(\omega)/\partial\omega$.

3.6.3 Polarization of transient strain spectroscopy

The technique of polarization memory decay (PMD) kinetics P(t), where

$$P(t) = \left(\frac{\Delta T_{\parallel}}{T_{\parallel}} - \frac{\Delta T_{\perp}}{T_{\perp}}\right) / \left(\frac{\Delta T_{\parallel}}{T_{\parallel}} + \frac{\Delta T_{\perp}}{T_{\perp}}\right) \tag{3.16}$$

is an ideal tool to distinguish between the various photoexcitation species in polymer films. The value of PMD kinetics for intrachain excitons and free polarons should be fast, since these species are very mobile among the polymer chains in the film. On the other hand, the excimer and polaron-pair species are more localized in places along the chains where the interchain distance between neighboring chains is the short; as a result, their binding energy is relatively larger than that of the more mobile species, and this increases their "stability." Hence, very slow PMD kinetics characterizes excimer and polaron-pair species [3.20].

Figure 3.19 shows the technique of polarization memory decay (PMD) kinetics P(t) of the RR – PTV at 1.81 eV. We found that ΔT(t) is initially polarized, having polarization degree P ≈ 0.5. However, at t > 10 ps, P(t) decays quickly to P = 0, which is reached at the peak of the second ΔT(t) component.

3.7 Conclusion

In this chapter, we studied two different derivatives of the PTV polymer. One is the RR – and RRa – PTV in which the $2A_g$ is the lowest excited state and consequently has very fast decay kinetics. The other derivative is the imide – PTV of which photophysics is dominated by mixture of the singlet energy state: $2A_g$ and $1B_u$.

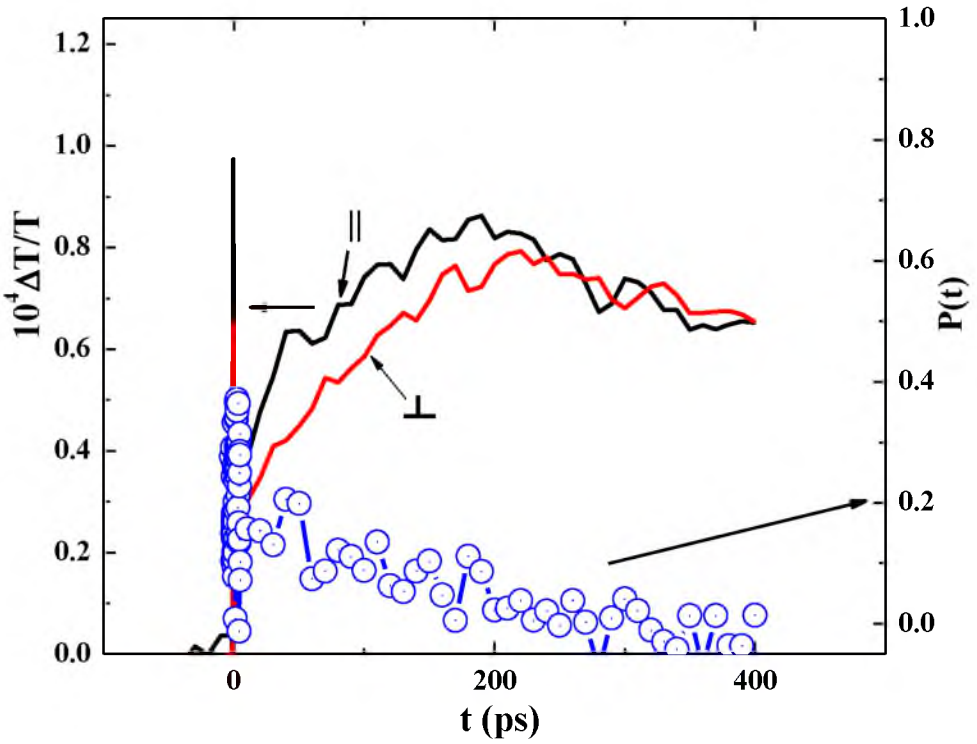

Figure 3.19: ΔT(t) parallel (||) and perpendicular (⊥) response dynamics and the resulting polarization degree, P(t), for a film with thickness of d ≈ 210 nm.

The RR – PTV ultrafast response is dominated by the fast decay of the photogenerated $1B_u$ excitons into the "dark" $2A_g$ exciton with lower energy; this limits the PLQE to $\approx 2 \times 10^{-4}$. From the measurements of PL, transient PM, and EA spectra, we determined the essential states in this NDGS polymer.

From the measurements of CW PA, DIA, and transient PM, we determined that triplet excitons are photogenerated in the imide – PTV polymer. However, since the CW PA and the transient PA do not show the same spectrum, we conclude that the triplets exciton do not form in the ps time domain.

The imide – PTV shows a different behavior compare with the RR – PTV. This is probably due to the different excited-state parabolic energy levels.

In the last part of the chapter, we demonstrated transient strain spectroscopy in RR – PTV thin films, where the ultrafast energy release associated with the exciton decay gives rise to substantial static and dynamic strains in the film that dramatically influence the film's transient PM response. We conclude that NDGS polymers with intrinsic weak PL may be used in nonlinear optical applications because of their ultrafast response, as well as in transducers for TS spectroscopic studies due to their ultrafast energy release.

3.8 Reference

[3.1] Z. G. Soos, S. Elemad, D. S. Galvao, and S. Ramasesha, Chem. Phys. Lett. 194, 341 (1992).

[3.2] J. H. Burroughes, D. D. C. Bradley, A. R. Brown, R. N. Marks, K. Mackay, R. H. Friend, P. L. Burns, and A. B. Holmes, Nature 347, 339 (1990)

[3.3] C.-X. Sheng, M. Tong, S. Singh, and Z. V. Vardeny, PRB, 73, 083206 (2007).

[3.4] A. J. Brassett, N. F. Colaneri, D. D. C. Bradley, R. A. Lawrence, R. H. Friend, H. Murata, S. Tokito, T. Tsutsui, and S. Saito, PRB, 41, 10386 (1990).

[3.5] F. Banishoeib, A. Henckens, S. Fourier, G. Vanhooyland, M. Breselge, J. Manca, T. J. Cleij, L. Lutsen, D. Vanderzande, L. H. Nguyen, H. Neugebauer, and N. S. Sariciftci, Thin Solid Films 316, 3978 (2008).

[3.6] E. Lafalce and X. Jiang,J. Phys. Chem. B, 113, 13139 (2011).

[3.7] C. Girotto, D. Cheyns, T. Aernouts, F. Banishoeib, L. Lutsen, T. J. Cleij, D. Vanderzande, J. Genoe, J. Poortmans, and P. Heremans, Org. Electron. 9, 740 (2008).

[3.8] S. N. Dixit, D. Guo, and S. Mazumdar, PRB 43, 6781 (1991).

[3.9] C. Thomsen, H. T. Grahn, H. J. Maris, and J. Tauc, Phys. Rev. B 34, 4129 (1986).

[3.10] G. S. Kanner, Z. V. Vardeny, and B. C. Hess, PRB, 42, 3403 (1990).

[3.11] G. S. Kanner, S. Frolov, and Z. V. Vardeny, PRL. 74, 1683 (1993).

[3.12] G. Lanzani, G. Cerullo, M. Zavelani-Rossi, S. DeSilvestri, D. Comoretto, G. Musso, and G. Dellepiane, PRL. 87, 187402 (2001)

[3.13] C. Zhang, T. Matos, R. Li, S.-S. Sun, J. E. Lewis, J. Zhang, and X. Jiang, Polym. Chem. 1, 663 (2010)

[3.14] S. Webster and D. N. Batchelder, Polymer, 37, 4961 (1996).

[3.13] C. Zhang, J. Sun, R. Li, S.-S. Sun, E. Lafalce, and X. Jiang, Macromolecules 44, 6389 (2011)

[3.16] Z. V. Vardeny and J. Tauc, Opt. Commun. 39, 396 (1991).

[3.17] M. Liess, S. Jeglinski, Z. V. Vardeny, M. Ozaki, K. Yoshino, Y. Ding, and T. Barton, PRB 36, 13712 (1997)

[3.18] N. T. Harrison, G. R. Hayes, R. T. Phillips, and R. H. Friend, PRL, 77, 1881 (1996).

[3.19] J. Orenstein and G. L. Baker, PRL, 49, 1043 (1982).

[3.20] Sanjeev Singh, Tomer Drori, and Z. Valy Vardeny, PRL, 77, 193304 (2008)

[3.21] B. C. Hess, G. S. Kanner, Z. V. Vardeny, and G. L. Baker, PRL, 66. 2364 (1991)

[3.22] T. Kobayashi Pure & Appl. Chern., 67, 387, (1995)

[3.23] A. J. Musser, M. Al-Hashimi, M. Maiuri, D. Brida, M. Heeney, G.Cerullo, R. H. Friend, and J.Clark, J. Am. Chem. Soc., 135, 12747 (2013).

[3.24] Smith, M. B. & Michl, J. Chem. Rev. 110, 6891 (2010).

[3.25] B. R. Gautam, T.D.Nguyen, E. Ehrenfreund, and Z.V Vardeny PRB 85, 205207 (2012)

CHAPTER 4

PHOTOEXCITATIONS OF LUMINESCENT CONJUGATED POLYMERS

4.1 Introduction

The derivatives of the polymer poly(phenylene-vinylene), referred to as PPV, are a variety of π – conjugated polymers that show high photoluminescence (PL) quantum efficiency and therefore, these polymers have been excellent candidates for active layers in electroluminescence devices, namely OLEDs. From the application point of view, the understanding of the photophysics of PPV polymers can help improve the PL quantum efficiency, and thus increase the electroluminescence output. Hence, the PPV derivatives have been the subject matter of a large body of experimental and theoretical research studies [4.14 – 4.17]. In this chapter, we focus on a specific PPV derivative, namely the poly(dioctyloxy) phenylenevinylene (DOO-PPV), and the influence of isotopes exchange on its ultrafast photophysics characteristic properties. The isotopes of DOO-PPV are: deuterated (D) – DOO-PPV, hydrogenated (H) – DOO-PPV, and ^{13}C-rich DOO-PPV, which for simplicity we will refer to as D – DOO-PPV, H – DOO-PPV, and C13 – DOO-PPV, respectively.

4.2 Materials

The DOO-PPV Isotopes that we used were synthesized in our laboratory by Mr. Leonard Wojcik. Synthetic reagents and solvents used in the preparation of the isotope-rich polymers were procured from Aldrich Chemical as reagent-grade and used as received. The detail synthesis process of D – polymer and H – polymer can be found in the supplementary information of a paper published by our group in Nature Materials, namely Tho et al. [4.13]. Their chemical structures are shown in Figure 4.1. The side groups attached to each benzene ring are two 4-phenyl-2-propyl-indene (C_8H_{17}) through oxygen, and two protonated hydrogen for H – polymer. When solutions based on aromatic solvents are cooled, the polymer forms gels that precipitate in clumps, making unsmooth films. However, short polymer chain length (or oligomers) tend to be more soluble in solvents such as toluene, orthodichlorobenzene (ODCB), and do not gel out easily. This was addressed by Hsieh [4.8] and Jiang-quing Pan [4.9], where they used a benzyl bromide end cap to shorten the polymer length. The synthesis of H – polymer was performed using polymerization of 2,5-bis(chloromethyl)-1,-4-dictyloxybenzene with potassium t-butoxide in refluxing p-xylene. This route allowed some control of the polymer chain length, and it is denoted by R1 in the chemical structure. The D – polymer contains deuterated hydrogen in place of protonated hydrogen. As for the C – polymer, some backbone ^{12}C carbon atoms have been replaced by ^{13}C isotope.

4.3. Linear absorption and photoluminescence spectra

The three DOO-PPV isotopes (namely D – polymer, H – polymer, and C – polymer) films were prepared under similar conditions. The linear absorption, in terms of

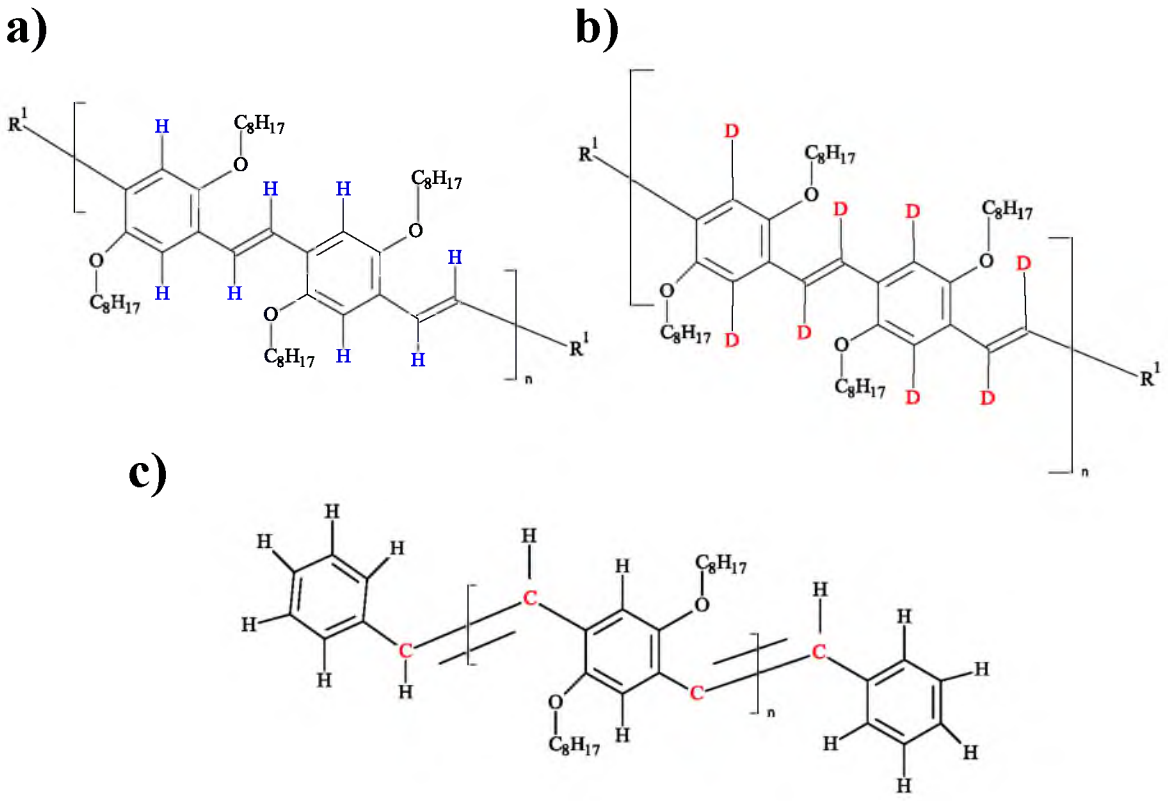

Figure 4.1: The basic repeat unit of the synthesized DOO-PPV polymer isotope of (a) H –, (b), D –, (c), ^{13}C – rich polymers.

optical density (O.D.), was measured using the Cary17 spectrometer. The photoluminescence (PL) was measured using the PL setup [Chapter 2]. These measurements were done by Mr. Tek Basel in our research group. Figure 4.2 shows a normalized O.D. and PL spectra of all three DOO-PPV isotopes. All three isotopes present similar absorption and emission spectra. For the absorption spectrum, a broad featureless band is observed at ≈ 2.5 eV. The absorption band above the optical band gap is due to $\pi - \pi^*$ transitions that lead to the formation of singlet exciton [4.1 – 4.3], whereas below the gap, the absorption is due to the presence of impurities and/or defects

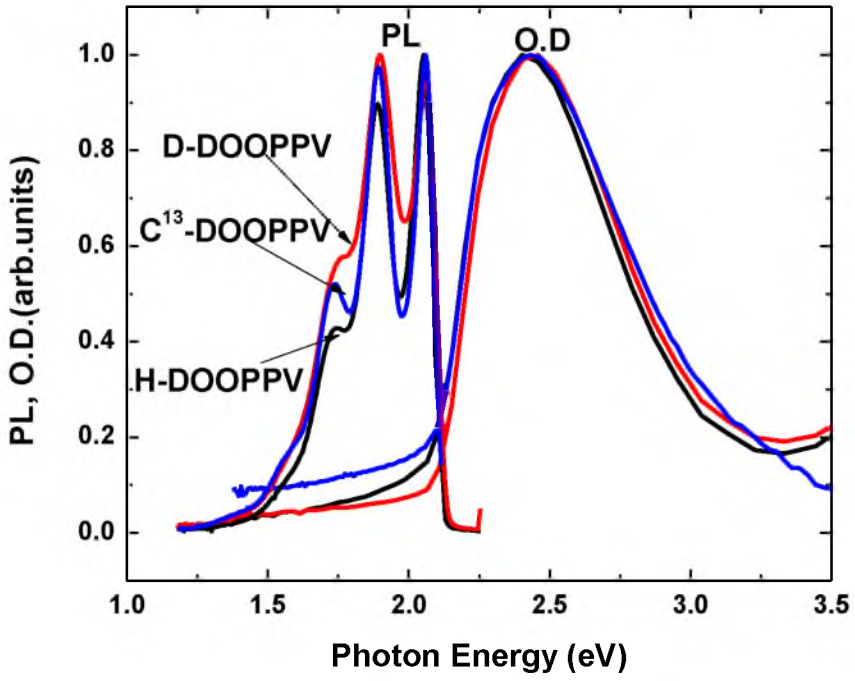

Figure 4.2: Normalized absorption and PL spectra of the three DOO-PPV isotopes. The absorption spectra were measured at 300 K, whereas the PL spectra were measured at 80 K.

in the samples that lead to an Urbach tail. The energy of the $\pi - \pi^*$ transition is dependent on the extent of the π-electron delocalization. In relatively disordered polymers such as the isotopes of DOO-PPV, the extent of delocalization tends to be limited by defects in the polymer chain, which lead to a range of $\pi - \pi^*$ energies for a given sample. The lack of vibronic structure in the absorption spectra is thus attributed to inhomogeneous broadening due to a distribution of conjugated lengths within the sample [4.4].

The PL spectra of all three isotopes show a similar emission band, having two phonon sideband. This verifies the polymer electronic structure, and also assures that the photoexcitation species such as excitons and polarons are the same in the D –, H –, and C – polymers [4.5]. Since the C = C stretching vibration in D – polymers is lower than in

the other two isotopes, we note that the emission replica of this polymer occurs at higher energies, namely closer to the 0 – 0 transition. The PL spectra of all three isotopes are Stokes–shifted from the absorption edges, and have clearly resolved vibronic structures. These observations have been explained by relocation of the photogenerated excitons to the lower energy (longer conjugation length) chain segments before radiative decay has time to occur [4.4, 4.6, and 4.7]. Therefore, the observed PL emission mainly originates from the lowest energy segments, leading to the observed Stokes shift and reduced inhomogeneous broadening when compared to the absorption spectra. The relative strength of the PL intensity of D – polymer is the highest among all isotopes, which is also consistent with the PL quantum efficiency (PLQE) measurements. These are: 11.5 % for H –, 12.8 % for D –, and 11.2 % for C – polymers, with uncertainty of 0.2%.

4.4 Photoexictations of DOOPPV isotopes

4.4.1 Transient photoinduced absorption of H – DOO-PPV (H – polymer) film

The transient ultrafast photomodulation (PM) spectrum of H – Polymer film in the photon energy spectral range of 0.3 – 2.4 eV is shown in Figure 4.3 (a) for two delay times, t, of t = 0 and 100 ps, respectively. The PM spectrum is divided into two different spectral regions: one region is below 1.7 eV where $\Delta T/T < 0$, whereas the other region is above 1.7 eV where $\Delta T/T > 0$. The PM spectrum at t = 0 ps contains the PA band at ≈ 1 eV (PA_1), and two other bands, namely stimulated emission (SE) at ≈ 1.9 eV, and photobleaching (PB) at ≈ 2.1 eV. The band just below the absorption of the H – DOO-PPV is due to SE [4.10], which is similar to the CW PL spectrum [Figure 4.3]. The band

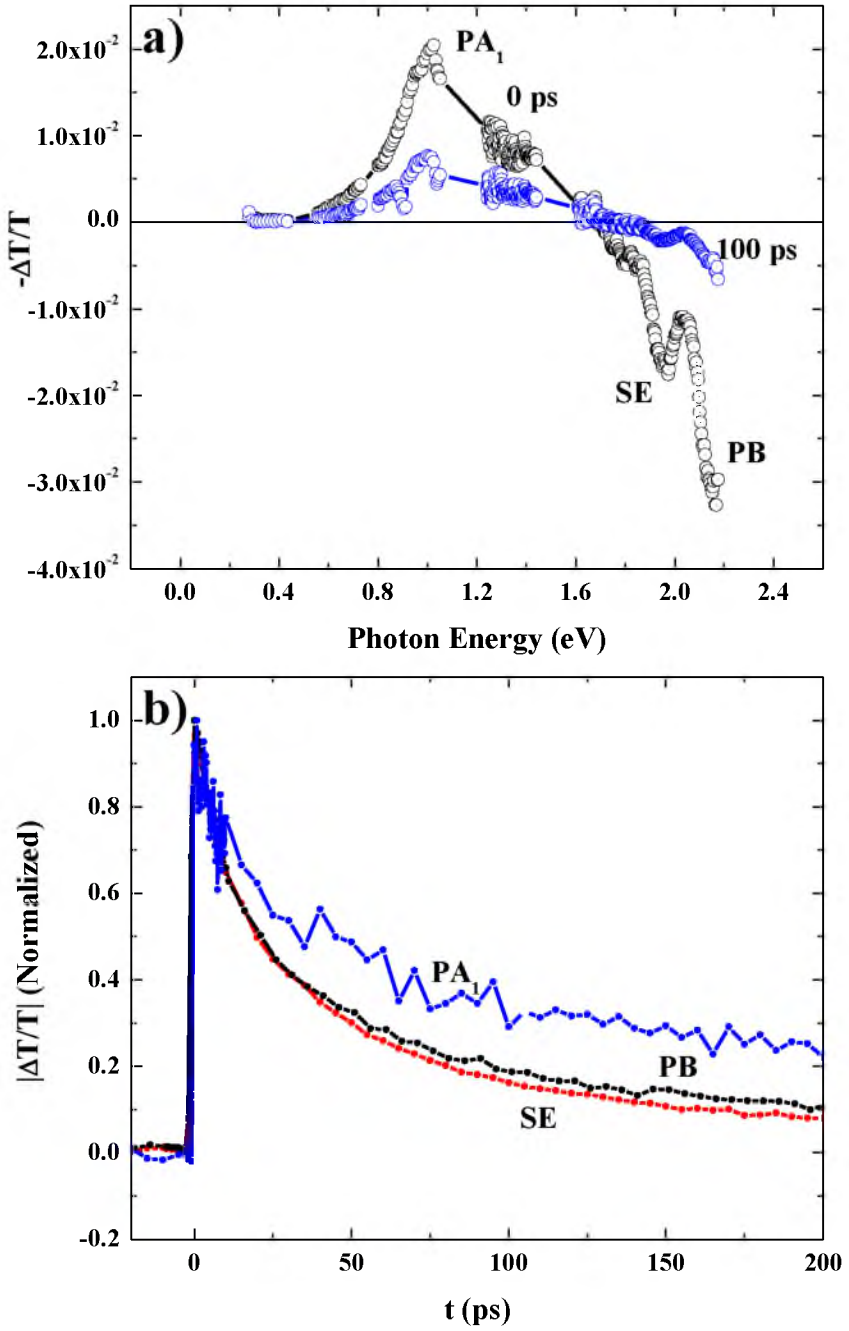

Figure 4.3: Transient PM (a) The spectrum of H – DOO-PPV film at t = 0 ps and 100 ps, respectively. (b) Decay dynamics of (a) at different probe energies.

above SE is assigned as PB because it is similar to the absorption spectrum.

We note that when the probe photon energy is above 1.7 eV, the change in the absorption is $\Delta T/T > 0$. For probe photon energy gain due to SE from photoexcited states, and, below 1.7 eV, the probe beam is absorbed due to photoinduced absorption (PA) from the photogenerated excitons to higher excited states, and shows an opposite signal as compared to the SE signal. We note, however, that at $t = 0$, the SE and PA bands spectrally overlap; otherwise, the SE band would have continued to lower photon energies. This is the case for other luminescent polymers, e.g., P3BT, PPE [4.11], and PPV [4.10]. At $t > 0$, the PM spectrum decays due to recombination of the photoexcited excitons.

The PM spectrum at $t = 100$ ps still consists of the singlet exciton band at $\approx$ 1eV along with SE and PB bands. Figure 4.3 (b) shows the transient decay behavior of the various bands PA_1, SE, and PB, measured at low excitation intensity. PA_1 does not show a significant intensity dependence and therefore, its decay dynamics was fitted with double exponential (rather than with bimolecular recombination kinetics that leads to power law decay) with time constants of $\tau_1 \approx 7$ ps (40%) and $\tau_2 \approx 55$ ps (60%). The decay dynamics are not the same across the spectrum, indicating that various photogenerated species contribute to the spectrum.

This is the reason for choosing the double exponential fitting. As we will show later on [section 4.6], the signal at 1.4 eV consists also of a triplet exciton. In contrast, SE and PB do not decay exactly the same as PA_1. We also note that the SE band decays a bit faster than the PB band. These decays could not be fitted with a single exponential; instead they were fitted, after taking into account the intensity dependence [Figure 4.4],

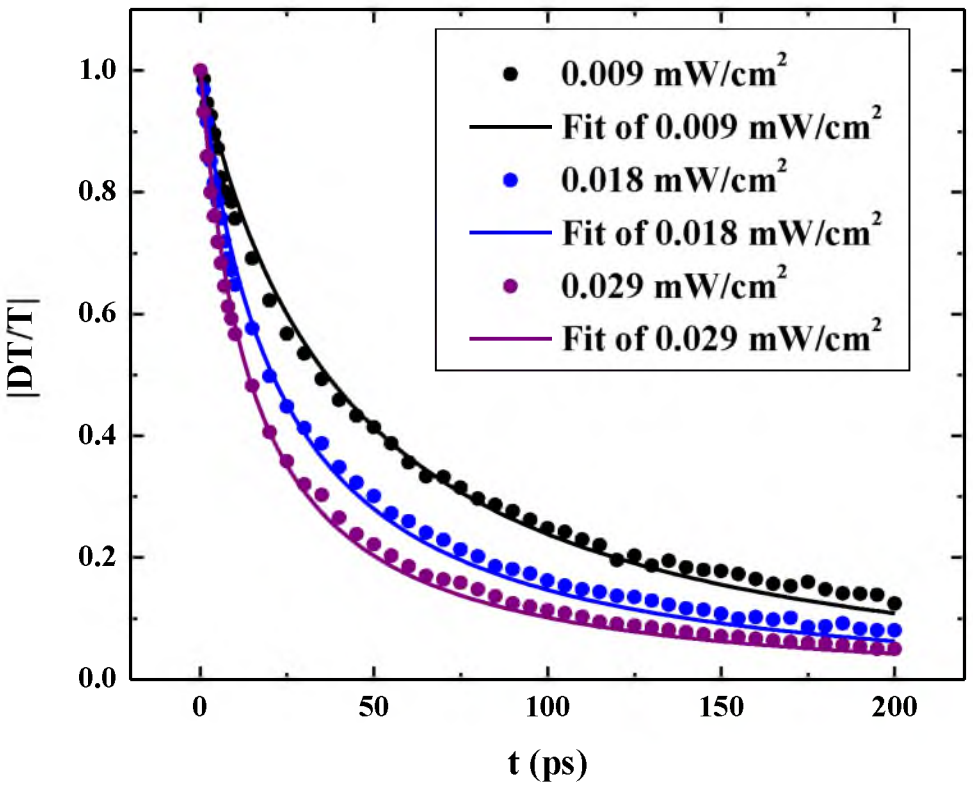

Figure 4.4: An example of the decay dynamics at different intensities at the SE band of the H- DOO-PPV film. The fit was done with the parameters: $\tau \approx 134$ ps and $b \approx 2 \cdot 10^{-20}$ cm^3/s.

with bimolecular recombination [4.12, Chapter 2]. For the H – polymer, the SE band decays with the bimolecular recombination parameters: $\tau \approx 134$ ps and $b \approx 2 \cdot 10^{-20}$ cm^3/s, whereas the PB band decays with the parameters: $\tau \approx 200$ ps and $b \approx 2 \cdot 10^{-20}$ cm^3/s.

The primary photoexcitations in PPV derivative polymers in dilute solutions are intrachain singlet excitons [4.18]. However, in films of PPV derivatives, species other than intrachain excitons can also be photogenerated [4.17] due to the increased interchain interaction. These species can be polaron pairs, excimers, and free polarons [4.14 – 4.19].

The technique of polarization memory decay (PMD) kinetics P(t), where

$$P(t) = \left(\frac{\Delta T_{\parallel}}{T_{\parallel}} - \frac{\Delta T_{\perp}}{T_{\perp}}\right) / \left(\frac{\Delta T_{\parallel}}{T_{\parallel}} + \frac{\Delta T_{\perp}}{T_{\perp}}\right) \quad (4.1)$$

is an ideal tool to distinguish between the various photoexcitation species in polymer films. The value of PMD kinetics for intrachain excitons and free polarons should be fast, since these species are very mobile among the polymer chains in the film. On the other hand, the excimer and polaron-pair species are more localized in places along the chains where the interchain distance between neighboring chains is the short; as a result, their binding energy is relatively larger larger than that of the more mobile species, and this increases their "stability." Hence, very slow PMD kinetics characterizes excimer and polaron-pair species [4.20].

Figure 4.5 shows the PMD kinetics of the H – polymer film at two probe frequencies; these are 1.34 eV [Figure 4.5 (a)], which is PA_1, and 1.96 eV [Figure 4.5 (b)], which is the SE. Figure 4.5 (c) compares between the two P(t) on a log-log scale. The polarization memory initial value P(0) is not the same for the SE ($\approx$ 0.25) and PA_1 ($\approx$ 0.5), this may be due to heat (that does not have PM), but the decay kinetics is roughly the same for the two probe frequencies, with $\tau \approx 7$ ps (SE) and 3 $\approx$ ps (PA_1). Since the SE band decay is correlated with that of the PA_1 band, we conclude that the primary photoexcitations in the H – polymer film are intrachain singlet excitons.

In π – conjugated polymers, the optical transitions between the ground state $1A_g$ and the Bu excited states are allowed, and therefore, the linear absorption spectrum shows mainly 1Ag $\rightarrow$ 1Bu and $1B_u \rightarrow mA_g$, or kA_g transitions. On the other hand, the optical transitions between the ground state $1A_g$ and other states with A_g symmetry are

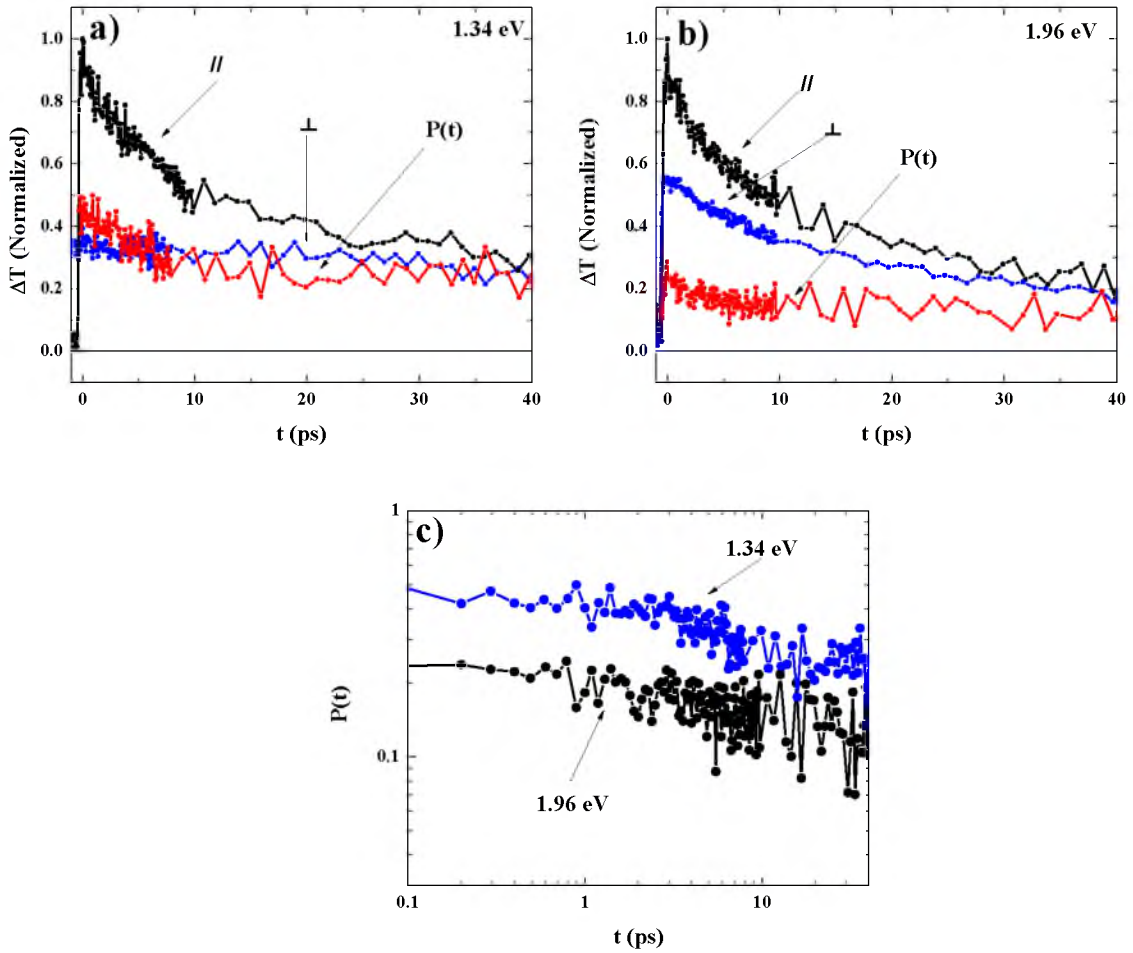

Figure 4.5: Polarization memory decay for the H – polymer at (a) 1.34 eV, (b) 1.96 eV. (c) The comparison of P(t) dynamics in (a) and (b).

forbidden.

However, these transitions become allowed when measuring two-photon absorption (TPA). Figure 4.6 shows the obtained TPA spectrum of H – polymer film; the technique of TPA measurements using pump-probe correlation is explained in section 2.3. It is seen that the TPA spectrum peaks at 3.65 eV having phonon side bands at 3.5, 3.3 eV, respectively, which are due to transitions into the kAg state at 3.3 eV (and vibronic progression). The other band seen at 3 eV is due to optical transition into the mA_g state.

4.4.2 Transient photoinduced absorption of D – DOO-PPV (D – polymer) film

Figure 4.7 (a) shows the ultrafast PM spectra of D – polymer film at t = 0 ps, 10 ps, and 100 ps in the spectral range from 1.25 – 2.1 eV, as obtained using pump excitation at 4.1 eV. The spectrum is dominated by the SE (1.9 eV) and PB (2.1 eV) bands. Also, the exciton (PA_1) tail is observed at 1.3 eV. At 100 ps, the spectrum is still clearly observed.

The decay dynamics of the SE, PB, and PA_1 are shown in Figure 4.7 (b). As with H – polymer, PA_1 here is fitted with a double exponential $\tau_1 \approx 5$ ps (10 %) and $\tau_2 \approx 90$ ps (90 %). Also, similar to the H – polymer, the SE and PB decays were fitted using bimolecular recombination kinetics. For the D – polymer, the SE band decays with the parameters: $\tau \approx 200$ ps and $b \approx 0.9 \cdot 10^{-20}$ cm^3/s and the PB band decays with the parameters: $\tau \approx 260$ ps and $b \approx 0.7 \cdot 10^{-20}$ cm^3/s.

Figure 4.8 shows the PMD kinetics of the D – polymer film at two probe frequencies; these are 1.34 eV [Figure 4.8 (a)], which corresponds to PA_1, and 1.96 eV

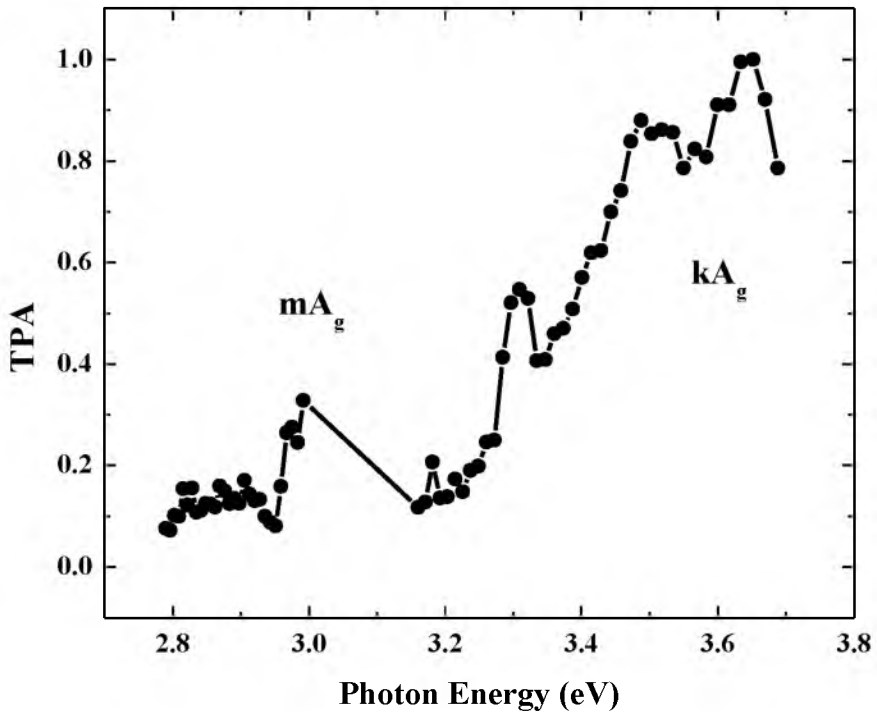

Figure 4.6: The two-photon absorption (TPA) spectrum of the H – DOO-PPV polymer.

[Figure 4.8 (b)], which corresponds to SE. Figure 4.8 (c) compares between the two P(t) on a log-log scale . The polarization memory initial value P(0) is not the same for the SE ($\approx$ 0.2) and PA_1 ($\approx$ 0.45). This can be due to heat, but the kinetics decay is roughly the same for the two probe frequencies, with $\tau \approx$ 2 ps (SE) and 2 ps (PA_1). Since the SE band decay is correlated with that of the PA_1 band, we can conclude that the primary photoexcitations in the D – polymer film are intrachain singlet excitons.

Figure 4.9 shows the TPA spectrum of D – polymer film. The TPA spectrum peaks at 4.6 eV, with no clear phonon side bands. These bands are due to kAg. The other band seen at 2.9 eV is due to transitions into the mA_g state.

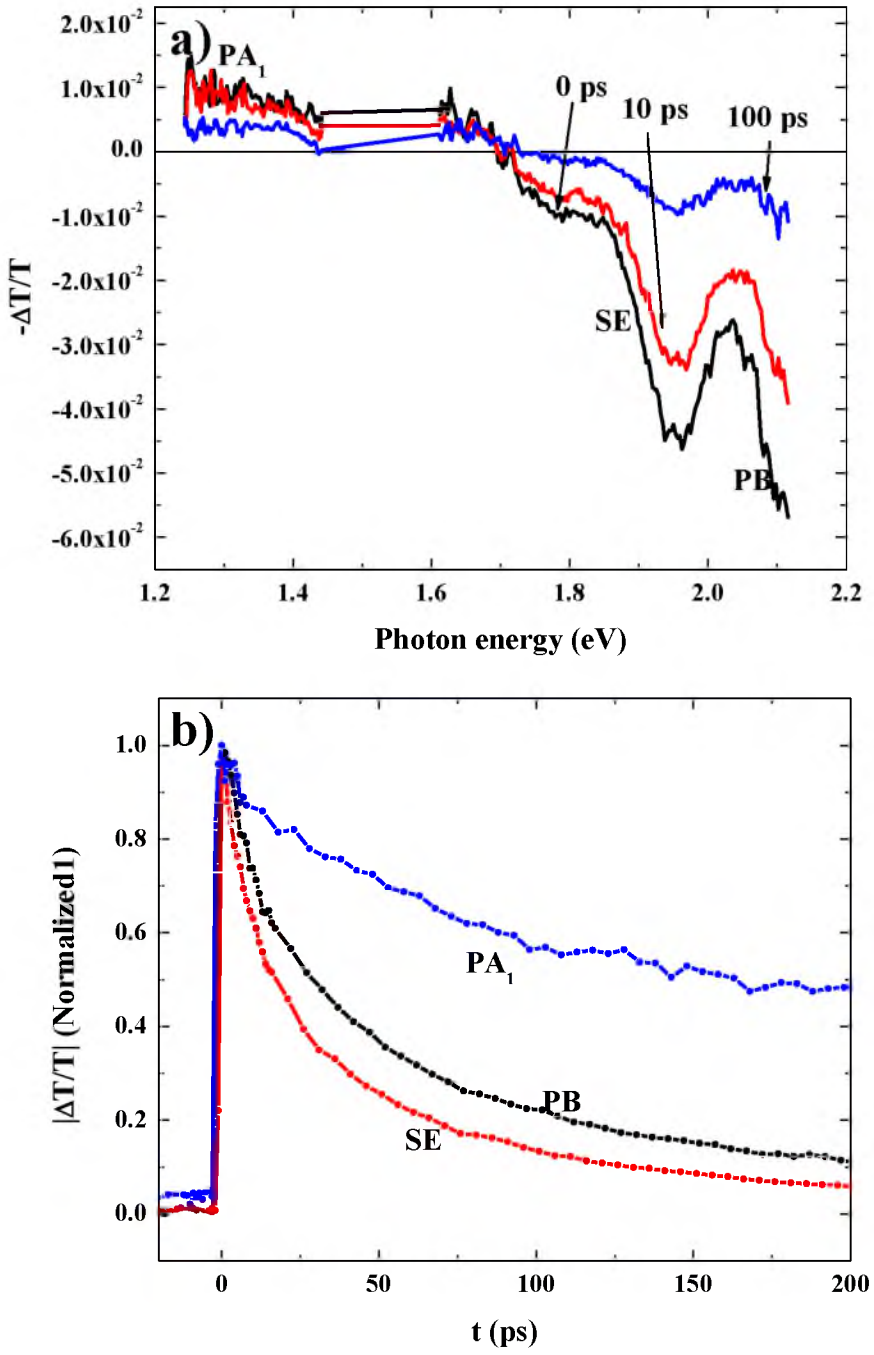

Figure 4.7: Transient PM. (a) The spectrum of D – DOO-PPV film at t = 0 ps, 10 ps, and 100 ps. (b) Decay dynamics at different probe energies of the D – DOO-PPV film.

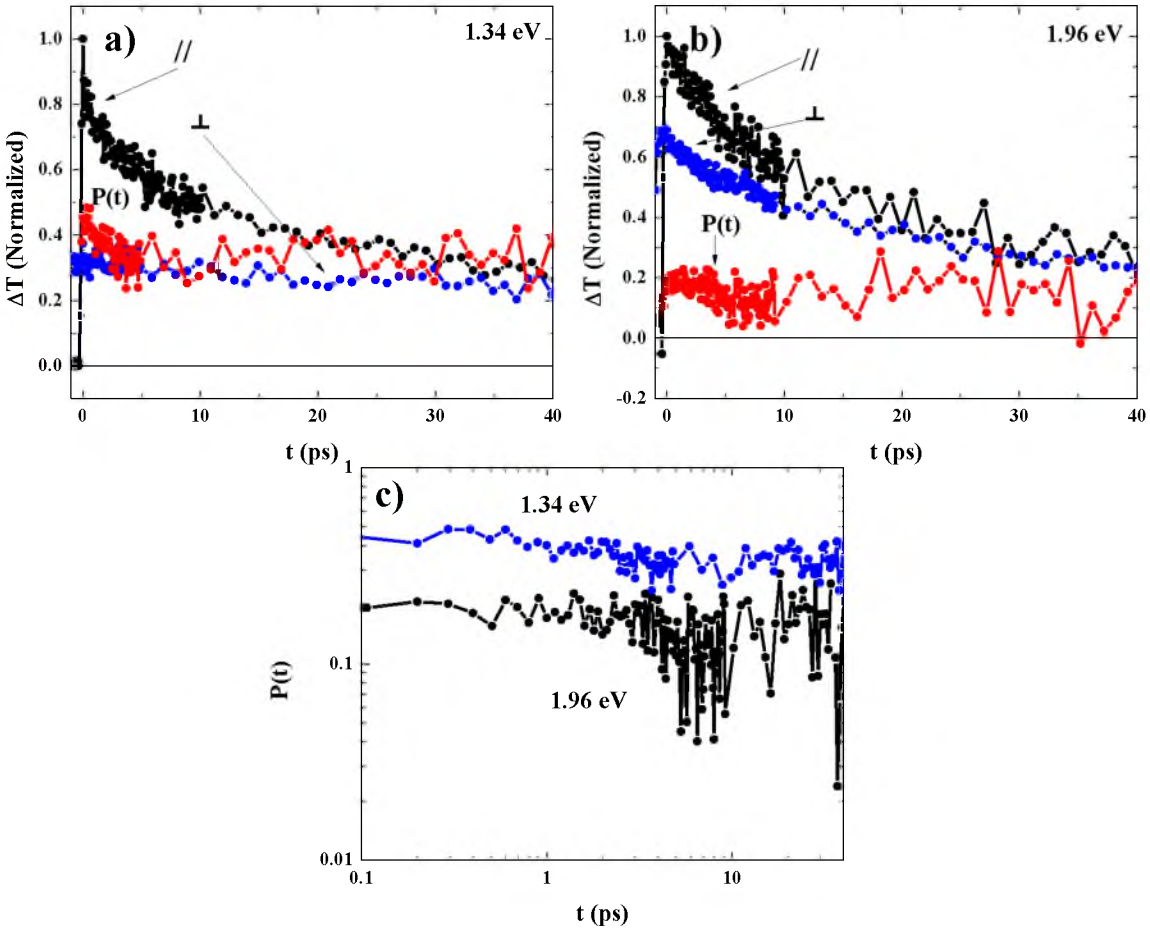

Figure 4.8: Polarization memory decays for the D – polymer at (a) 1.34 eV (b) 1.96 eV. (c) Comparison of P(t) dynamics of (a) and (b).

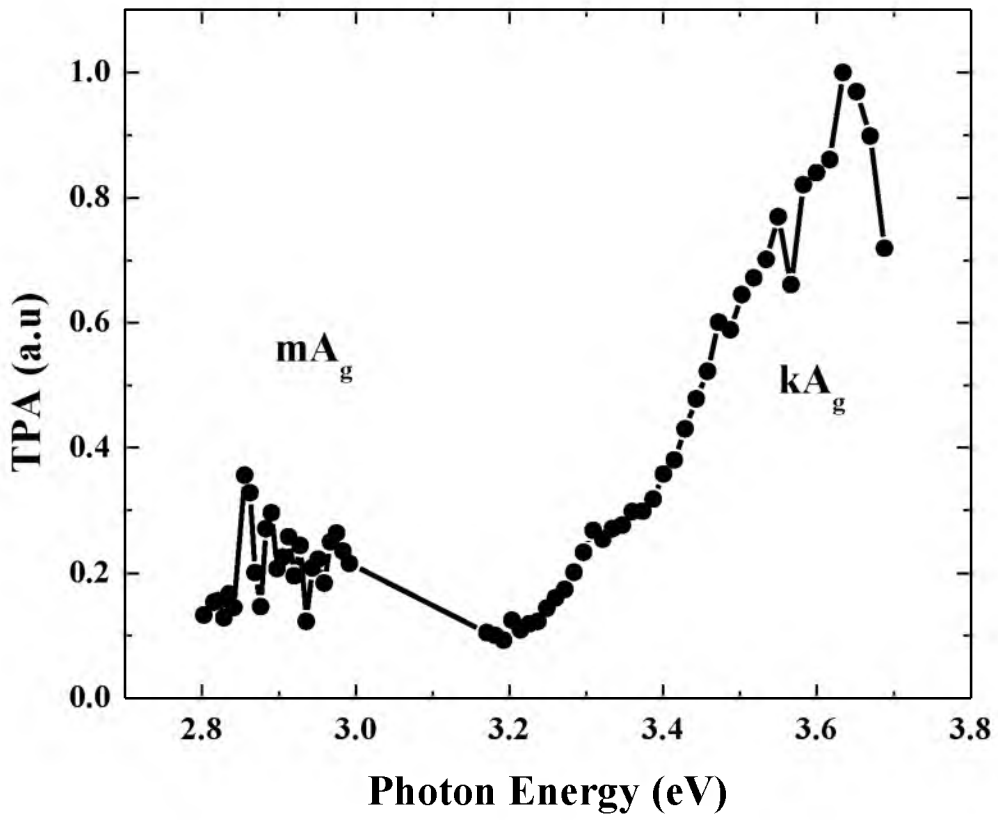

Figure 4.9: The two-photon absorption (TPA) spectrum of D – polymer.

4.4.3 Transient photoinduced absorption of C13 – DOO-PPV (C – polymer) film

Figure 4.10 (a) shows the ultrafast PM spectra of C – polymer film, in the visible range, at t = 0 ps, 10 ps, 100 ps, respectively, using pump excitation at 4.1 eV. Similarly to the other two polymers discussed above, the visible near-IR spectrum here contains SE and PB bands, and a tail of the PA_1 band. The decay dynamics of these bands are shown in Figure 4.10 (b).

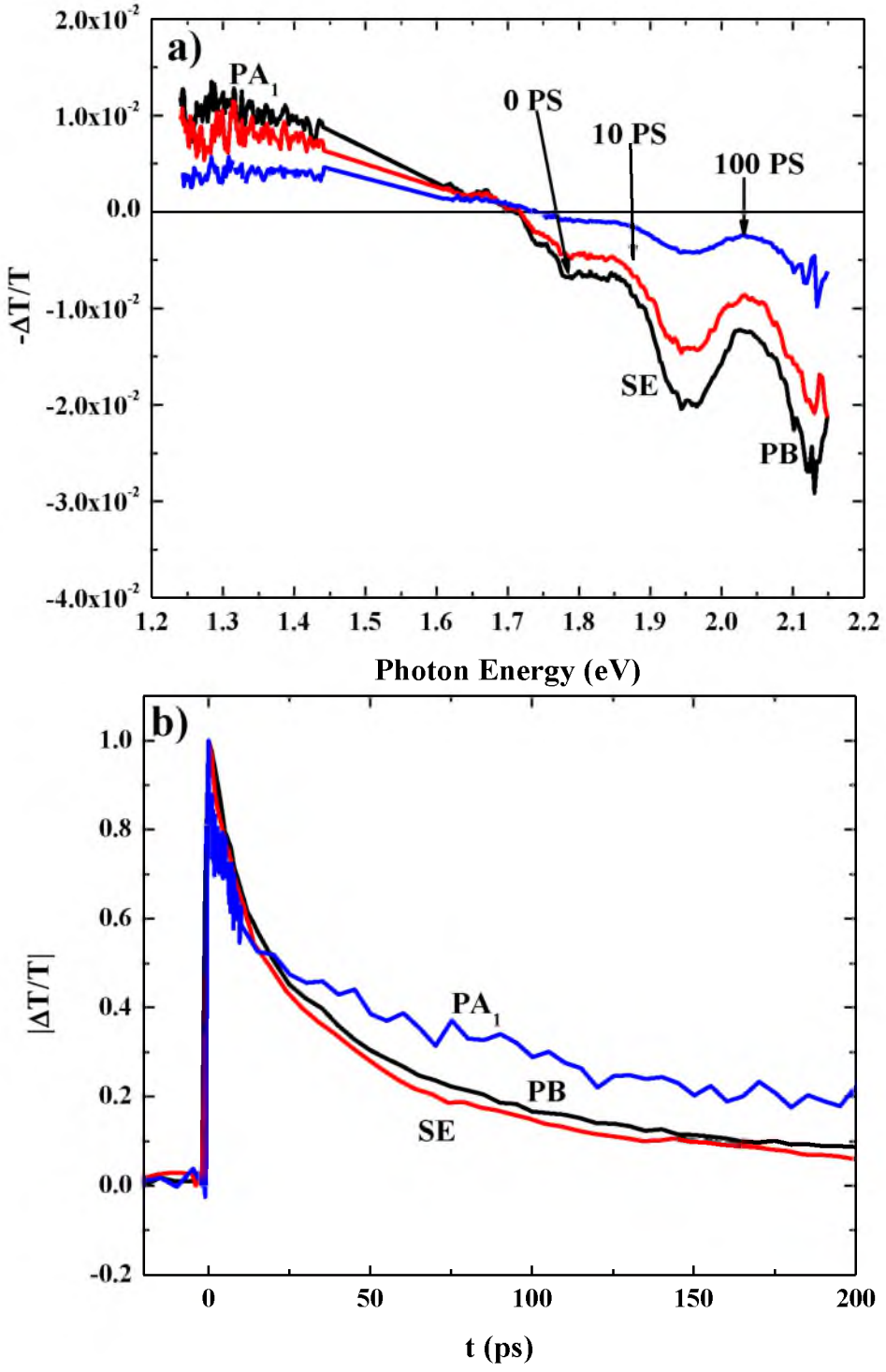

Figure 4.10: Transient PM. (a) The spectrum of C-DOO-PPV film at t = 0 ps, 10 ps, and 100 ps. (b) Decay dynamics at different probe energies of the C – DOO-PPV film.

PA_1 band decay was fitted with a double exponential with time constants of $\tau_1 \approx 8$ ps with 40 % and $\tau_2 \approx 110$ ps with 60 %. The SE and PB were fitted with bimolecular recombination. For the C – polymer, the SE band decays with the parameters: $\tau \approx 112$ ps and $b \approx 0.9 \cdot 10^{-20}$ cm^3/s and the PB band decays with the parameters: $\tau \approx 180$ ps and $b \approx 0.8 \cdot 10^{-20}$ cm^3/s.

4.4.4 Comparison of the obtained photophysics of the pristine isotopes films

Figure 4.11 shows the ultrafast PM spectra of the three isotopes (H –, D –, and C – polymers) of DOO-PPV at t = 0 ps measured under similar conditions such as pump photon energy (3.1 eV), excitation intensity, and temperature. In all three polymer isotopes we observed the same type of PM spectrum that consists of the three bands, SE at 1.8 eV, PB at 2.1 eV, and PA_1 tail at 1.3 eV. When comparing all three isotope films, the H – polymer and C – polymer have the same spectrum. The only difference between the two polymers is the PB, which is stronger in the H – polymer. The D – polymer has a stronger PB and SE, which is in agreement with the longer τ (200 ps). Another difference between the three polymers is the tail of PA_1, which is observed at 1.61 eV in the D – polymer but is not observed in the H, C – polymers.

In order to compare the dynamics of the SE and PB of all three isotopes, we measured the decay at different intensities. The decay rates of the SE and PB were then fitted with bimolecular recombination. Tables 4.1 (PB) and 4.2 (SE) summarized the decay rates, τ's, and the coefficients, b, for all three isotopes.

From this comparison, we can see that the D – polymer has the longest life time

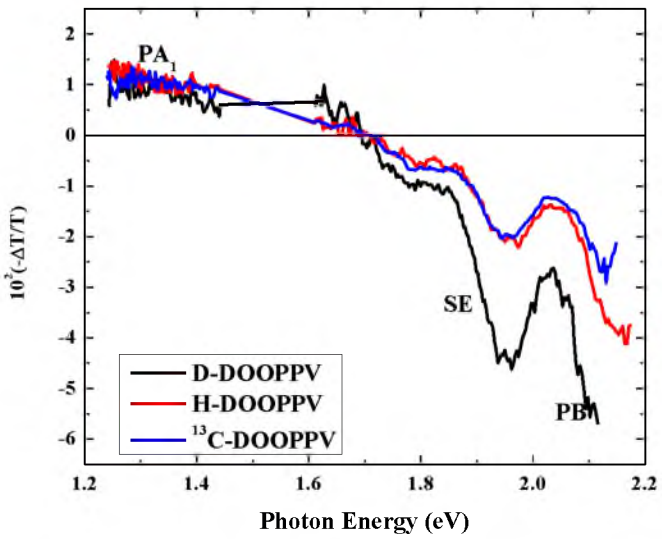

Figure 4.11: The transient PA spectra at t = 0 ps for all three DOO-PPV isotope films (H-, D-, and C- polymers).

Table 4.1: The best fit parameters, τ and b, of the exciton dynamics for the three DOO-PPV isotopes measured at the PB range, using bimolecular recombination kinetics.

	τ	**b**
^{13}C-DOOPPV	180±5	8±1 x10^{-21}
H-DOOPPV	200±7	2±0.4 x10^{-20}
D-DOOPPV	260±10	7±1 x10^{-21}

Table 4.2: The best fit parameters, τ and b, of exciton dynamics for the three DOO-PPV isotopes measured at the SE band, using bimolecular recombination kinetics.

	τ	**b**
^{13}C-DOOPPV	112±2	9±1 x10^{-21}
H-DOOPPV	134±3	2±0.6 x10^{-20}
D-DOOPPV	197±7	9±1 x10^{-21}

for the SE and PB as compared to the other two isotopes. There is not much difference in the decay rate between the H, C – polymers (see Discussion).

Figure 4.12 shows the Raman scattering measurement of the D – polymer and H – polymer (the C – polymer is not shown but the C, H – polymer Raman spectra are similar). The Raman scattering spectra show two main Raman-active vibrational modes: one at $\nu \approx 1300$ cm^{-1}, which is related to the C – C stretching mode, and another at $\nu \approx 1500$ cm^{-1}, which is related to the C = C stretching mode. As seen, the D – polymer Raman spectrum is red-shifted by ≈ 3 % from the H – polymer [4.5]; this is in agreement with the expected isotope shift of the CH (CD) units resulting from the square root of the mass ratio rule [4.13], namely $\nu(CH)/\nu(CD) = [m(CD)/m(CH)]^{1/2} \approx 1.037$.

The change in the isotope molecular weight leads to a change in the polymer vibrational frequencies. In turn, the vibration of the polymer is associated with the electronic configuration of the material and affects the optical transitions.

Figure 4.13 shows the PMD kinetics of the H, D – polymer film at the two probe frequencies: 1.34 eV [Figure 4.13 (a)], which corresponds to PA_1 and 1.96 eV [Figure 4.13 (b)], which corresponds to the SE. For the PA_1 band, the polarization memory initial value P(0) is roughly the same for the H (≈ 0.5) and D (≈ 0.46) – polymers. The decay constant, τ, is approximately the same with 3 ps for the H – polymer and 2 ps for the D – polymer. As for the SE band, again the polarization memory initial value P(0) is roughly the same for the H (≈0.25) and D (≈0.2) – polymers. The decay constant, τ, is roughly the same with 7 ps for the H – polymer and 2 ps for the D – polymer. We can conclude that there is not a significant difference in the PMD between the D and H – polymer.

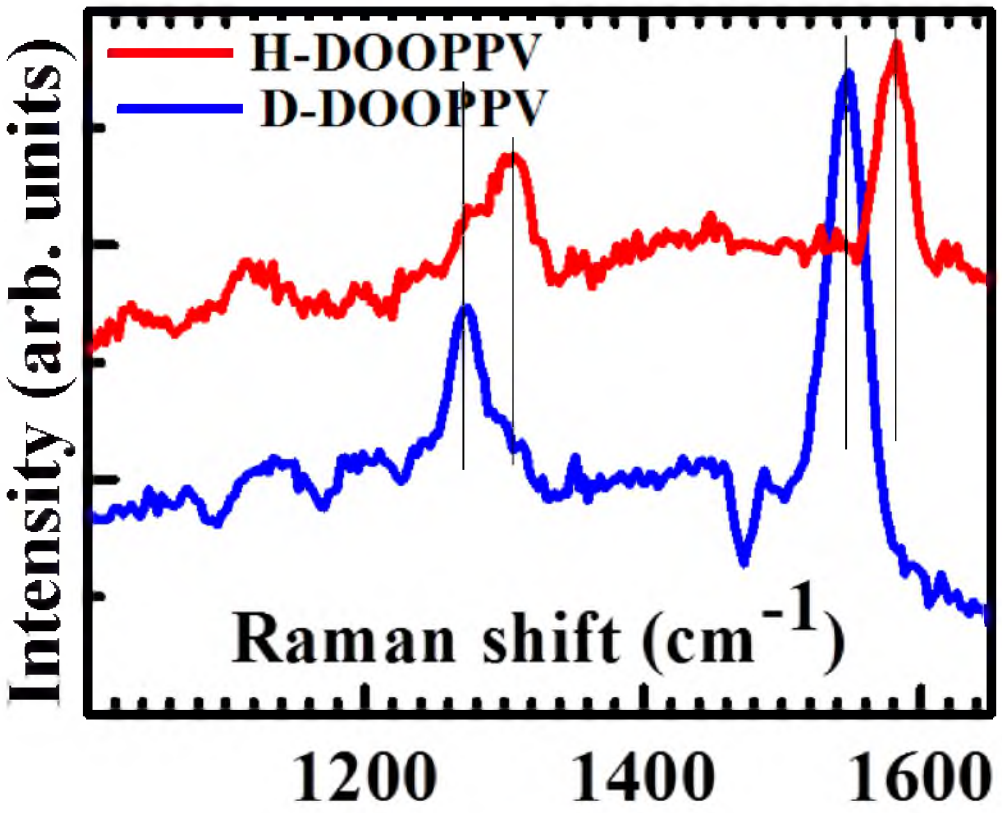

Figure 4.12: The resonant Raman spectra of H-DOO-PPV and D-DOO-PPV polymers that show isotope shift for both C-C and C=C stretching vibration frequencies.

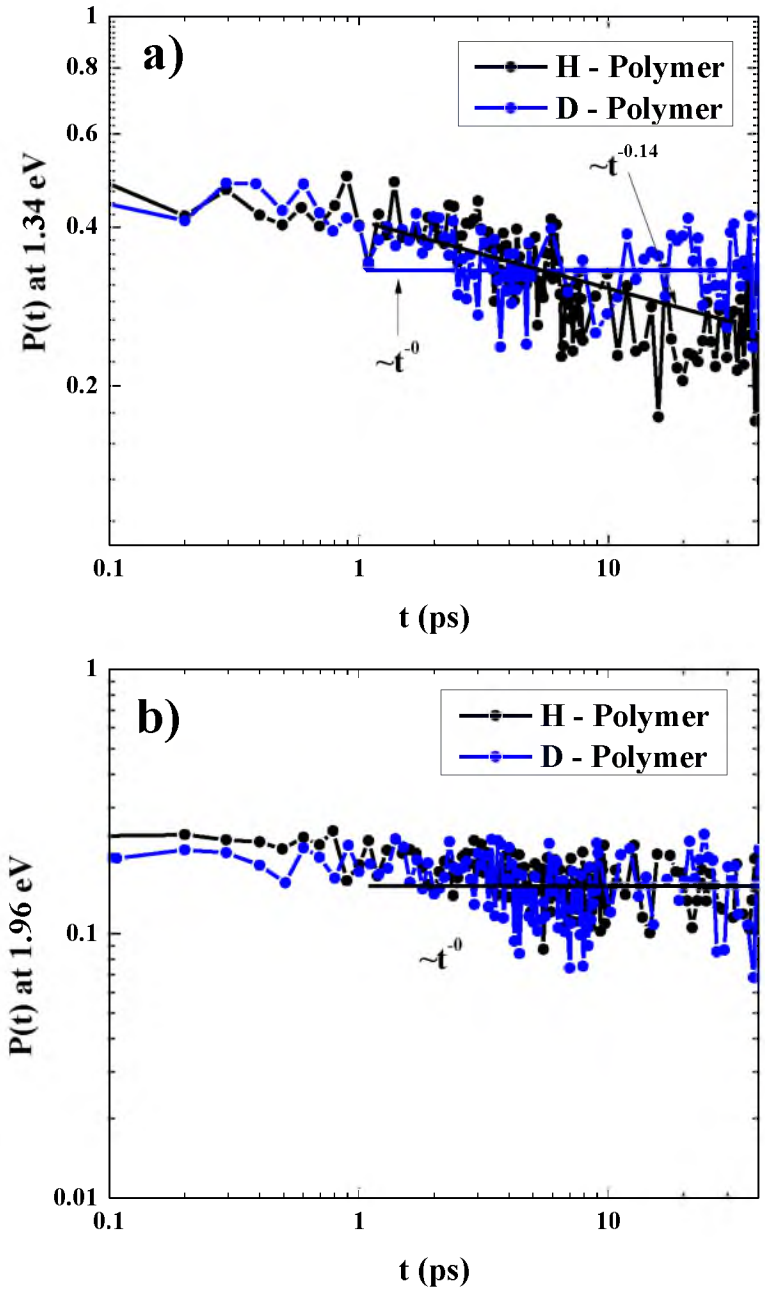

Figure 4.13: Comparison of the polarization memory decay of the H, D – polymer on a log-log scale at (a) 1.34 eV and (b) 1.96 eV. (c) The comparison of P(t).

Figure 4.14 compares the TPA spectra of H and D – polymer films. For both polymers, the band related with the kA_g state is at 3.6 eV, but the H – polymer shows phonon side bands, whereas the D – polymer does not show prominent phonon side bands. The band which related to the mA_g state of the D – polymer (2.9 eV) is red-shifted compared to that in H – polymer (3 eV).

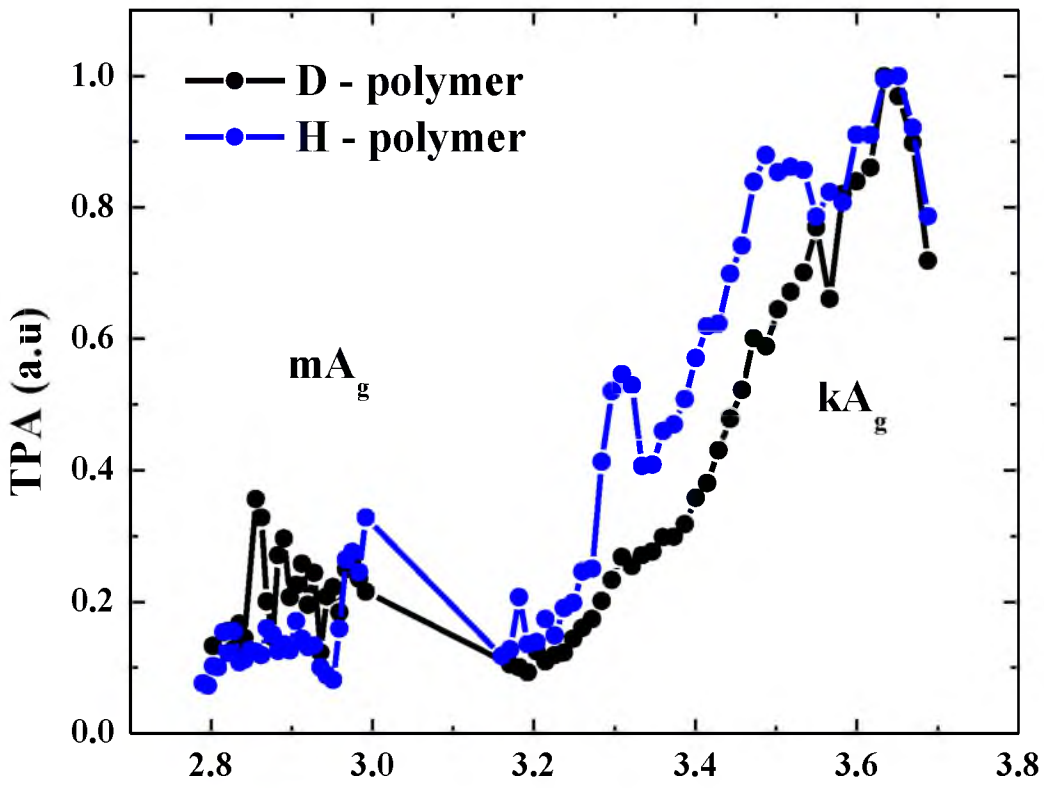

Figure 4.14: Comparison of TPA spectrum of D, H – polymer.

4.4.5 Discussion

The main purpose of studying transient photomodulation (PM) spectroscopy of DOO-PPV isotope-rich films is to see if and how the isotope effect comes into play in the PM spectrum, the formation of different types of photogenerated species within the spectral range of our interest, and whether or not the transient decay mechanism is affected by the change in the molecular isotopes. In order to accomplish these goals, the three isotope films (D – polymer, H – polymer, and C – polymer) were prepared, and PM measurements were carried out under similar conditions.

We have found that the PM spectra are roughly the same in all three isotopes, except for the fact that the D – polymer SE and PB intensity is stronger than the other two polymers. The tail of the exciton band, PA_1 appears at 1.6 eV. By taking into account the PM spectra and PMD, which are relatively similar for all polymers, we can claim that the PA_1 band is due to intrachain singlet excitons.

The PM spectrum of excitons in DOO-PPV is schematically explained in Figure 4.15, which shows the ground and excited electronic levels and their associated transitions in a configuration coordinate (Q) diagram. The pump beam induces the transitions from the ground state ($1A_g$) to the first allowed excitonic state ($1B_u$), which contains many vibrational states, following a relatively small relaxation to the lowest vibronic state ($\approx$ 0.1 eV). SE (and PL) occurs between the relaxed $1B_u$ and $1A_g$. In addition to the SE and PL, a PA transition from $1B_u$ to higher energy levels can occur between two even-parity states, i.e., mA_g at $\approx$ 3 eV and $kA_g \approx$ 3.6 eV. The energy of the $1B_u$ state is extracted from the electroabsorption (EA) spectrum [4.21] at the zero crossing $\approx$ 2.25 eV. It is due to the quadratic Stark-shift of the $1B_u$ exciton at this energy

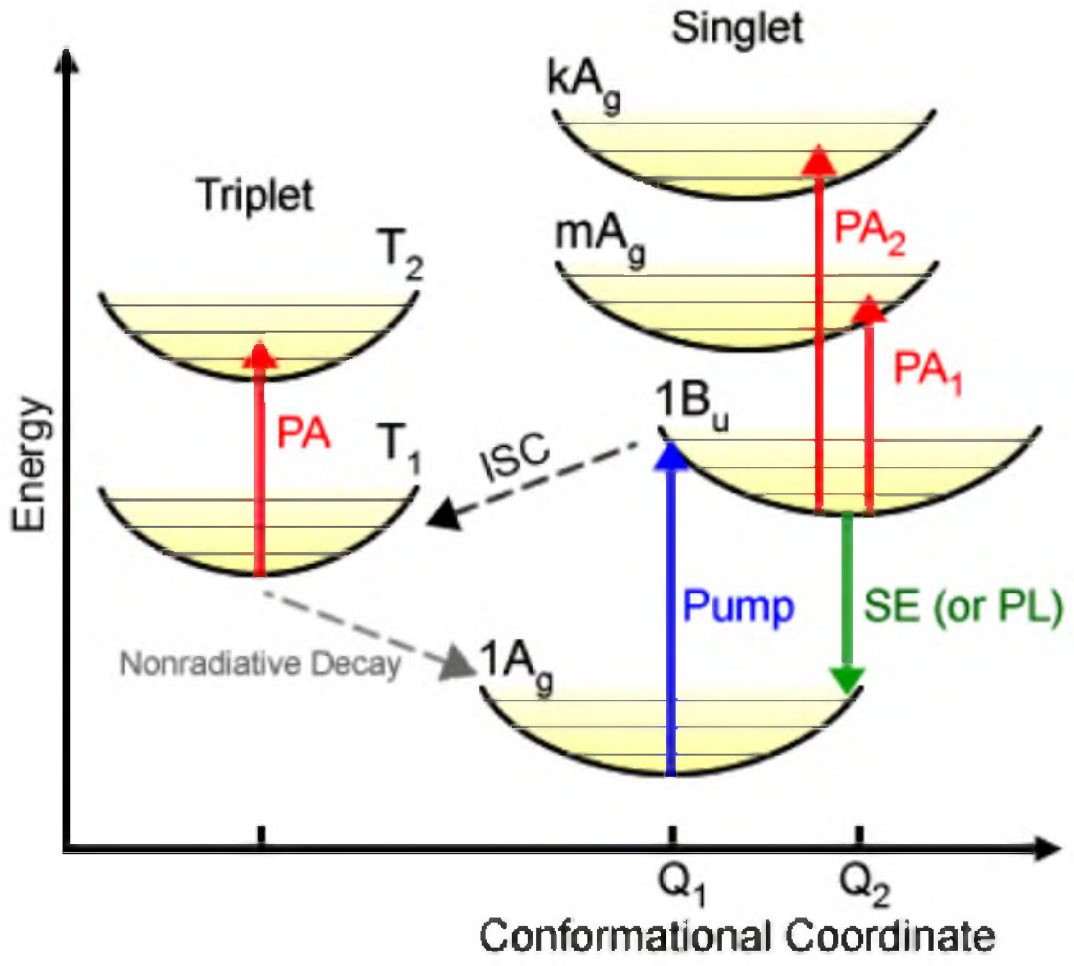

Figure 4.15: Photoexcitation model in conjugated polymers with nondegenerate ground states.

[4.22]. The EA spectrum can also give us the two A_g states. These two bands are due to even parity states (mA_g and kA_g), which become partially allowed in EA due to symmetry breaking caused by the applied electric field. The energy difference between $1B_u$ and mA_g is ≈ 0.75 eV; however, we have observed the PA_1 band at a higher energy range than this value in all three DOO-PPV isotopes ≈ 1 eV.

The reason for the blue shift of the singlet exciton band in our PM spectrum as compared to the singlet exciton band inferred from the EA and TPA measurements can be due to the fact that the $1B_u$ level is composed of many vibrational states, in which the lowest has index 0 and above it, the index is 1, 2, 3, etc. an increase of $\approx$ 0.18 eV. The exciton PA peak observed in our transient PM spectrum of isotopes might not be the 0 – 0 transition. When looking at the TPA, the D – polymer mA_g state is red-shifted compared with the H – polymer. This shift can indicate that the peak is sensitive to the vibrational mode frequency, which changes according to the isotope molecular mass. The increase in molecular mass always reduces the C = C stretching vibrational frequency, and consequently, the 0 – n transition associates with the reduced vibrational frequency are red-shifted. The red-shift in the vibrational frequency of the D – polymer is verified by the Raman scattering spectroscopy. We may conclude that the main reason for the red-shift in the DOO-PPV film of the mA_g state is the decrease in frequency of the C = C stretching vibration.

The other goal of this study on PM spectroscopy is to examine the isotope's effect on the transient decay kinetics. The comparison of decay dynamics of all three isotopes at the same probe energy [Table 4.1, Table 4.2] shows that the SE and PB decay slower in the D – polymer.

This also fits with the results of the PLQE where the D – polymer has the highest value: $\eta \approx 13$ %.

The decay kinetics of the excitons in DOO-PPV is schematically explained in Figure 4.16. The exciton recombination kinetics in all three isotopes is composed of both monomolecular (intrinsic) and bimolecular (exciton-exciton annihilation) processes

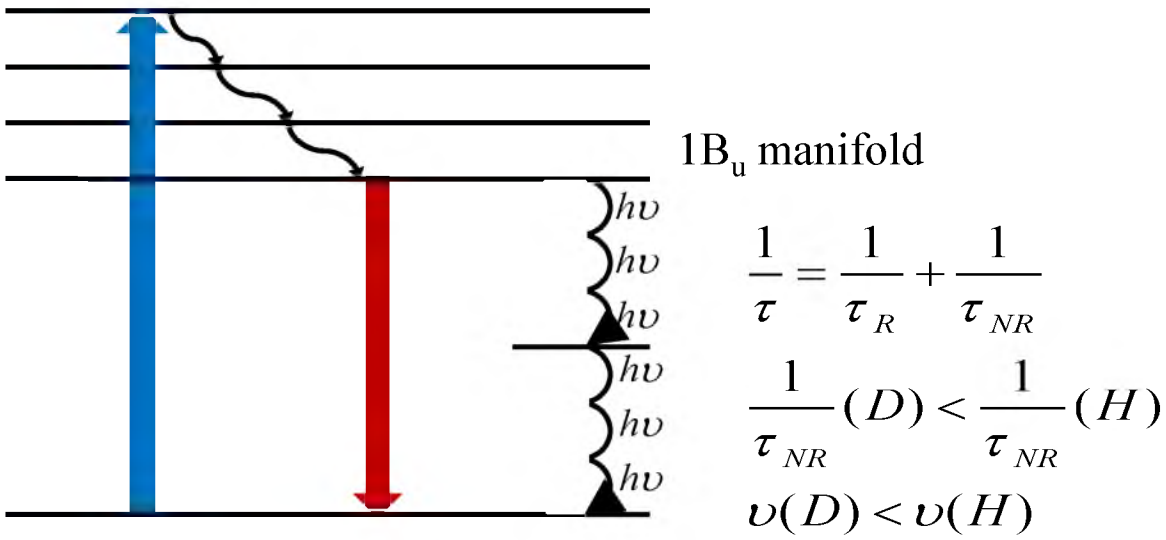

Figure 4.16: Schematic description of exciton recombination processes in DOO-PPV polymer.

[4.12]. The dynamic of the D, H, ^{13}C – polymers was fitted with global fitting by using Equation 2.28. We found that the bimolecular coefficient, b, is roughly the same for all the isotopes films, but the monomolecular coefficient, τ, was longest for the D – polymer. Therefore, we can conclude that the exciton recombination in DOO-PPV consists of two processes: one is intrinsic monomolecular (where τ is not constant), and the second is exciton-exciton annihilation having bimolecular kinetics (where b is similar for all polymers).

The intrinsic process also consists of two components: radiative and non-radiative. If we assume that the radiative rate does not change with the isotope exchange, we found that the intrinsic nonradiative (INR) rate depends on the isotope, since the decay kinetics are the slowest in D – polymer. The INR rate depends on the number quanta of vibrations that take part in the process.

Since the vibrational frequencies of D – DOO-PPV are small, the INR process requires more vibrational quanta, and thus, the INR rate of this isotope is the smallest. This may explain the slow kinetics of the PA obtained for this isotope.

4.5 Singlet fission in D – polymer

The traditional solar cells create one electron-hole pair for each absorbed photon. In order to improve solar-cell efficiency, two (or more) electron-hole pairs may be generated from just one photon. Singlet fission is a process in which the singlet state may convert into two triplet exactions, each with half the energy of the original singlet. In solar cells, this could potentially double the photocurrent.

Taking the thermal loss into account, the maximum solar-to-electric power conversion efficiency of the traditional solar cell is determined by the Shockley–Queisser limit of $\approx$ 31% [4.23]. With SF, the power conversion efficiency can reach 45 %

Harvesting of multiple electron–hole pairs from singlet fission was confirmed in pentacene/C_{60} or tetracene/C_{60} solar cells [4.24 – 4.26]. A major obstacle to the application of singlet fission in solar cells is that high singlet-fission yields can be found only in a few molecular systems such as tetracene and pentacene [4.27].

In order to have singlet fission, the singlet (S) exciton energy has to possess at least twice the triplet (T) energy, i.e., $E(S) \geq 2 \times E(T)$ [4.27].

Figure 4.17 (a) shows the decay kinetics of the D – polymer at different probe energies up to 2 ns. The dynamic at 1.6 and 1.34 eV both belong to the singlet exciton, which peaks at $\approx$ 1 eV. It is obvious that the decay dynamics of the exciton are not the same across the spectrum; this indicates that various photoexcitations contribute to the

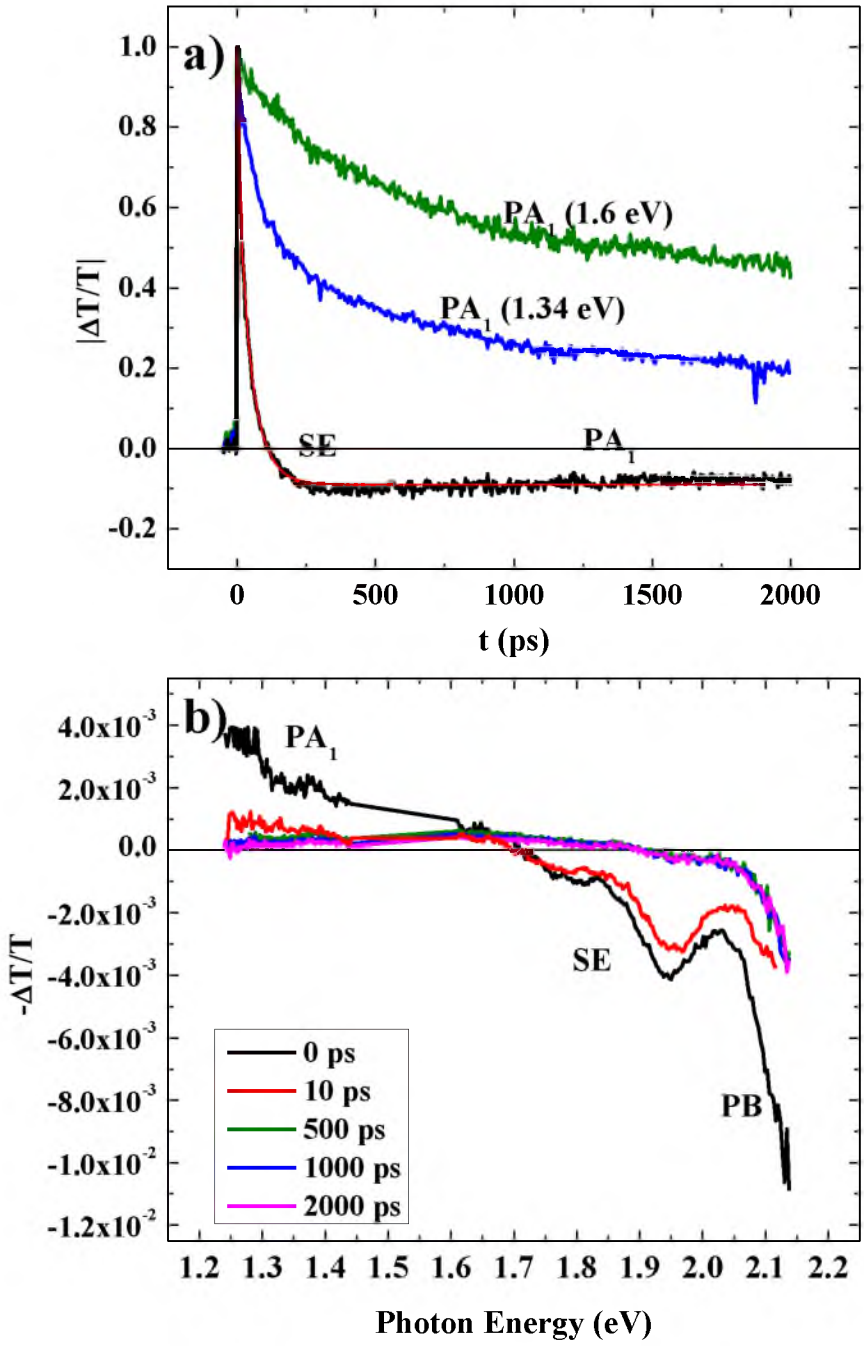

Figure 4.17: The D – polymer decay kinetic on longer time scale. (a) Decay kinetics at different probe energies up to 2 ns. (b) Spectrum of the D – polymer at different delay times.

spectrum. From the decay kinetics, is it clear that the SE converts into the singlet exciton at around 100 ps (the SE was measured at 1.8 eV).

The transient ultrafast photomodulation (PM) spectra of D – polymer film at photon energy spectral range from 1.2 – 2.4 eV is shown in Figure 4.17 (b). The PM spectra were measured at t = 0 and 10, 500, 1000, 2000 ps time delay. At t > 500 ps, the SE band already converted into PA of the singlet exciton. However, the spectrum still contains the PB and PA_1 bands. In order to try to identify the different photoexcitations that contribute to the spectrum at longer time, we subtract the signal at 1 ns from the signal at 0 ns; this is shown in Figure 4.18. The result is the formation of a photoinduced absorption band in 1 ns at 1.4 eV.

Figure 4.19 (a) shows the CW photoinduced absorption at low temperature. The band at 1.4 eV is identified as a triplet [4.18]. By comparing the CW PA and the resulting spectrum at 1 ns, we can conclude that the signal at 1 ns is due to the triplet exciton. The intersystem crossing (ISC) process occurs in the time domain of 10 to 100 ns [4.28]. Therefore, the triplet exciton generation cannot be via ISC process. Figure 4.19 (b) summarizes the processes that take place in the D – polymer.

From TPA data, we found that the mAg state is at 2.9 eV. The pump-probe measurements were done using 3.1 eV as the excitation source. This suggests that the mAg state is also excited. From other measurements of the triplet energy, we get 2 X energy(triplet) = 2.8 eV. Therefore, mA_g can undergo fission into two triplets (2x1.4 eV) during the thermalization process and this can explain the triplet exciton that is observed in less than 1 ns.

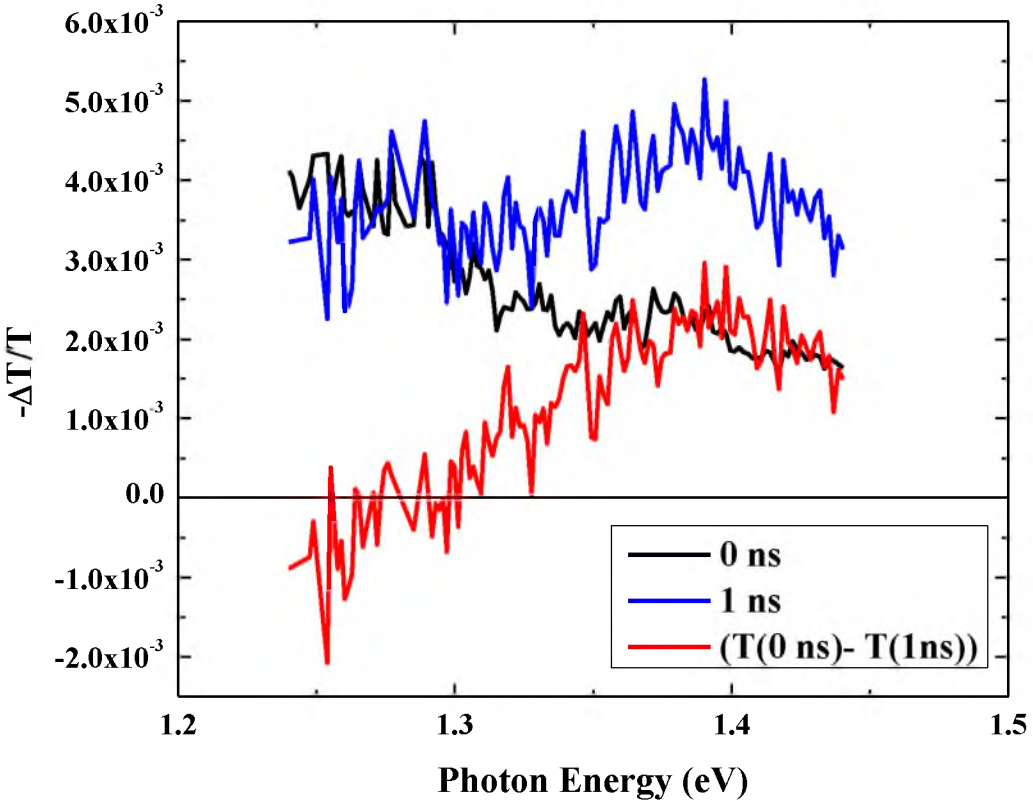

Figure 4.18: The difference (shown in red) between the D-polymer spectrum at 0 ns (black) and the spectrum at 1 ns (blue).

4.6 Conclusion

In this chapter, we used the pump-probe spectroscopy technique to study the transient ultrafast photophysics of pristine films of three DOO-PPV isotopes (D – polymer, H – polymer, and C – polymer). The linear absorption spectra, PL spectra, and PLQE measurements were also performed on films of all isotopes. The transient spectra of all three pristine isotope films at t = 0 ps were found to be similar to each other.

From the transient decay kinetics measurements, we found that the exciton recombination in DOO-PPV consists of two processes. These are: intrinsic

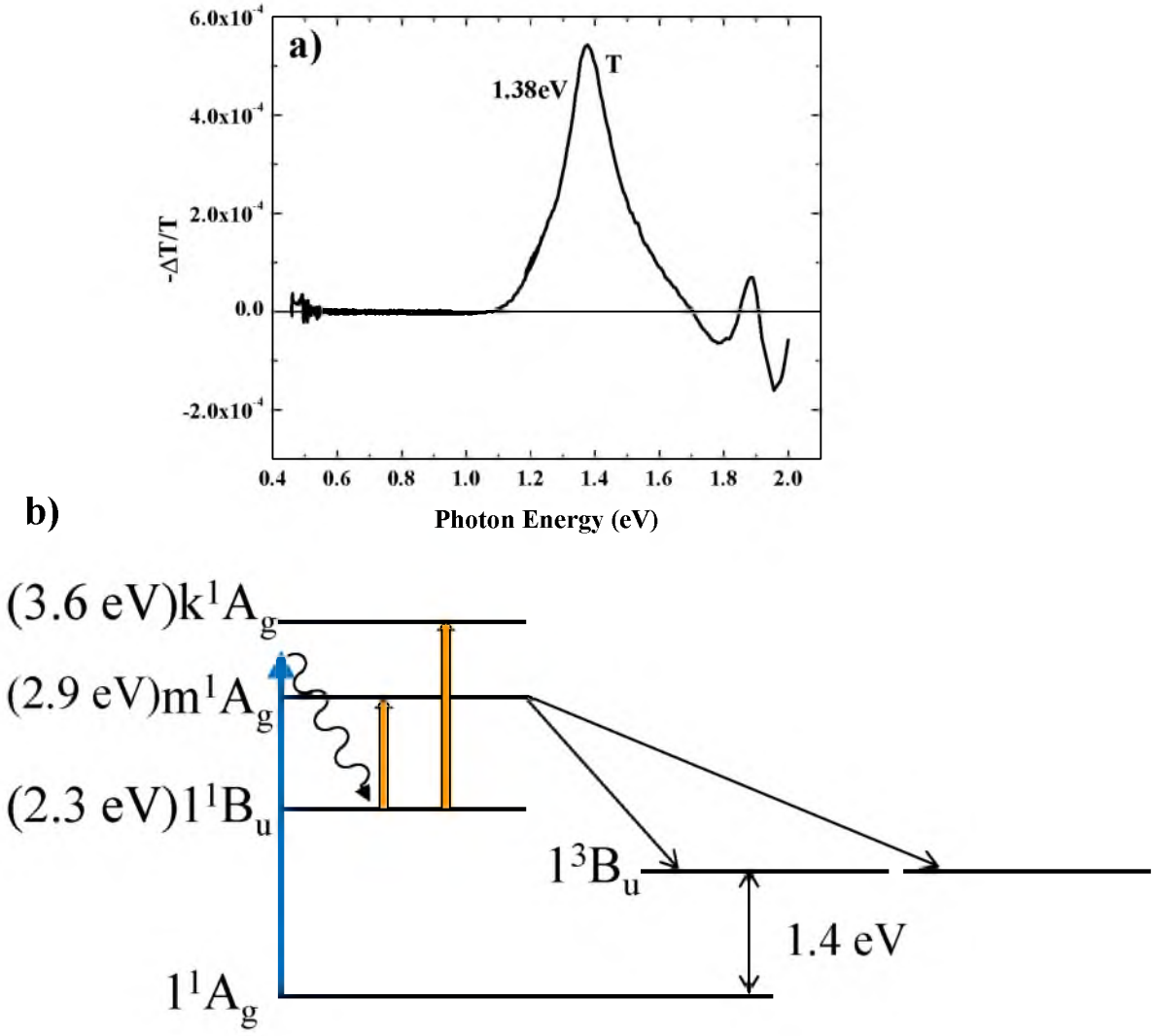

Figure 4.19: Singlet fission in D – polymer; (a) The CW photoinduced absorption spectrum of the D – polymer. (b) Schematic description of the formation of triplet exciton processes in DOO-PPV polymer via singlet fission.

monomolecular, and exciton-exciton annihilation (bimolecular). The SE and PB decay kinetics are the slowest in the D – polymer.

This can be due to the increase of the molecular mass, which ultimately decreases the vibrational frequency coupled to the electronic transitions (phonon replica); this leads, in turn, to the decrease of the intrinsic nonradiative (INR) rate and as a result, the increased time constant. We also saw the effect of the increase in molecular mass in the TPA measurements were the D – polymer is red-shifted compare to the H – polymer. The red-shift in the vibrational frequency is confirmed using Raman spectroscopy. The polarization memory results of the H, D – polymers were similar.

In the D – polymer, different probe frequencies of PA_1 show different decay kinetics, which result from various photoexcitations that contribute to the spectrum. Comparing the spectrum at 1 ns time delay to the CW PA shows the formation of triplet exciton in less than 1 ns. This is possible due to singlet fission of mA_g (at 2.9 eV) into two triplets (2 X 1.4 eV).

4.7 Reference

[4.1] M. Furukawa, K. Mizuno, A. Matsui, S.D.D.V. Ruhoopth, and W. C. Walker. J. Phys. Soc. Japan 58, 2976 (1989).

[4.2] U. Rauscher, H. Bassler, D. D. C. Bradley and M. Hennecke, PRB 42, 9840 (1990).

[4.3] H. Bassler, M. Gailberger, R. F. Mahrt, J. M. Oberski, and G. Weiser. Synth. Metals 49, 341 (1992).

[4.4] S. Webster and D. N. Batchelder, Polymer, 37, 4961, (1996).

[4.5] T. D. Nguyen, G. H. Markosian, F. Wang, L. Wojcik, X. G. Li, E. Ehrenfreund and Z. V. Vardeny, Nature Mater. 14 (2010).

[4.6] R. Mahrt, J. Yang, A. Greiner, H. Bessler and D.D.C. Bradley, Macromol. Chem. Rapid Commun. 11, 415 (1990).

[4.7] I. D.W. Samuel, B. Crystall, G. Rumbles, P.L. Burn, A. B. Holmes, and R.H. Friend, Synth. Metals 54, 281 (1993).

[4.8] B. R. Hsieh, Y. Yu, A. C. Vanlaeken, and H. Lee, Macromolecules 30, 8094 (1997).

[4.9] J. Q. Pan, Z. K. Chen, Y. Xiao, and W. Huang, Chinese J. Poly. Sci. 18, 541 (2000).

[4.10] M .Yan, L. J. Rothberg, F. Papadimitrakopoulos, M. E. Galvin, and T. M. Miller, PRL. 72, 1104 (1994).

[4.11] S. V. Frolov, Ph.D thesis, University of Utah, (1996).

[4.12] I. Martini, A. D. Smith, and B. J. Schwartz, PRB 69, 035204 (2004)

[4.13] Z. V. Vardeny, O. Brafman, E. Ehrenfreund, Solid State Commun. 53, 615 (1985).

[4.14] M. Chandross, S. Mazumdar, M. Liess, P. A. Lane, Z. V. Vardeny, M. Hamaguchi, and K. Yoshino, PRB 55, 1486 (1997).

[4.15] S. V. Frolov, M. Shkunov, Z. V. Vardeny, and K. Yoshino, PRB 56, R4363 (1997)

[4.16] S. V. Frolov, Z. Bao, M. Wohlgenannt, and Z. V. Vardeny, PRB 65, 205209 (2002).

[4.17] C.-X. Sheng, M. Tong, S. Singh, and Z. V. Vardeny, PRB 75, 085206 (2007).

[4.18] Handbook of Conducting Polymers, 3rd ed., edited by T. A. Skotheim and J. R. Reynolds CRC, Boca Raton, (2007).

[4.20] S. Singh, T. Drori, and Z. Valy Vardeny, PRB 77, 195304 (2008)

[4.21] S. V. Frolov, M. Liess, P. A. Lane, W. Gellermann, Z. V. Vardeny, M. Ozaki, and K. Yoshino PRL 78, 4285 (1997).

[4.22] S. Guha, J. D. Rice, Y. T. Yau, C. M. Martin, M. Chandrasekhar, H. R. Chandrasekhar, R. Guentner, P. Scanduicci de Freitas, and U. Scherf, PRB 67, 125204 (2003).

[4.23] Shockley, W. & Queisser, H. J. J. Appl. Phys. 32, 510, (1961).

[4.24] Jadhav, P. J., Mohanty, A., Sussman, J., Lee, J. & Baldo, M. A. Nano Lett. 11, 1495, (2011)

[4.25] Daniel N. Congreve, Jiye Lee, Nicholas J. Thompson, Eric Hontz, Shane R. Yost, Philip D. Reusswig, Matthias E. Bahlke, Sebastian Reineke, Troy Van Voorhis, Marc A. Baldo, science, 340, 334, (2013).

[4.26] A. Rao, M.W.B. Wilson, J. M. Hodgkiss, S.A. Seifried, H. Bassler, and R.H. Friend, J. Am. Chem. Soc. 132, 12698 (2010)

[4.27] M.. Smith, and J. Michl, Chem. Rev. 110, 6891, (2010)

[4.28] M.C Hanna, A.J Nozik. J. Appl. Phys. 100, 074510 (2006)

CHAPTER 5

TIME-RESOLVED ENERGY TRANSFER IN POLYMERS DOPED WITH 'HEAVY ATOMS' MOLECULES

5.1 Introduction

Organic light emitting diodes (OLEDs) have been the subject of interest for lighting applications due to their potentially large area, 2-dimensional light sources, the possibility of tunable electro-optical properties, and relatively cheap production. In order to achieve white broadband emission for organic lighting, the combination of organic polymers and molecules with different emission spectra were investigated in this work.

Figure 5.1 (a) shows the working principal of OLEDs. It is quite simple. First, charged carriers are injected into the device, and then, the carriers are transported into the active layer. In the active layer, the electrons and holes recombine to basically form an exciton. Eventually, the exciton decays and emits light. Figure 5.1 (b) shows an OLED device layout. In this work, we used the blend of Polyfluorene (PFO), a host, and Iridium III molecule ($Ir(btp)_2acac$), which acts as a guest, as the active material for the OLED device.

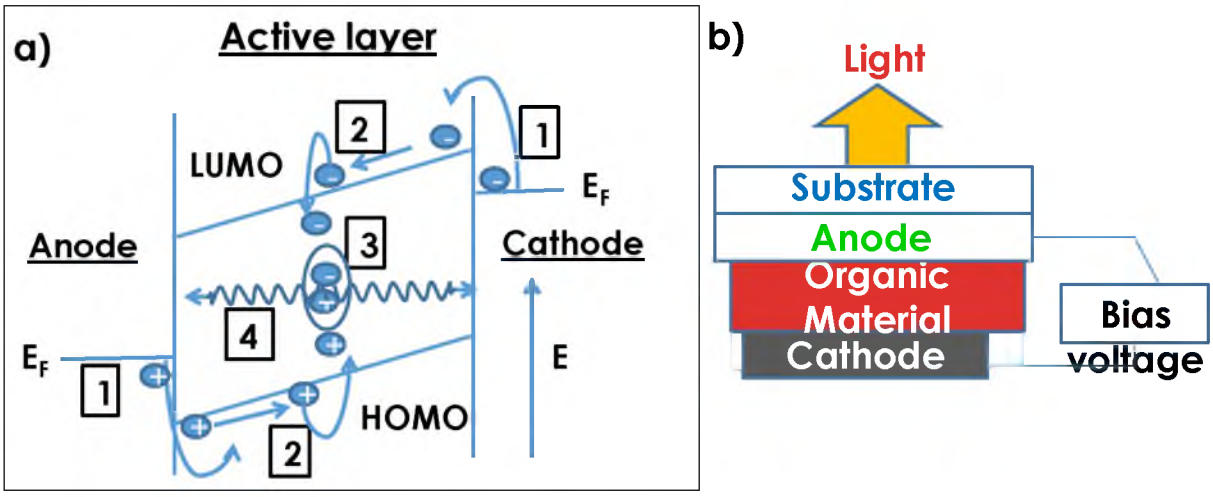

Figure 5.1: The OLED picture. (a) The working principal of OLEDs. (b) OLED device layout.

The PFO is an attractive material for applications in optoelectronics [5.1, 5.2]. The PFO has a high photoluminescence quantum efficiency (about 40%), good charge-transport characteristics, thermal stability, and the ability to change physical parameters, such as the emission wavelength, by blending with other polymers to create copolymers [5.3 – 5.5]. PFO also has a complex morphological behavior with a variety of phases, creating different electronic and optical properties [5.6, 5.7].

PFO presents different forms of (para)crystalline order. A spin-cast PFO film from a solution creates a glassy sample: α phase. With thermal treatment, the β phase can be obtained. The optical properties of phase β and α are completely different from one another [5.6]. In this work, all films were spin cast from solutions; therefore, the focus of this chapter is on phase α of PFO.

The efficiency of OLEDs has been dramatically improved by using heavy metal phosphorescent molecules. This is because heavy atoms induce spin orbit coupling, which increases the efficiency for the intersystem crossing process from the singlet to the

triplet state. As a result, this leads to very efficient OLED devices that are able to use both singlet and triplet electrogenerated excited states [5.8 – 5.10].

Cyclometalated Ir(III) complexes are promising candidates for phosphorescent dopants because they can emit with high efficiency, at room temperature, from the triplet metal-to-ligand charge transfer (^{3}MLCT) state [5.17, 5.18].

In this work, we used Iridium (III)complex; $Ir(btp)_2acac$, since the absorption spectrum of the Ir molecule complex overlaps with the emission spectrum of PFO. This can increase the efficiency of the energy transfer for nearly 100% overall [5.19].

5.2 Materials

For the host polymer, we used Poly[2,7-(9,9-di{(S)-3,7 dimethyloctyl}fluorene)] (**PFO**), [Figure 5.2 (a)] and for the guest molecule, we used Iridium (III) bis(2-(2'-benzo-thienyl) pyridinatoN,$C^{3'}$) (acetyl-acetonate) (**$Ir(btp)_2acac$**) [Figure 5.2 (b)].

Both materials powders were originally dissolved in toluene solvent. The PFO was dissolved with the ratio of 10 mg to 1 ml and the Ir molecule was dissolved at 1 mg to 1 ml. Afterward, both solutions were mixed with a different percentage of the guest molecule (0, 0.02, 3, 5, 7). Finally, the solutions were spin cast into films, at a speed of 800 rpm, on either sapphire or glass substrates.

5.3 Linear absorption and photoluminescence spectra

Figure 5.3 (a) shows a normalized O.D. and PL spectra of the PFO and Ir complex. The linear absorption, in terms of optical density (O.D.), was measured using a

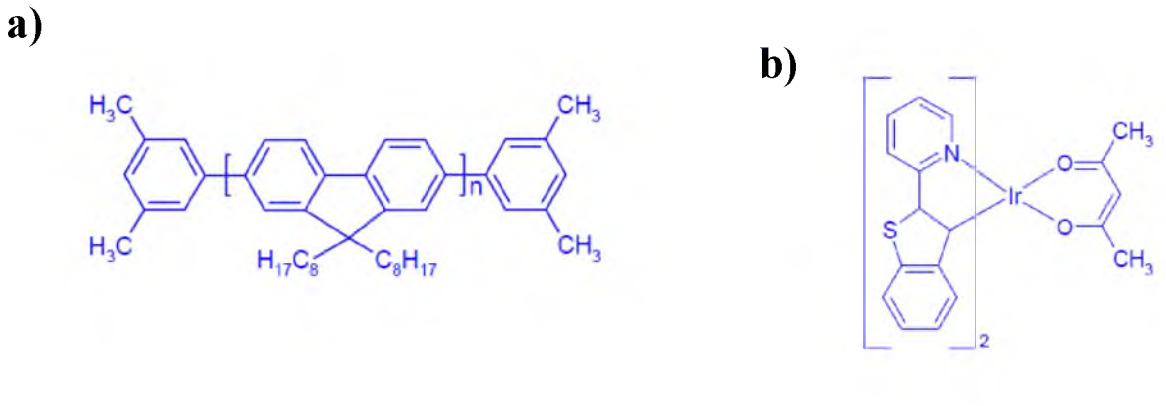

Figure 5.2: The chemical structures of (a) Poly[2,7-(9,9-di{(S)-3,7 dimethyloctyl}fluorene)] (**PFO**), the host polymer and (b) Iridium (III) bis(2-(2'-benzo-thienyl) pyridinatoN,$C^{3'}$) (acetyl-acetonate) (**Ir(btp)$_2$acac**), the guest molecule.

Cary17 spectrometer. The photoluminescence (PL) was measured using the PL setup [Chapter 2].

The PFO absorption onset occurs at ≈ 2.9 eV, with a maximum at ≈ 3.2 eV, which is due to delocalized $\pi - \pi^*$ transitions involving optical transitions from the ground state (1^1A_g) to the first excited state (1^1B_u). The PFO PL spectrum is red-shifted with respect to the absorption and shows a clear vibronic structure with picks at ≈ 2.76 (0 – 0), 2.6 (0 – 1), and 2.43 (0 – 2) eV, respectively. A fourth band occurs at 2.25 eV, and could be a fourth phonon transition 0 – 3. This relatively obvious substructure in the PL spectrum is due to the relocation of the photoexcited excitons towards the longest conjugation chain segments before radiative decay occurs and, as a result, makes the PL band narrower than the absorption band.

The absorption of the Ir(III) complex has two absorption bands: one band with onset at ≈ 3.2 eV and another weak band at ≈ 2.5 eV. The absorption band at higher energies is mostly assigned to the ligand-centered (LC) (btp), spin-allowed $\pi - \pi^*$

transitions. The weaker band at 2.5 eV is assigned to both allowed and spin-forbidden ^{1,3}MLCT transitions [5.26]. The Ir(III) complex PL spectrum is red-shifted with respect to the absorption and shows a clear vibronic structure with picks at ≈ 2 (0 – 0), 1.85 (0 – 1), and 1.65 (0 – 2) eV, respectively. The emission with clear vibronic structure is typically from ligand-based excited states in the Ir(III) complex, from the triplet $\pi - \pi^*$ transition [5.26].

Figure 5.3 also demonstrates why these materials were chosen; the guest, which is the Ir(III) complex, absorption band overlaps well with the host, which is the PFO polymer, emission band, forming an efficient energy transfer. The host/guest blend at all the measurements was pumped at 3.1 eV (unless it is stated otherwise), meaning that only the host material was photoexcited.

5.4 Processes in accepter/donor interface

5.4.1 Energy transfer channels in guest/host blend

Figure 5.4 (a) summarizes the energy process between the guest (acceptor) and the host (donor) in the blend. When exciting the host in the blend, an e-h pair, exciton is created. The exciton can be relocated from the host polymer to the guest molecule, via a nonradiative process of energy transfer. At the end of the process, the exciton in the guest molecule is recombined and decays to the ground state via a phosphorescent process.

There are two main energy transfer processes that can take place: Förster and Dexter processes. The mechanisms of these two energy transfer processes are distinguished [Figure 5.4].

The Förster mechanism is based on dipole-dipole interaction and occurs when the

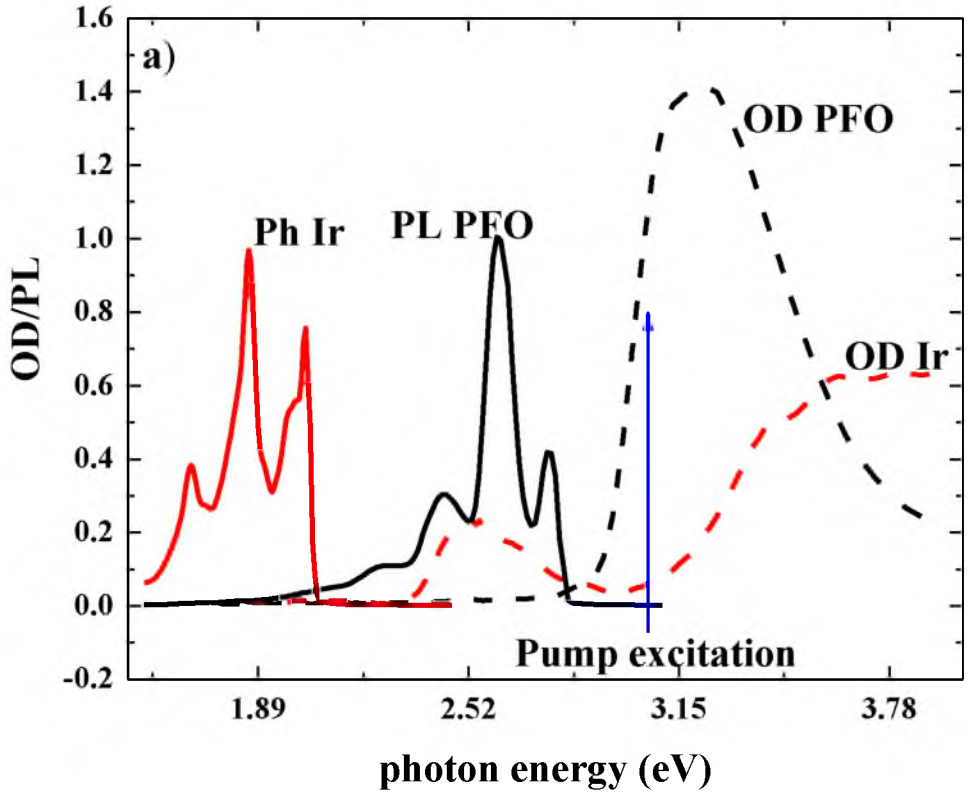

Figure 5.3: The normalized absorption and PL spectra of PFO and Ir complex.

emission spectrum of the host is overlapped with the absorption spectrum of the guest. As a result, this type of energy transfer is called resonant energy transfer (FRET). The efficiency of FRET decreases with the distance, R, between the host and guest with a factor of R^{-6}. The FRET process occurs within 10 nm, which means it is a long-range energy transfer [5.13]. Basically, in the Förster mechanism, there is energy transfer between the singlet excitons of the guest and host. However, a triplet exciton that is located at a phosphorescent host also can undergo FRET.

In the Dexter energy transfer process, an exchange of electrons, between host and

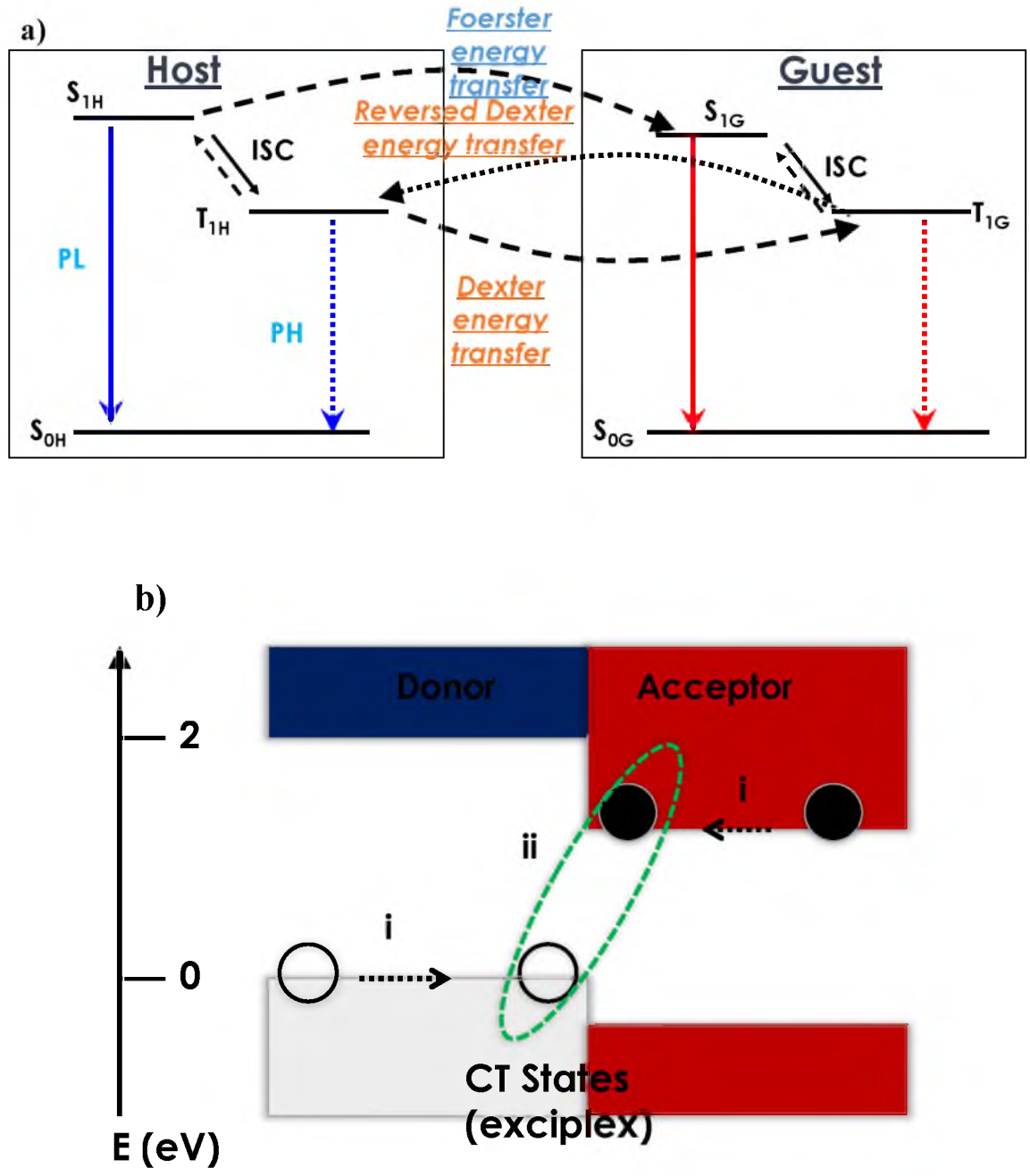

Figure 5.4: The different processes that can occur at the donor/acceptor interface; (a) Two main energy transfer processes: (i) Foerster energy transfer; FRET (ii) Dexter energy transfer. Another possibility: reversed Dexter energy transfer. (b) Charge transfer states.

guest, occurs within the overlap of the wavefunctions [5.11]. The transfer exponentially decays as the distance increased. It is a very short-range energy transfer, typically 1nm. In this process, usually, the exciton at the host undergoes internal ISC. Therefore, triplets may be transferred between the host and the guest.

In contrast to FRET, Dexter energy transfer does not require the overlap between emission and absorption spectra of the host and guest molecules. However, the exciton energy levels of the guest should be lower than the ones of the host molecule for efficient transfer.

5.4.2 Charge transfer at the accepter/donor interface

Another possibility for transfer between the guest and host polymer chain is charge transfer exciton. When an exciton located on a conjugated chain reaches the interface with a second polymer, (1) the exciton can be transferred to the second material where it may decay radiatively (luminescence characteristic of the second polymer) or nonradiatively, (2) the exciton remains in the first material where it decays radiatively (luminescence characteristic of the first polymer) or nonradiatively, or (3) the exciton dissociates by transfer of a single charge to the second material, leaving behind an opposite charge in the first material.

The schematic diagram of charge transfer is shown in Figure 5.4 (b). (i) The charged carriers are transported into the interface. (ii) At the interface, the electron and hole recombine and form exciton, creating charge transfer state. The charge transfer state is often refered to as an exciplex [5.30]

5.5 EL and PL spectra of host/guest blend

Figure 5.5 (a) shows the EL spectrum of a device based on a host/guest blend of PFO mixed with 0.02% $Ir(btp)_2acac$ molecules, in which the PFO (host) shows blue fluorescence, whereas the Ir-complex (guest) has red PH emission. As stated before in section 5.3, the PFO emission spectrum matches the absorption band of the Ir-complex, and this may induce an efficient energy transfer from the PFO host to the Ir-complex guest molecules [5.10, 5.21]. The emission spectrum of the blend OLED at 10K with different guest, Ir-complex, percentages is shown in Figure 5.5 (b). The EL spectrum reveals three distinct bands across the visible spectrum: blue fluorescence from the PFO, green fluorescence from the band marked as EX, and red PH emission from the Ir-complex. Therefore, the device may be considered to be a "white OLED." The emission spectrum shows three bands: a blue doublet at $\approx$ 3.0 eV that originates from EL of singlet excitons in the PFO host, a broad green emission band (EX) centered at $\approx$ 2.5 eV that is also related to the PFO host, and a red sharp doublet band at $\approx$ 2 eV that originates from the EPH of triplet excitons in the Ir-complex molecules. The origin of the EX band is still debated in the literature; this EL emission may be due to excimers [5.22], aggregates, or intrachain defects [5.23]. In any case, it belongs to the PFO host, since it also occurs in pristine PFO EL emission [Figure 5.5 (a)].

Figure 5.5 (b) shows the PL of the guest/host organic blend at different Ir-complex percentages. It shows the same spectrum as the EL spectrum. It presents the same three distinct bands across the visible spectrum. In order to show the three bands (blue, green, and red) across the visible spectrum, more Ir-complex percentage was needed (3%) in order to compare to the EL measurement. This is due to the fact that in

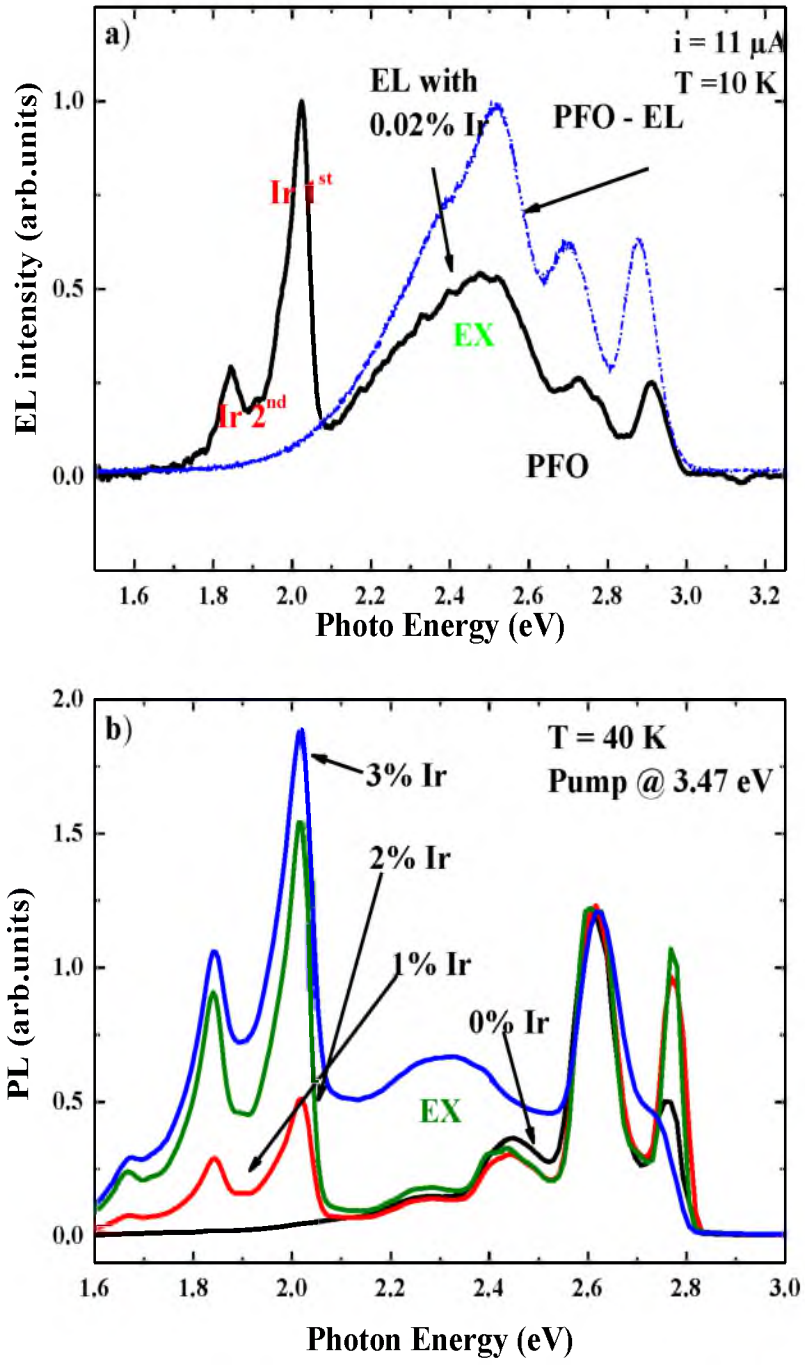

Figure 5.5: The emission in the host/guest blend. (a) The EL of the guest/host organic blend with 0.02 % of the guest molecule. (b) The PL of the guest/host organic blend at different percentages.

the EL experiment, the singlet and triplet levels of the host, the PFO, have been populated by carrier injection, which causes a Dexter transfer mechanism, compared with the PL experiment, in which only the singlet levels of the host have been populated with the carrier injection [5.24].

5.6 PL decay kinetic of PFO/Ir blend

Figure 5.6 shows the PL decay kinetic of PFO + Ir5%, excited at 3.55 eV with different probe frequencies.

For $t < 0.4$ μs, the dynamics of all the probe frequencies show similar behavior. The decay kinetic shows the PL dynamic of the host, the PFO polymer.

For $t > 0.4$ μs, the decay kinetic at probe energies of the PH emission, namely, 1.83, 2.01, 1.65 eV, show another contribution to the dynamics. This decay is fairly slow compared to the PFO dynamic. Most likely, this contribution comes from the PH of the Ir(III) complex. The decay kinetic for the probe frequencies 2.06 and 2.32 eV are most likely from the PFO polymer. It can be due to excimers [5.22], aggregates 0, or intrachain defects [5.23].

The delay in the Ir(III) complex PH emission indicates that there is energy transfer between the PFO emission and the Ir(III) complex absorption.

5.7 Picosecond transient photomodulation of guest/host blends

The picosecond transient photomodulation spectra of pure PFO films are shown in Figure 5.7 (a), for the visible – NIR spectral range for probe time delay t = 0, 5, 10, and 50 ps. The PM spectrum at t = 0 contains a sharp PA band at 1.63 eV. A SE band

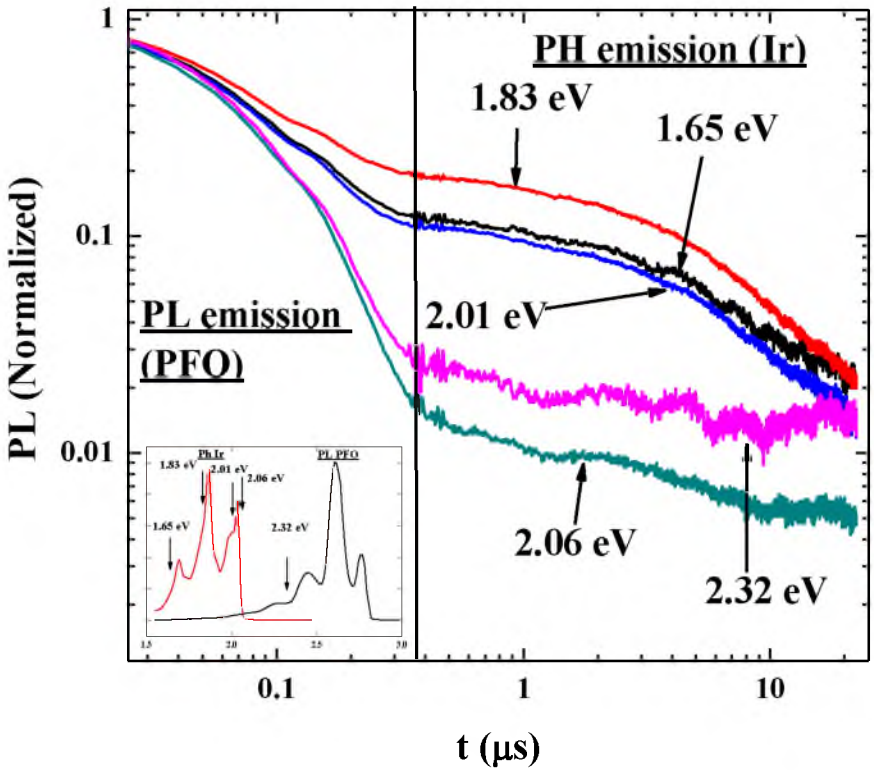

Figure 5.6: PL dynamics of PFO + Ir5% on a log-log scale. Excited at 3.55 eV, with different probe frequencies. The insert shows the probe frequencies.

was not seen, as expected, above 2.5 eV. This can be due to the thickness of the film (≈ 100 nm). However, the isosbestic point was identified at ≈ 2.5 eV. The PA band was identified as a singlet exciton, PA_2, [2.25].

The PM spectra at t = 5 and 10 ps still consist of the singlet exciton band at ≈ 1.63 eV; however, at 50 ps, the singlet exciton band almost disappears. Figures 5.7 (b) – (d) show the picosecond transient PM spectra of PFO/Ir blend with different guest (Ir complex) percentages of 3, 5, and 7 %, respectively. Overall, all different blend spectra present similar spectra to the pristine PFO film.

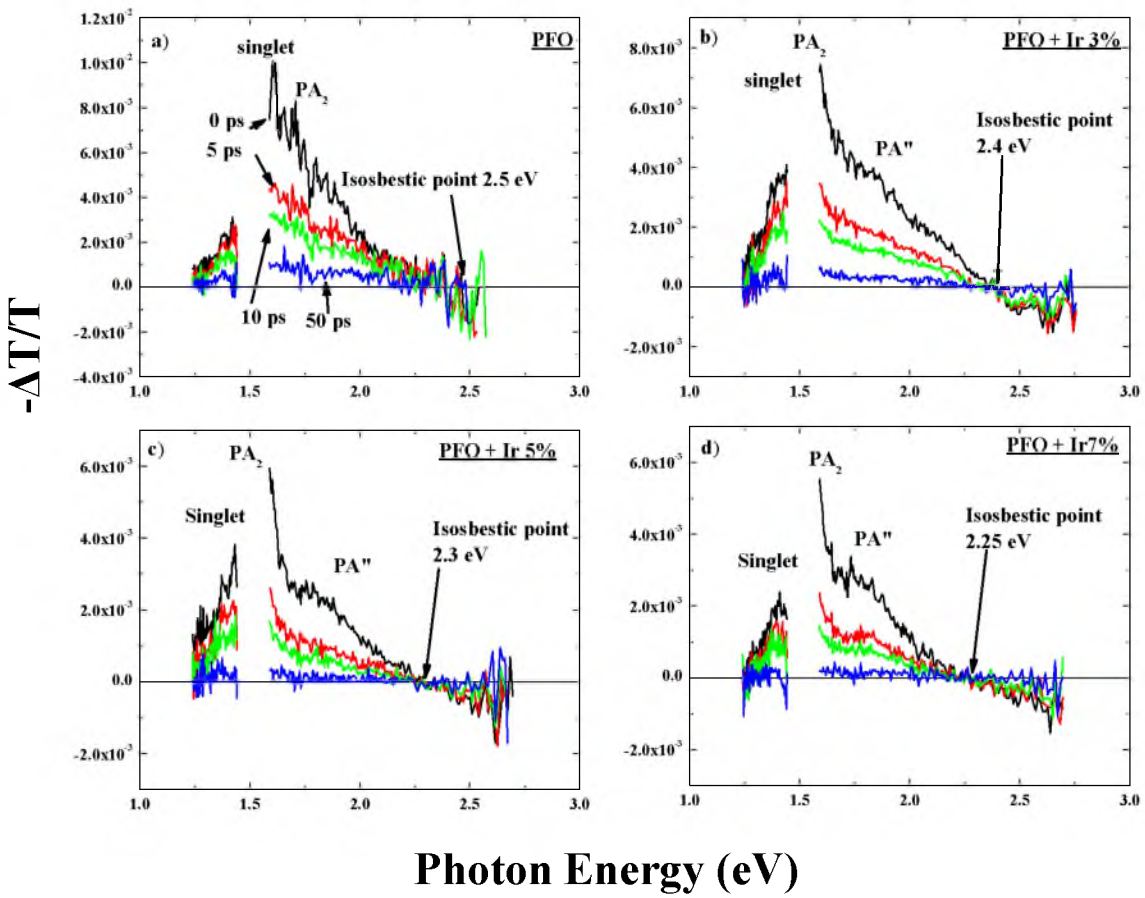

Figures 5.7: The picosecond transient PM spectra of PFO/Ir blend with different guest (Ir complex) percentage of (a) 0, pure PFO. (b) 3%. (c) 5%. (d) 7%.

However, there are two changes in the spectra the occur with the increase of the Ir complex percentage in the blend; first, the isosbestic point is red-shifted with the increase of the Ir(III) complex percentage. This shows that another process is taking place already at t = 0 [5.28]. Second, the formation of another band at ≈ 1.75 eV, PA, is observed. The intensity of this new band increases with the increase of the Ir complex percentage. However, at 5% of the Ir complex, the band reaches saturation as there is no difference between the spectrum of 5 and 7% of Ir complex.

Another indication of the formation of another blend is the comparison of the decay kinetic at different probe frequencies with different Ir complex percentages [Figure 5.8].

Figure 5.8 (a) shows the decay kinetic of the pure PFO at probe frequencies 1.6 eV and 1.75 eV. It is very clear that both decay kinetics are the same and belong to the singlet exciton of the PFO polymer. Figure 5.8 (b) shows the decay kinetic of the PFO with 5% of Ir complex, at probe frequencies 1.6 eV and 1.75 eV. It is obvious that there is a difference in the decay kinetic of the two frequencies.

In order to understand the different processes that take place in the blend, Figures 5.8(c – d) show the decay kinetic of the guest\host blend for different guest percentages (1, 2, and 3%) at probe frequencies 1.6 eV (d) and 1.75 eV (c). The decay kinetic, at both probe frequencies, shows similar behavior. The dynamics, instead of becoming faster with the increase of the percentage of the guest molecule, as expected [5.29], is slower.

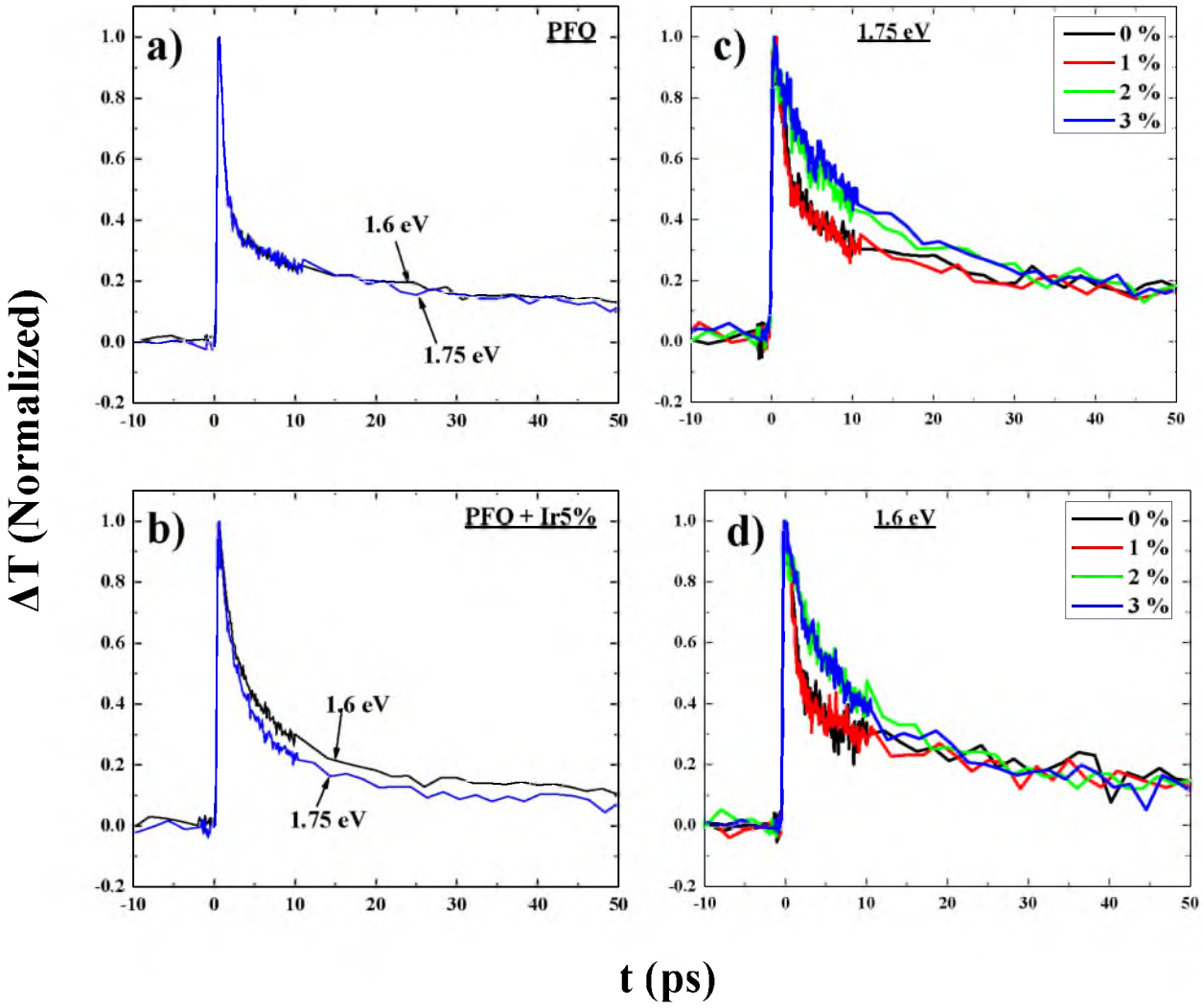

Figure 5.8: The decay kinetic of (a) pure PFO at probe frequencies 1.6 eV and 1.75 eV. (b) PFO with 5% of the Ir complex, at probe frequencies 1.6 eV and 1.75 eV. (c) Guest\host blends for different guest percentages (1, 2, and 3%) at probe frequency 1.75 eV. (d) Guest\host blends for different guest percentages (1, 2, and 3%) at probe frequency 1.6 eV.

5.8 Discussion

When the guest absorption band overlaps well with the host emission band, the possibility for an efficient FRET increases. As demonstrated, the host emission, the PFO polymer, overlaps well with the guest, the Ir(III) complex. In addition, the heavy atoms induce spin orbit coupling, which increases the efficiency for intersystem crossing processes from the singlet to the triplet states. As a result, this leads to very efficient OLED devices that are able to use both singlets and triplets for emission. This was demonstrated well with the EL where, with only 0.02 % of Ir (III), the EL spectrum reveals three distinct bands across the visible spectrum, blue fluorescence from the PFO, green fluorescence from the band marked as EX, and red PH emission from the Ir-complex. In addition, the delay decay kinetic of the PH from the guest molecule confirms the energy transfer from the host polymer, the PFO, to the guest molecule, the Ir(III) complex. However, the FRET was not detected in the decay kinetic measurements. This indicates that the energy transfer from the singlet states of the host to the singlet states of the guest molecule occurs very fast, in less than 1 ps.

The transient PM measurements reveals another PA band around 1.7 eV when increasing the Ir(III) complex percentage. This PA band is interpreted as the charge transfer state, exciplex, where an exciton is created in the interface of the donor and acceptor. The fact that decay kinetic dependence on the Ir(III) complex percentage becomes slower when increasing the guest percentage supports this interpretation.

Figure 5.9 summarized the processes that occurs between the host and the guest.

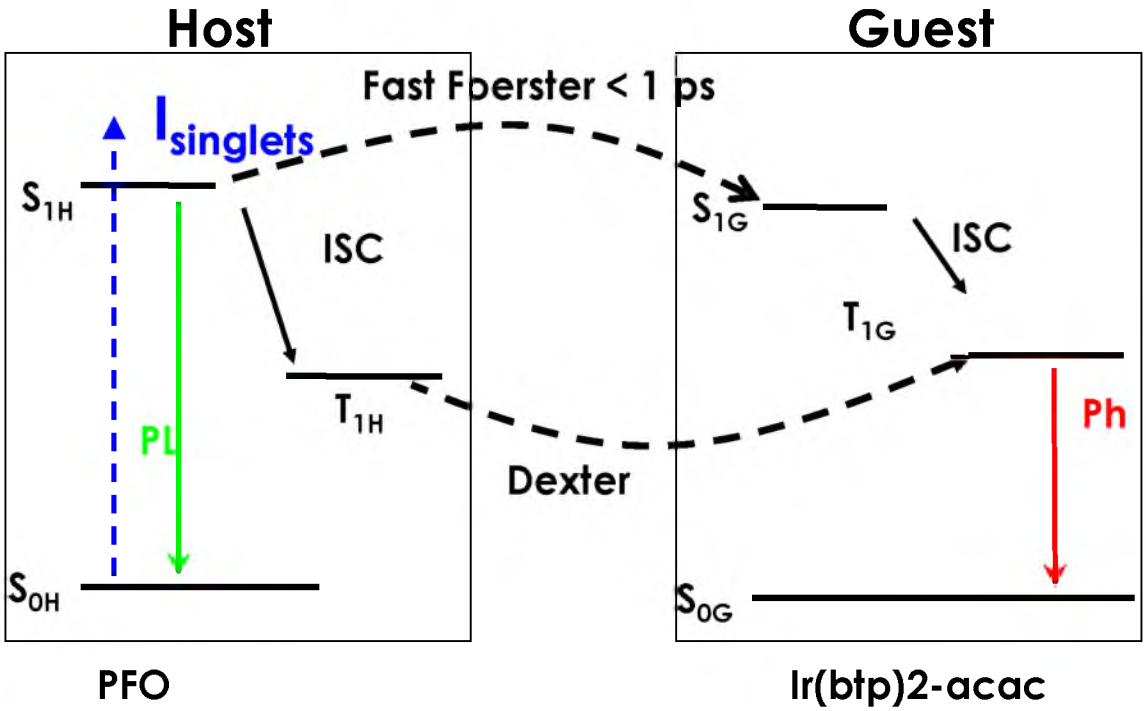

Figure 5.9: The energy transfer processes between the host and the guest.

5.9 Conclusion

The OLED device based on a host/guest blend of PFO mixed with X% of $Ir(btp)_2acac$ molecules, in which the PFO (host) shows blue fluorescence, whereas the Ir-complex (guest) has red PH emission, proven to be a "white OLED," since, the PFO emission spectrum matches the absorption band of the Ir-complex, and this induces an efficient energy transfer from the PFO host to the Ir-complex guest molecules. As a result, the emission spectrum of the blend OLED shows three distinct bands across the visible spectrum, blue fluorescence from the PFO, green fluorescence from the band that is marked as EX, and red PH emission from the Ir-complex. Therefore, the device may be considered to be a "white OLED."

5.10 Reference

[5.1] A.W. Graice, D.D.C Bradley, M.T. Bernius, M. Inbasekaran, W.W. Wu, and E.P. Woo. Appl Phys Lett 73, 629 (1998).

[5.2] M. Grell, D.C. Bradley, M. Inbasekaran, E.P. Woo, Adv. Mater. 9, 798 (1997)

[5.3] P. Sreearunothai, A.C. Morteani, I. Avilov, J. Cornil, D. Beljonne, R.H. Friend, R.T. Phillips, C. Silva, and L.M. Herz, PRL 96, 117403 (2006).

[5.4] A.C. Morteani, P.Sreearunothai, L.M. Herz, R. H. Friend, and C. Silva, PRL 92, 247402 (2004).

[5.5] L. Lu, D. Kabra, K. Johnson, and R.H. Friend, Adv. Funct. Mater. 22, 144 (2012).

[5.6] A. J. Cadby, P. A. Lane, H. Mellor, S. J. Martin, M. Grell, C. Giebeler, D. D. C. Bradley, M. Wohlgenannt, C. An, and Z. V. Vardeny, PRB 62, 15604 (2000).

[5.7] A. Hayer, A. L. T. Khan, R. H. Friend, and A. Köhler, PRB 71, 241302 (2005).

[5.8] M. A. Baldo, S. Lamansky, P. E. Burrows, M. E. Thompson, and S. R. Forrest, Appl. Phys. Lett. 75, 4 (1999)

[5.9] K. Goushi, H. Sasabe, R. C. Kwong, J. J. Brown, and C. Adachi, J. Appl. Phys. 95, 7798 (2004)

[5.10] Y. Kawamura, K. Goushi, J. Brooks, J. J. Brown, H. Sasabe, C. Adachia. Appl. Phys. Lett. 86, 071104 (2005).

[5.11] D. L. Dexter, J. Chem. Phys. 21, 836 (1953).

[5.12] D. L. Dexter, R. S. Knox, T. Förster, Phys. Status Solidi B, 34, 159, (1969)

[5.13] W. A. Luhman and R. J. Holmes, Adv. Funct. Mater. 21, 764 (2011).

[5.14] V. Cleave, G. Yahioglu, P. L. Barny, R. H. Friend, N. Tessler, Adv. Mater., 11, 285 (1999).

[5.15] V. Cleave, G. Yahioglu, P. Le Barny, D. H. Hwang, A. B. Holmes, R. H. Friend, N. Tessler, Adv. Mater., 13, 44 (2001).

[5.16] Y. Kawamura, J. Brooks, J. J. Brown, H. Sasabe, C. Adachi, PRL, 96, 017404 (2006)

[5.17] C. Adachi, M. A. Baldo, S. R. Forrest, S. Lamansky, M. E. Thompson, and R. C. Kwong, Appl. Phys. Lett. 78, 1622 (2001).

[5.18] K. A. King, P. J. Spellane, and R. J. Watts, J. Am. Chem. Soc. 107, 1431 (1985).

[5.19] C. Adachi, M. A. Baldo, and S. R. Forrest, J. Appl. Phys. 90, 5048 (2001)

[5.20] Lemmer, U. et al. Chem. Phys. Lett. 240, 373-378 (1995).

[5.21] X. Gong, W. Ma, J.C. Ostrowski, G.C. Bazan, D. Moses, A. J. Heeger, Adv. Mater. 16, 615 (2004).

[5.22] Herz, L. M. and Phillips, R. T.. PRB, 61, 13691 (2000).

[5.23] X. Gong, P.K. Iyer, D. Moses, G.C. Bazan, A.J. Heeger, S.S. Xiao, Adv. Funct. Mater. 13, 325 (2003).

[5.24] J.S. Wilson, A.S. Dhoot, A.J.A.B. Seeley, M. S. Khan, A. Köhler and R. H. Friend Nature 413, 828. (2001).

[2.25] M. Tong, C.-X. Sheng, and Z. V. Vardeny PRB 75, 125207, (2007)

[5.26] S. Lamansky, P. Djurovich, D. Murphy, F. Abdel-Razzaq, C. Adachi, P. E. Burrows, S. R. Forrest, and M. E. Thompson, J. Am. Chem. Soc. 123, 4303 (2001).

[5.27] J.-P. Duan, P.-P. Sun, and D.-H. Cheng, Adv. Mater. 15, 224 (2003).

[5.28] J. Roncali, P. Marque, R. Garreau, F. Gamier, and M. Lemaire, Macromolecules, 23, 1347 (1990)

[5.29] L. M. Herz, C. Silva, A. C. Grimsdale, K. Müllen,3 and R. T. Phillips, PRB 70, 165207 (2004)

[5.30] A.C. Morteani1, A.S. Dhoot, J.-S. Kim, C. Silva, N.C. Greenham, C. Murphy ,E. Moons, S. Cinà, J.H. Burroughes, R.H. Friend., Adv. Mater, 15, 1708 (2003).

[5.31] W.E.B. Shepherd, A.D. Platt, M.J. Kendrick, M.A. Loth, J.E. Anthony, and O. Ostroverkhova, J. Phys. Chem. Lett. 2, 362, (2011)

CHAPTER 6

SUMMARY AND FUTURE PLANS

In this chapter, we summarize what was presented in Chapters 1 through 5 and expose the conclusions drawn from various experimental tools in brief in order to provide a clearer picture of the thesis to the casual reader.

In Chapter 1, we explained in detail the basic model that might happen in π – conjugated polymers during photoexcitation. The neutral and charged photoexcitation energy level diagrams and the allowed optical transitions in dipole-moment approximation are clearly presented. The theoretical models used to describe the photoexcitations in π – conjugated polymers are presented in a simple way for better understanding.

In Chapter 2, we presented the experimental techniques that we used in this work in order to measure linear absorption in terms of optical density (O.D.), photoluminescence (PL), electroabsorption (EA), continuous wave (CW), photoinduced absorption (PA), and transient PA in the visible and mid-IR range.

In Chapter 3, we studied different derivatives of the PTV polymer. One is the RR- and RRa – PTV in which the $2A_g$ is the lowest excited state and consequently has very fast decay kinetics. The other derivative is the imide – PTV of which photophysics is dominated by mixture of the singlet energy state: $2A_g$ and $1B_u$. The imide – PTV shows a

different behavior compared with the RR – PTV, which is probably due to the different excited state parabolic energy levels.

In the last part of Chapter 3, we demonstrated transient strain spectroscopy in RR – PTV thin films, where the ultrafast energy release associated with the exciton decay gives rise to substantial static and dynamic strains in the film that dramatically influence the film's transient PM response.

In order to understand better the processes in the derivatives of the PTV polymer, it is a good idea to study the different derivatives under pressure. Applying pressure is a tool to change the polymer optical properties (such as absorption) without changing the chemical structure of the material. We expect that under pressure, the RR, RRa – PTV decay kinetics become a lot slower.

In Chapter 4, we used the pump-probe spectroscopy technique to study the transient ultrafast photophysics of pristine films of three DOO-PPV isotopes (D – polymer, H – polymer, and C – polymer). The linear absorption spectra, PL spectra, and PLQE measurements were also performed on films of all isotopes. The transient spectra of all three pristine isotope films at t = 0 ps were found to be similar to each other. From the transient decay kinetics measurements, we found that the exciton recombination in DOO-PPV consists of two processes. These are: intrinsic monomolecular, and exciton-exciton annihilation (bimolecular). The SE and PB decay kinetics are the slowest in the D – polymer. This can be due to the increase of the molecular mass, which ultimately decreases the vibrational frequency coupled to the electronic transitions (phonon replica); this leads, in turn to the decrease of the intrinsic nonradiative (INR) rate and as a result, the increased time constant. We also saw the effect of the increase in molecular mass in

the TPA measurements were the D – polymer is red-shifted compare to the H – polymer. The red-shift in the vibrational frequency is confirmed using Raman spectroscopy. The polarization memory results of the H, D – polymers were similar. In the D – polymer, different probe frequencies of PA_1 show different decay kinetics, which result from various photoexcitations that contribute to the spectrum. Comparing the spectrum at 1 ns time delay to the CW PA shows the formation of a triplet exciton in less than 1 ns. This is possibly due to singlet fission of mA_g (at 2.9 eV) into two triplets (2 X 1.4 eV). Future plans include using different wavelength for excitation and seeing the influence on the singlet fission.

In the last chapter, Chapter 5, we show an OLED device based on a host/guest blend of PFO mixed with X% of $Ir(btp)_2acac$ molecules, in which the PFO (host) shows blue fluorescence, whereas the Ir-complex (guest) has red PH emission, proven to be a "white OLED." Therefore, the PFO emission spectrum matches the absorption band of the Ir-complex, and this induces an efficient energy transfer from the PFO host to the Ir-complex guest molecules. As a result, the emission spectrum of the blend OLED shows three distinct bands across the visible spectrum, blue fluorescence from the PFO, green fluorescence from the band which is marked as EX, and red PH emission from the Ir-complex. Therefore, the device may be considered to be a "white OLED."